Kaj Lampio

Optimization of Fin Arrays Cooled by Forced or Natural Convection

Tampere 2018

Kaj Lampio

Optimization of Fin Arrays Cooled by Forced or Natural Convection

Thesis for the degree of Doctor of Science in Technology to be presented with due permission for public examination and criticism in Festia Building, Auditorium Pieni Sali 1, at Tampere University of Technology, on the 24th of August 2018, at 12 noon.

Doctoral candidate: Kaj Lampio
                        Chemistry and bioengineering
                        Natural Sciences
                        Tampere University of Technology
                        Finland

Supervisor: Jukka Konttinen, professor
                        Chemistry and bioengineering
                        Natural Sciences
                        Tampere University of Technology
                        Finland

Instructor: Reijo Karvinen, professor
                        Tampere University of Technology
                        Finland

Pre-examiners: Kemal Hanjalić, professor
                        Department of Chemical Engineering
                        Delft University of Technology
                        Netherlands

                        Jussi Hakanen, adjunct professor
                        Faculty of Information Technology
                        University of Jyväskylä
                        Finland

Opponents: Bengt Sundén, professor
                        Department of Energy Sciences
                        Lund University
                        Sweden

                        Jussi Hakanen, adjunct professor
                        Faculty of Information Technology
                        University of Jyväskylä
                        Finland

Abstract

Electronic components must be cooled to maintain their operating temperatures below the specified limits. If the maximum permissible limit of a component is exceeded, its service life decreases considerably. With increasing power densities in recent decades, the use of heat sinks to improve component cooling has become virtually mandatory in many applications. However, designing a heat sink, which optimally compromises its material weight and its heat transfer performance, is a difficult task because the result depends heavily on its geometrical structure and its operating conditions.

In this thesis, a fast way to optimize industrial heat sinks with a fixed set of heat dissipating components is presented. In a typical optimization case, several hundred temperature field evaluations are needed to find the optimal geometry. These evaluations consume a lot of CPU - time if done with conventional CFD. The main objective of this thesis is, therefore, to present a new calculation model, which can handle these temperature field evaluations in a much shorter time. In the model, the speedup is obtained by replacing the slow 3D CFD -solution of air velocity and temperature distributions with 1D solutions for the mean values of these distributions, where convective heat transfer and shear stress are calculated from analytical correlations. A complete 3D numerical solution is only performed for the solid temperature field. These modifications make the new model at least a thousand times faster than CFD.

The calculation model is then tested for accuracy in many test cases, where its results are compared to those calculated with CFD and analytical solutions. These comparisons ensure that the model operates with the precision needed for optimization to predict the maximum temperature of the components. This is important because, in optimization, the maximum temperature of the components is the most crucial quantity.

After accuracy testing, the use of the model as part of an efficient multi-objective optimization algorithm is demonstrated in many distinct cases. Instead of just one optimal solution, multi-objective optimization results in a set of best compromise solutions, called the Pareto optimal set, according to the chosen criteria. Usually, the optimization criteria are the maximum temperature of the components and the weight of the material, or the external volume, of the heat sink. A well-performed optimization can allow a significant reduction of the solid material used. In the heat sink manufacturing industry, the potential for total savings in material, energy, and CO_2 emissions is significant as the global market size of thermal management technology is vast.

Tiivistelmä

Elektroniset komponentit tarvitsevat jäähdytystä, jotta niiden käyttölämpötilat pysyvät sallittujen raja-arvojen sisällä. Mikäli sallitut käyttölämpötilat ylitetään, komponenttien käyttöikä laskee merkittävästi. Haasteena onkin, että komponenttien tehotiheydet ovat kasvaneet merkittävästi viime vuosikymmeninä, jolloin niiden lämmönpoisto vaatii käytännössä jäähdytyspinta-alan kasvattamista jäähdytysrivastojen avulla. Optimaalisen jäähdytysrivaston suunnittelu ei ole kuitenkaan helppoa, koska sen geometrinen rakenne, ja käyttöympäristö, vaikuttavat sen lämmönsiirtotehoon.

Tässä työssä esitetään nopea metodi tietyn komponenttijakauman jäähdyttämiseen tarkoitetun jäähdytysrivaston optimoinnille. Optimoinnissa vaaditaan yleensä vähintään satojen erilaisten rakenteiden lämpötilajakaumien laskeminen, jotta löydetään optimaalinen geometria. Nämä laskennat kuluttavat paljon CPU-aikaa, jos ne tehdään virtauslaskennalla (CFD). Ratkaisuna tässä työssä esitetään nopea laskentamalli, joka suoriutuu lämpötilakentän laskennasta huomattavasti CFD:tä nopeammin. Laskentamallissa hyödynnetään nopeita 1D-ratkaisuja ilmavirtauksen keskimääräisille nopeus- ja lämpötilajakaumille, ja niillä korvataan CFD:n yksityiskohtaisemmat ilman nopeus- ja lämpötilajakaumien 3D-ratkaisut. Ainoastaan jäähdytysrivaston lämpötilakenttä ratkaistaan kolmiulotteisesti. Näillä muutoksilla uusi laskentamalli on yli tuhat kertaa CFD:tä nopeampi jäähdytysrivaston lämpötilakentän laskennassa.

Laskentamallin soveltuvuutta optimointiin testattiin vertailemalla sillä laskettuja arvoja analyyttisiin laskentoihin, CFD-laskentoihin ja kokeellisiin tuloksiin. Laskentamallin antamat tulokset komponenttien maksimilämpötiloille poikkesivat alle 10 % vertailuarvoista kaikissa testitapauksissa. Tulos oli hyvä, koska maksimilämpötilan tarkka laskenta on tärkeää optimoinnin onnistumisen kannalta.

Laskentamallia käytettiin maksimilämpötilojen määrittämiseen monitavoitteisessa optimoinnissa, jossa etsitään matemaattisesti parhaat kompromissit, Pareto optimaaliset ratkaisut, valittujen kriteerien mukaan. Useimmiten optimointikriteerit ovat komponenttien maksimilämpötilat, rivaston massa ja ulkotilavuus. Optimoinnin avulla voidaan saavuttaa merkittäviä materiaalisäästöjä. Esimerkiksi tyypillisessä tämän työn tapauksessa jäähdytysrivaston massaa saatiin vähennettyä noin 50 %. Koska kansainvälisten markkinoiden koko tehostetulle lämmönsiirrolle on valtava, optimoinnilla voidaan saavuttaa merkittäviä kokonaissäästöjä materiaalin ja energian kulutuksessa sekä CO_2-päästöissä.

Preface

This thesis was written during my time at the Department of Energy and Process Engineering (2012), at the Department of Engineering Design (2013-2014), at the Department of Mechanical Engineering and Industrial Systems (2015 – 2016), and at the Department of Chemistry and Bioengineering (2017 – 2018) in Tampere University of Technology. I would like to thank all the personnel at all departments and all my coworkers who assisted me with this thesis.

Especially I would like to thank my first supervisor, prof. Reijo Karvinen (2012 – 2017), for his guidance, advice, and co-authoring during the work. He led me into the field of fluid dynamics and heat transfer and he has been a source of inspiration for his passion for perfecting the profession. Equally, I want to thank my second supervisor, prof. Jukka Konttinen (2017-2018), for supporting me to finish this thesis. I want to thank Dr. Matti Lindstedt for him contribution of being the first author in Publication III. I want to thank also Dr. Henrik Tolvanen, who helped me to figure out the overall structure of this thesis.

I would also like to express my sincere thanks for my pre-examiners prof. Kemal Hanjalic and adjunct professor Jussi Hakanen for their evaluations of this thesis and their suggestions for amending the manuscript.

I would also like to thank Risto Laurila, Timo Koivuluoma, and Jorma Manninen from ABB Drives for plating the seed for this great research project, financing its beginning, and for the interesting discussions on the practical side of heat sink designs.

For financial assistance, I would like to thank the Department of Chemistry and Bioengineering for believing in me to complete this work and financing its completion.

Finally, I want to thank my parents and friends for their support. Lastly, thank you Terhi, Linnea, and Lenni, my own loved ones, for reminding me every day what is ultimately important in life.

Tampere, 31th May, 2018

Kaj Lampio

Contents

List of symbols

Latin symbols

A	Area	m^2
A_{b-f}	Coefficient in Eq. (4.3)	WK^{-1}
A_E	East side coefficient in Eq. (4.2)	WK^{-1}
A_N	North side coefficient in Eq. (4.2)	WK^{-1}
A_P	Control volume P coefficient in Eq. (4.2)	WK^{-1}
A_S	South side coefficient in Eq. (4.2)	WK^{-1}
A_W	West side coefficient in Eq. (4.2)	WK^{-1}
b	Base plate thickness	m
C	Coefficient related to Nusselt number (Chimney effect)	-
C_1	Coefficient related to Sutherland Eq. (2.5)	$kgm^{-1}s^{-1}K^{-1/2}$
c_1	Cognitive component in PSO – algorithm	-
c_2	Social component in PSO – algorithm	-
c_3	Inertia component in PSO – algorithm	-
c_p	Specific heat	$Jkg^{-1}K^{-1}$
d	Channel width	m
d_b	Diameter of pin fin	m
d_h	Hydraulic diameter = $2d$ (for parallel plates)	m
$d_{i,h}$	Distance between swarm member i and target h in optimization	-
d_{LE}	Distance from the leading edge	m
El	Elenbaas number = $g\beta\Delta Td^4\mathrm{Pr}/(v^2L)$	-
f	Mean Fanning friction factor = $\tau_s/(0.5 \times \rho V^2)$	-
$\boldsymbol{f(x)}$	Vector of objective functions in optimization	-
$f_i(\boldsymbol{x})$	Objective function i in optimization	-
$F_i(\boldsymbol{x})$	Modified objective function i in optimization	-
f_{max}	Large number in optimization	-
fRe	Fanning friction factor times Reynolds number	-
$\boldsymbol{g}$	Vector of gravitational acceleration	ms^{-2}
g	Acceleration of gravity = 9.81	ms^{-2}
$\boldsymbol{g(x)}$	Vector of inequality constraints in optimization	-
gbest	Global optimum in PSO-algorithm in optimization	-
$g_i(\boldsymbol{x})$	Inequality constraint i in optimization	-
G_n	Constants (Eigen functions) in Table 1	-
h	Heat transfer coefficient	$Wm^{-2}K^{-1}$
$\boldsymbol{h(x)}$	Vector of equality constraints in optimization	-
$h_j(\boldsymbol{x})$	Equality constraint j in optimization	-
H_k	Function for calculating variance in Eq. (3.9) in optimization	-
K	Coefficient in Eqs. (2.30) and (2.31)	$m^{-1/2}$
k	Thermal conductivity	$Wm^{-1}K^{-1}$
K_{in}	Minor loss coefficient (inlet)	-
K_{out}	Minor loss coefficient (outlet)	-
L	Length in x-direction	m
l	Fin height	m

L^*	Dimensionless length = $L/(\mathrm{RePr}d_h)$	-
L_d	Distance between components in Fig. 16	m
l_e	Extended fin height in Eqs. (2.30) and (2.31)	m
l_t	Coefficient in Eq. (3.10) in optimization	-
m	Mass	kg
m_c	Fin constant in Eq. (2.26)	m^{-1}
N	Number of fins OR Number of particles in optimization	-
n	Number of design variables	-
N_{ch}	Number of channels	-
n_{ec}	Number of equality constraints h_j in optimization	-
n_{ie}	Number of inequality constraints g_i in optimization	-
Nu	Mean Nusselt number = hL/k_f	-
$\mathrm{Nu_a}$	Asymptotic Nusselt number	-
$\mathrm{Nu_x}$	Local Nusselt number = hx/k_f	-
$\mathrm{Nu_\xi}$	Nusselt number = $h\xi/k_f$ in Eq. (2.20)	-
P	wetted perimeter of channel cross-section	m
p	Pressure	Pa
pbests	Best solution achieved for specific swarm member so far in optimization	-
Pe	Peclet number = RePr	-
Pr	Prandtl number = $\mu c_p/k_f$	-
q	Heat flux	Wm^{-2}
Q	Volumetric flow	$\mathrm{m}^3\mathrm{s}^{-1}$
Q_p	Source term in Eq. (4.2)	W
R	Gas specific constant = 287 (for air)	$\mathrm{Jkg}^{-1}\mathrm{K}^{-1}$
r	L/d – ratio in Section 2.3.2	-
Ra_L	Rayleigh number = $g\beta\Delta TL^3\mathrm{Pr}/v^2$	-
Ra_ξ	Rayleigh number = $g\beta\Delta T\xi^4\mathrm{Pr}/(v^2L)$	-
Re	Reynolds number = Vd_h/v	-
REP	Repository of non-dominated Pareto optimal solutions in optimization	-
r_i	Vector of random numbers in optimization	-
S	Coefficient related to Sutherland Eq. (2.5)	K
t	Time	s
T	Temperature	K
T_{avg}	Fluid average temperature in a channel	K
t_b	Fin thickness at fin base ($z = 0$)	m
$T_{i,j}$	Temperature at location (i, j)	K
T_m	Fluid mean temperature	K
t_t	Fin thickness at fin tip ($z = l$)	m
$\boldsymbol{u}$	Design variable vector in Eq. (3.3)	-
u	Velocity component in x-direction	ms^{-1}
U_∞	Ambient flow velocity	ms-1
$\boldsymbol{v}$	Design variable vector in Eq. (3.3)	-
v	Velocity component in y-direction	ms^{-1}
V	Mean velocity OR Volume	ms^{-1} OR m^3
$\boldsymbol{V}$	Velocity vector = $(u, v, w)^{\mathrm{T}}$	ms^{-1}
$\boldsymbol{V}_{i,k}$	Velocity component vector of swarm member i in optimization	-
w	Velocity component in z-direction	ms^{-1}
W	Width in y - direction	m
Δz_1	Base plate side control volume height in Eq. (4.3)	m
Δz_2	Fin side control volume height in Eq. (4.3)	m

x	x-coordinate	m
$\boldsymbol{x}$	Design variable vector in optimization $= (x_1, x_2, \ldots, x_n)^\mathrm{T}$	-
X	Location of component cluster in x-direction	m
x^*	Dimensionless coordinate $= x/(\mathrm{RePr}d_\mathrm{h})$	-
$\boldsymbol{x}^*$	Pareto optimal design variable vector in optimization	-
x^+	Dimensionless coordinate $= x/(\mathrm{Re}d_\mathrm{h})$	-
$\boldsymbol{X}_C$	Location vector of components in x-direction	m
$\boldsymbol{x}_{i,k}$	Design variable vector of swarm member i in optimization	-
$\boldsymbol{x}_l$	Design variable vector lower bound in optimization	-
$\boldsymbol{x}_u$	Design variable vector upper bound in optimization	-
y	y-coordinate	m
Y	Location of component cluster in y-direction	m
$\boldsymbol{Y}_C$	Location vector of components in y-direction	m
z	z-coordinate	m

Greek symbols

α	Channel aspect ratio ≥ 1 OR angle in Fig. 7	-
β	Volumetric expansion coefficient, for gas $= 1/T_\infty$	K^{-1}
Δp	Pressure loss	Pa
ΔT	Case specific temperature difference	K
Δx	Length of single control volume in x - direction	m
Δy	Length of single control volume in y - direction	m
Δz	Length of single control volume in z - direction	m
ε_i	Constraining value for objective i in ε-constraint method in optimization	
η	Fin efficiency $= \phi/\phi_i$	-
θ	Temperature excess $= T - T_\infty$	K
λ_n	Eigenvalue in Table 1	-
μ	Dynamic viscosity	Pas
μ_a	Coefficient in Eq. (2.31)	-
μ_b	Coefficient in Eq. (2.31)	-
v	Kinematic viscosity	$\mathrm{m}^2\mathrm{s}^{-1}$
ξ	Characteristic length in Eq. (2.22)	-
ξ_d	Dummy coordinate variable in Eq. (2.9)	-
ρ	Density of fluid	kgm^{-3}
ρ_s	Density of solid	kgm^{-3}
τ_s	Mean surface shear stress	Pa
ϕ	Heat transfer rate	W
ϕ'_{CFD}	Heat transfer rate per unit length with CFD in Table 11 (W/m)	Wm^{-1}
ϕ'_m	Heat transfer rate per unit length with calculation model in Table 11	Wm^{-1}
ϕ'_{sp}	Heat transfer rate per unit length with superposition principle in Table 11	Wm^{-1}
ϕ_i	Heat transfer rate from isothermal channel/fin	W
ϕ_m	Heat transfer rate with calculation model in Table 8	W
ϕ_T	Heat transfer rate with Teertstra model in Table 8	W
Ω	Feasible region in optimization	-

Subscripts

0	value at $x = 0$
∞	ambient property
avg	average value
b	base plate property
c	component or component cluster property
cs	cross section property
eff	effective property
f	fluid property
L	characteristic length L OR value at $x = $ L
m	mean value
max	maximum value
min	minimum value
s	solid property
w	wall property

Abbreviations

CFD	computational fluid dynamics
CPU	central processing unit
EU	European Union
LcRiPSO	locally convergent rotationally invariant particle swarm optimization
MOO	multi-objective optimization
MOPSO	multi-objective particle swarm optimization
PCB	printed circuit board
PSO	particle swarm optimization
SOO	single objective optimization
sPSO	standard particle swarm optimization

List of publications

The present thesis is based on the following five publications, referred to as Publications I-V. Some previously unpublished material is also presented and discussed in the compilation of the thesis.

I.   R. Karvinen, K. Lampio, "Combined numerical and analytical method for fin array heat transfer", Proc. of CHT-12, July 1-6, 2012, Bath, England.

II. R. Karvinen, K. Lampio, "Multi-objective optimization of electronics heat sink geometries", Proc. of IWHT 2013, October 18-21, 2013, Xi'an, China, Invited lecture.

III. M. Lindstedt, K. Lampio, R. Karvinen, "Optimal shapes of straight fins and finned heat sinks", ASME J. Heat Transfer (2015), 137 (6), 061006-1-8.

IV. K. Lampio, R. Karvinen, "A new method to optimize natural convection heat sinks", Heat and mass transfer (2017), in press, published online 14 August 2017.

V.   K. Lampio, R. Karvinen, "Optimization of convectively cooled heat sinks", Microelectronics reliability (2017), 79, 473-479.

Author's contribution

I. The author (Lampio) presented the method for forced convection cooling and preformed the calculations. The author and the co-author wrote the manuscript.

II. The author presented the multi-objective optimization method for forced convection cooling using the method presented in Publication I, performed the calculations and optimizations. The author and the co-author wrote the manuscript.

III. The author was involved with the calculations of fin arrays by performing the calculations and multi-objective optimizations for fin arrays with trapezoidal fins and checked the results of rectangular fins. The author had a minor role in writing the manuscript. Lindstedt presented the fin array results with rectangular fins and with professor Karvinen the results on single fin optimization. Lindstedt and Karvinen were the main authors of the manuscript.

IV. The author presented a new calculation method suitable for multi-objective optimization of fin arrays cooled by natural convection, and performed optimization calculations. The author and the co-author wrote the manuscript.

V. The author conducted preliminary calculations for pin fins for further study. The author reviewed and refined the previous conference and journal publications with the co-author and compiled the manuscript together with co-author.

The work was conducted under the supervision of prof. Reijo Karvinen (2012 – 2017); and prof. Jukka Konttinen (2017 - 2018), whereas prof. Reijo Karvinen was the main scientific contributor to the work.

Chapter 1

Introduction

Electronic components require cooling to keep their operating temperatures below specified limits. If the maximum permissible limit is exceeded, the service life of a component decreases significantly. As pointed out in [1] when the first digital computers, such as the Harvard Mark I, shown in Fig. 1, were used between the 1940s and -60s, sufficient thermal control was achieved by simply removing the hot air from the computer room. In the 1970s and 1980s, transistors were made smaller, and the components were mounted on a printed circuit board (PCB). Adequate cooling was achieved by stacking the PCBs in a row as a card cage and by creating sufficient airflow through the channels, as shown in Fig. 2. After the 1990s, sole reliance on these cooling methods has become obsolete, because of continually increasing power densities. Currently, an average heat flux from a component may correspond to that of a nuclear blast, and the maximum heat flux from hot spots may equal even that of the outer surface of the Sun. However, the surface temperature of the Sun is about 5800 K, but these components must operate typically at around 300 – 400 K. In power electronics, similar challenges has been encountered in cooling of IGBT devices, where the cooling requirements have become the major barrier for developing advanced power electronics for electronic vehicles [2]. These constantly increasing challenges have been the main driver behind the development of cooling equipment.

The heat sink cooled by forced (in Fig. 3a) or natural convection (in Fig. 3b) has served as a typical solution for enhancing heat transfer from electronic components and other engineering applications [3]. The main idea of a heat sink is to extend the size of the heat transfer surface that is in direct contact with the cooling medium. Forced convection heat sinks can remove much larger heat loads, but because of a possible fan failure, natural convection heat sinks have also many applications, such as those used in base station cooling in Fig. 3c. The performance of a heat sink is sensitive to its geometrical structure because the overall heat transfer is constrained by conduction resistance imposed by the solid geometry and the convection resistance of the airflow in the heat sink channels. Consequently, the optimal dimensions of a heat sink are highly application dependent, and designing a well performing heat sink is a challenging task.

Figure 1. Harvard Mark I of the 1950s.

Figure 2. Example of a card cage cooled by a fan.

Forced flow from fan

Buoyancy driven natural flow

(a)   (b)   (c)
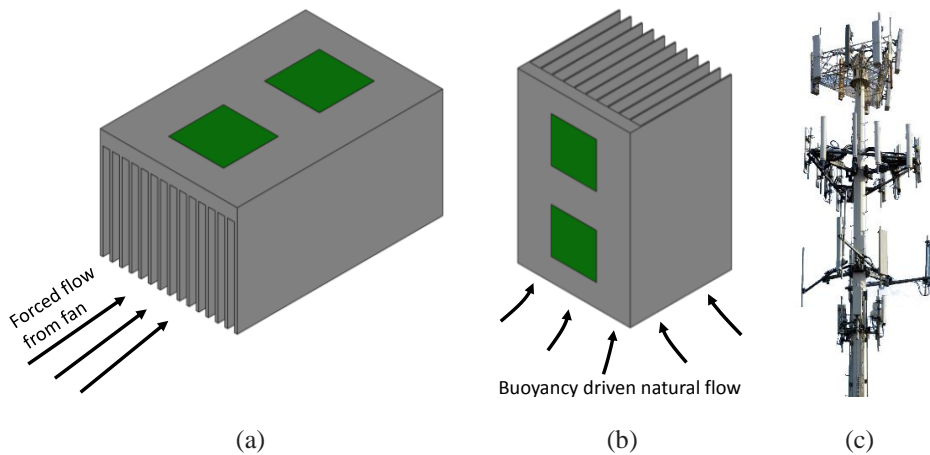
Figure 3. Cooling of two heat dissipating components (shown green) with a heat sink operated by forced convection (a) or natural convection (b), and also a base station cooled by natural convection (c).

In industry, a typical heat sink has many different components mounted on its base plate, and the optimal heat sink design must be determined case specifically. Lehtinen [4] pointed out that the optimal design should minimize the following criteria: component maximum temperatures, heat sink mass, outer volume, manufacturing and operating costs, and noise level. When the designer optimizes a heat sink, the most challenging task is to determine its temperature distribution for a given set of components. The maximum temperature depends on component locations, heat dissipation rates, heat sink dimensions, and flow condition, i.e., whether the flow is created by a fan or a buoyant force. The requirement of minimizing several conflicting design criteria forms a multi-objective optimization problem, as pointed out in Publications II and IV.

Computational fluid dynamics (CFD) software is a good option to obtain a temperature field for single case calculation. However, it is typically too slow for optimization, because hundreds of different geometries must be evaluated in order to obtain an optimum solution. One alternative is to build multiple different prototypes and measure them directly. However, this is an expensive and slow process and one not typically carried out without special reasons.

Finally, the materials selected for a heat sink may significantly affect its performance. Typically, selection is made between aluminum and copper. Copper has about two times higher thermal conductivity but 3.3 times higher density than aluminum. The price of copper is currently about three times higher per mass unit than that of aluminum [5]. When the density difference is taken into account, the price of copper is about ten times higher per volume unit than that of aluminum. In many cases, the extra price of copper is not worth the marginal increase in heat transfer capability, and aluminum has been the most used material. Copper is mainly used in special environments, such as ships and other marine vessels, where corrosion restricts using aluminum.

1.1 Objective of present thesis

The main objective of the present thesis is to provide a fast performing way to optimize material weight, maximum temperature, and outer volume of industrial heat sinks with a fixed set of heat dissipating components. The main emphasis is in material weight reduction where a well-performed optimization may allow significant reductions (up to 60 %). However, even small improvements have a meaningful impact because the global saving potential is huge. The thermal management technology market is expected to reach $ 14.7 billion by 2019, and fans and heat sinks account about 84 % of the size [6]. When inspecting an individual heat sink, an estimate of energy consumption in the manufacturing process was about 85 kWh/kg in 1999 [7]. This approximate figure takes into account the energy used for extrusion, assembly and transportation, and includes material wastage and use of some recycled material in the process. The efficiency of the process has probably improved over the last two decades, yet the above energy consumption figure is still likely to be a good approximation when estimating potential savings.

To fulfill the objective of a fast performing optimization tool, the selected approach in the present thesis is to create a new calculation model, which yields the temperature field evaluations of a heat sink in a much shorter CPU -time than conventional CFD. This allows the new model to be used as a part of an efficient multi-objective optimization algorithm, which finds optimal geometry candidates according to selected criteria. In a typical optimization case, this approach

allows a significant reduction in heat sink mass without affecting the heat sink performance. Such reductions do matter as saved energy (see the previous paragraph) and CO_2 emissions when a company produces heat sinks in large quantities.

Understanding how CO_2 emissions affect our planet's climate have increased in recent decades. Therefore, companies must pay for CO_2 emission allowances, which were between €4 to €6 per CO_2 tonne throughout 2016 and 2017 in the European Union [8]. The price of emission allowances may increase in future, because the EU has set a goal for reducing greenhouse gas emissions by 2030. Currently (2018), these reduction goals depend on the country between 0 - 40 % of the CO_2 emission levels in 1990 [9]. For Finland, the present target is -39 %.

The specific objectives of the thesis are to:

- present a calculation model for forced convection heat sinks (Publication I)
- extend the model for natural convection heat sinks (Publication IV)
- test the model accuracy against analytical, experimental, and CFD results (Publications I, II, III, IV and V)
- demonstrate the use of the model in multi-objective optimization (Publications II, III, IV and V)

1.2 State-of-the-art in optimization of heat sinks

The optimization of a single fin has been studied extensively, and solutions for a constant heat transfer coefficient with constant fin mass exist in the literature [3]. Optimal solutions for fins, which take into account the effect of surface temperature distribution on the heat transfer coefficient, are presented in [10, 11]. Optimal dimensions can be obtained from non-dimensional variables, and these results are also presented in Publication III. These single fin optimization results can help to understand the effect of fin shape on heat transfer performance in heat sinks. However, optimizing fin arrays is a more complicated problem than single fin optimization, because the flow in the channels must be taken into account.

The simplest case to optimize is an isothermal heat sink, which is presented in *forced convection* cases in the literature [12, 13, and 14]. Optimization was performed using a numerical and an analytical approach, and optimal fin spacing was obtained for various flow boundary conditions. The analytical formula was based on intersection of asymptotes, which is a simple and effective way to obtain optimal fin spacing. Muzychka [15] used the same method of intersection of asymptotes to derive optimal channel passage size to its length -ratio for various different cross sectional channel shapes. Lindstedt and Karvinen [16] conducted multiple different multi-objective optimization studies for isothermal arrays, such as "minimum thermal resistance with fixed volume and pressure drop". The results of optimal structures were presented using three different non-dimensional variables. They made also an important finding that at least one design parameter from fin height, fin thickness, number of fins, or flow mean velocity has to be fixed in the optimization, or no meaningful geometry can be found.

For a constant heat flux base plate, which resembles more electronics cooling applications, many optimization studies in *forced convection* case have been published in the literature. In [17] Ruy

et al. found that the channel width is the most crucial parameter in optimization if pumping power is fixed. In [18] Kim et al. found surprising result that the optimal fin thickness was independent of the pumping power, and the length of the channels. Additional finding was that the optimal fin thickness was proportional to the fin height linearly. In [19] Kim et al. studied the effect of variable fin thickness and found that when minimizing the thermal resistance with a fixed pumping power, the optimal fins are those whose are thinnest at the base plate and increase their thickness towards their tips (upward trapezoidal shape). Of course, this fin shape is not probably optimal if also fin mass is taken in the consideration in optimization.

If the heat flux is brought to the base plate from a smaller area than the entire base plate, such as from individual components, the temperature distribution of the base plate changes considerably. Biswal et al [20] made an interesting analytical study of cooling a single heat source with *forced convection* using liquid as a coolant. The flow was laminar in the study, and they studied how different design parameters effect on total heat transfer. The varied parameters were the thickness of the base plate, the channel aspect ratio, the number of channels, etc. For a single centered heat source case they found that if the base plate thickness is too thin, the spreading resistance disturbs efficient heat transfer, but too thick values also have large conduction resistances. Therefore, an optimal base plate thickness exists for the best thermal performance.

For multiple components in a full 3D heat sink case cooled by a *forced convection*, Lehtinen [4] constructed an analytical formula using a truncated Fourier series for plate fin heat sinks and tested it in the case of laminar flow. Lindsted [21] exploited the formula and optimized a fin array with nine components in the case of turbulent flow. In his thesis, Aho [22] performed an interesting study of the optimal location of components on a printed wired board (PWB). He conducted a multi-objective optimization whose conflicting criteria were average maximum temperatures of the components and the total wiring length between the components. He also extensively reviewed the work done in the field.

Researchers have also developed alternative approaches to finding the optimal structures inspired by thermodynamics. Examples of these are the cases of *entropy generation minimization* [23] or *entransy minimization* [24]. Of these two, the more recent, entransy, has lately been subjected to criticism [25, 26] in that it is, e.g., an unnecessary, redundant, and not a new physical quantity. However, some authors such as [27] are more open to a new concept and remind us that its applications are still being developed. Entropy generation minimization has been used, e.g., in [28] to optimize an example heat sink and examined in more detail in [7], where also total energy consumption (manufacturing, transportation, operational costs) was a subject of minimization. In the latter paper, an interesting finding was also that in a turbulent flow situation typically from 20 to 90 W of cooling power of heat dissipating components can be cooled with a 1 W power fan. For practical problems, however, the complex concepts of entropy and entransy may be too sophisticated, and they have not been widely used [21].

In optimization of *natural convection*, the paper of Bar-Cohen et al. [29] was the starting point. The authors optimized an isothermal 2D channel for its width with several different boundary conditions. Later Bar-Cohen et al. optimized natural convection heat sinks with an isothermal base plate [30]. They found out that the classical least material optimum of single fin in Ref. [3] can be combined with the optimum spacing result from [29]. When they are combined, a

thermally superior optimum is obtained easily for isothermal base plate heat sink without any mathematical optimization process.

In a case of *natural convection* cooled heat sink with a constant heat flux at the base plate, Kim [31] optimized the fin shape in respect to its thermal resistance. He found that if the fin thickness was let to vary, the thermal resistances were reduced up to 10 % from the uniform fin thickness case. However, he also pointed out that the obtained benefit decreases if the heat flux to the base plate or the length of the heat sink in the flow direction decreases.

In *natural convection* cooling, the direction of gravitational field in respect to heat sink orientation affects the behavior of buoyant plumes. The cases mentioned in the paragraphs above dealt with vertically oriented natural convection heat sinks. Shen et al. [32] studied the effect of orientation, and found that arrays with denser fins were more sensitive to orientation, and that small inclinations from vertical position do not affect significantly to heat transfer performance.

Besides rectangular heat sinks, another interesting heat sink type in *natural convection* cooling is a radial heat sink. It is often used to cool a single heat source, such as LED, and some important experimental work has been carried out recently in the literature [33, 34, and 35] considering calculation of heat transfer coefficient for radial heat sinks in natural convection with straight, triangular and branching fins.

All the cases above dealt with plate fins. In *forced convection*, a pure plate fin heat sink can be improved by introducing a combination of a plate fin heat sink and a pin fin heat sink. Pin fins are placed in between two parallel plate fins to increase the turbulence in the channels. According to Yu [36], the intrinsic shortcoming of plate fin heat sinks is that airflows in them are smoother than with pin fins, which act as turbulence promoters. In their example comparison case of plate-pin fin and pure plate heat sinks, thermal resistance dropped about 30 %, but the pressure drop was many times larger.

Simpler methods, such as cutting unified rectangular fins as a series of short fins in flow direction, have same kind effects. These interrupted fins enhance the heat transfer by increasing the flow mixing and thus thinning the thermal boundary layers. Teertsrta et al. [37] showed experimentally that the interrupted fins enhance the heat transfer significantly in *forced convection*. In *natural convection*, Ahmadi et al. [38] encountered similar heat transfer improvement and they also published an analytical formula, from which the optimal gap length between two fins in flow direction can be calculated.

Information supporting the optimality of the interrupted plate and pin fins has also been obtained in other studies. Ndao et al. [39] compared plate, pin and interrupted fins in *forced convection* in their multi-objective optimization study and found that when pressure drop was constrained the interrupted fins outperformed pin fins, which again outperformed plate fins with same pumping power. Another interesting way to optimize heat sinks is to use topology optimization, whereby the heat sink material is removed bit by bit according to selected criterion. In a *natural convection* study, Bornoff et al. [40] chose the criterion to be a so-called BottleNeck number, which is the dot product of heat flux and temperature gradient vectors. It was used in their CFD-based calculations to find the thermally least important parts of a heat sink during the topology

optimization process. This gradual material reduction changed the heat sink geometry significantly during the process. As a solution, they obtained a curve of thermal resistances as a function of material weight. Even the starting point was a plate fin heat sink; it quickly became some combination of uniform and interrupted plate fins. In their case, mass was reduced about 40 % without significant increase in thermal resistance. Some of the interrupted plate fins were short and resembled pin fins.

1.3   Outline of the thesis

The present thesis has the following structure: Following the introduction in Chapter 1, Chapter 2 presents the background of the governing equations of fluid flow and heat transfer, fin theory, and fin array heat transfer. Chapter 3 introduces multi-objective optimization and the optimization algorithms used. Chapter 4 focuses on the calculation model, the test cases for studying the model accuracy, and the multi-objective optimization cases. Chapter 5 reports the results of the test cases and optimizations. Chapter 6 summarizes the most important results of the work. Chapter 7 proposes future study in the field.

Chapter 2

Fin array heat transfer

This chapter deals with the general equations governing fluid flow and temperature distributions and the theory of fin array heat transfer. With aluminum heat sinks, the main heat transfer mechanisms are heat conduction and convection. Thermal radiation is ignored due to the low emissivity of aluminum surfaces. Heat conduction is caused by the temperature gradient, and heat convection is the transport of heat carried by a flowing fluid, either gas or liquid. Heat flow through a solid-fluid interface, namely convective heat transfer, is a complex combination of heat conduction and transport within a thin boundary layer close to a solid surface. It is computationally time consuming to solve the governing partial differential equations, and thus results are usually presented in a compact form using dimensionless Nusselt number correlations, which depend on geometry and surface temperature distributions. Heat conduction and convection are coupled in fin array applications and must be solved simultaneously as a conjugated heat transfer problem. [3, 41]

2.1   General equations of fluid flow

The partial differential equations that govern the general fluid flow and heat transfer phenomena are in the case of incompressible fluid given with constant thermal properties. In fin arrays, temperature and pressure variations within the fluid are small, and thus in practical engineering justify the assumption of flow incompressibility and constant thermal properties. With these assumptions, the continuity equation is

$$\nabla \cdot \mathbf{V} = 0,$$

(2.1)

where $\mathbf{V} = (u, v, w)^{\mathrm{T}}$ is the velocity vector, and u (ms^{-1}), v (ms^{-1}) and w (ms^{-1}) are its components in the x, y and z-directions, respectively. The fluid velocity distribution is governed by its momentum equations, which are presented using vector notations as

$$(\mathbf{V} \cdot \nabla)\mathbf{V} = -\frac{1}{\rho}\nabla p + \nu\nabla^2\mathbf{V} + \mathbf{g},$$

(2.2)

In the above equation, p (Pa) is the pressure, ν (m²s^{-1}) is the kinematic viscosity, ρ (kgm^{-3}) is the density and $\mathbf{g}$ (ms^{-2}) is the vector of gravitational acceleration. The temperature distribution is governed by the fluid energy equation, which for an incompressible constant property fluid is without frictional heating terms

$$\rho c_p \left(\frac{\partial T}{\partial t} + (\mathbf{V} \cdot \nabla)T\right) = k_f \nabla^2 T.$$

(2.3)

In Eq. (2.3), c_p (Jkg^{-1}K^{-1}) is the specific heat, T (K) is the temperature, t (s) is time, and k_f (Wm^{-1}K^{-1}) is the thermal conductivity of fluid. An additional useful equation for ideal gas is the equation of state

$$\frac{p}{\rho} = RT$$
(2.4)

where R (Jkg^{-1}K^{-1}) is the gas specific constant (for air = 287 Jkg^{-1}K^{-1}). In numerical modelling of the above equations (CFD), the effect of temperature on viscosity is easily taken into account by using the Sutherland viscosity law:

$$\mu = \rho v = C_1 \frac{T^{3/2}}{(T + S)}$$
(2.5)

where μ (Pas) is the dynamic viscosity, and for air $C_1 = 1.458 \times 10^{-6}$ (kgm^{-1}s^{-1}K$^{-1/2}$) and $S = 110.4$ (K).

2.2   Convective heat transfer

Convective heat transfer is a complex phenomenon, in which heat is exchanged at the fluid-solid interface between the regions. In heat sink channels, flow can be laminar or turbulent, and the surface temperature distribution can be arbitrary. Such phenomena are particularly complex, because convection and conduction occur simultaneously in the fluid. In addition, if turbulence occurs, it adds a complex momentum and energy mixing to the flow. Therefore, convective heat transfer analysis of heat sinks is often time consuming with CFD. A computationally faster way is to use convective heat transfer correlations, which are obtained either analytically from fundamental equations or from a vast number of published experimental results in the literature. These results are presented using the basic formula of convective heat transfer, so-called Newton's law of cooling, which is

$$\phi = hA_w\Delta T,$$
(2.6)

where ϕ (W) is the heat transfer rate, A_w (m^2) is the surface area of a wall, h (Wm^{-2}K^{-1}) is the convective heat transfer coefficient, and ΔT (K) is the case specific temperature difference. Newton, however, did not formulate the concept of the heat transfer coefficient [42] but merely said that heat transfer is proportional to the temperature difference between the surface and flowing air temperatures. The concept of the heat transfer coefficient was later developed by Fourier in the 1800s, and it was presented in its modern form by Nusselt in 1915 [43]. The most difficult part of convective heat transfer analysis is to evaluate the heat transfer coefficient, which is usually presented using the non-dimensional Nusselt number

$$\text{Nu} = \frac{hL}{k_f}$$
(2.7)

where L (m) is the case specific characteristic length. The Nusselt number can be a local Nu_x or a mean value Nu, which is obtained by integrating Nu_x over the heat transfer surface.

2.2.1 Forced convection in channels

Airflow in fin channels can be approximated as a 2-dimensional flow between the adjacent parallel plates. The mean Nusselt numbers for forced flow between isothermal parallel plates of length L (m) are [44, 45]

$$\text{Nu} = \frac{h d_h}{k_f} = \begin{cases} 7.55 + \dfrac{0.024(L^*)^{-1.14}}{1 + 0.0358(L^*)^{-0.64}\text{Pr}^{0.17}} & \text{for laminar flow} \\[4mm] \dfrac{\left(\frac{f}{2}\right)(\text{Re} - 1000)\text{Pr}}{1 + 12.7\left(\frac{f}{2}\right)^{\frac{1}{2}}(\text{Pr}^{2/3} - 1)}\left[1 + \left(\frac{d_h}{L}\right)^{2/3}\right] & \text{for turbulent flow} \end{cases}, \quad (2.8)$$

where the dimensionless length $L^* = L/(\text{RePr} d_h)$ (-), the Reynolds number $\text{Re} = V d_h/\nu$ (-), the Prandtl number $\text{Pr} = \mu c_p/k_f$ (-) (for air = 0.7), the mean velocity in the channel V (ms^{-1}), and the Fanning friction factor $f = \frac{\tau_s}{1/2\rho V^2}$ (-), where τ_s (Pa) is shear stress at the surface. The friction factor correlations are presented later in Chapter 4. The hydraulic diameter is defined as $d_h = 4A_{cs}/P$ (m), where A_{cs} (m^2) is the cross-sectional flow area and P (m) is the wetted perimeter of the channel cross-section. In the case of a parallel plates channel $d_h = 2d$, where d (m) is the channel width. For turbulent flow, heat transfer is nearly independent of the boundary condition, which in a practical heat sink means that the wall temperature distribution does not significantly affect the Nusselt number.

The laminar flow case, however, is highly sensitive to the wall temperature distribution. For an arbitrary surface temperature distribution, we can obtain the local heat flux in laminar flow by using the superposition principle and the step change solution of temperature for a fully developed velocity profile ($\text{Pr} \geq 1$). Graetz [46] was the first to study this problem, known as the Graetz problem. An extension to the parallel plates channel can be found e.g. in Ref. [41]. Heat flux from the parallel plates channel with an arbitrarily varying surface temperature is

$$q(x) = \frac{4k_f}{d_h}\sum_{n=0}^{\infty} G_n\left[\theta_0 e^{-2\lambda_n^2 x^*} + \int_0^{x^*} e^{-2\lambda_n^2(x^*-\xi)}\frac{\partial\theta_m(\xi_d)}{\partial\xi_d}d\xi_d\right] \quad (2.9)$$

where the eigenvalues λ_n (-) and eigen functions G_n (-) are presented in Table 1. In Eq. (2.9), $q(x)$ (Wm^{-2}) is the local heat flux, $x^* = x/(\text{RePr} d_h)$ (-) the dimensionless coordinate, ξ_d (-) the dummy integration variable, $\theta_0 = T_0 - T_w(0)$ (K) the temperature excess at $x = 0$, and $\theta_m = T_m(x) - T_w(x)$ (K) the temperature difference between local fluid mean temperature $T_m(x)$ (K) and wall temperature $T_w(x)$ (K).

Table 1. Eigenvalues and -functions for an isothermal parallel plates duct

n	λ_n	G_n
0	3.885	1.717
1	13.09	1.139
2	22.32	0.952
> 2	$\dfrac{16}{\sqrt{3}}n + \dfrac{20}{3\sqrt{3}}$	$2.68\lambda_n^{-1/3}$

The local heat flux from the wall surface to flowing air is

$$q(x) = h(x)\big(T_m(x) - T_w(x)\big) \tag{2.10}$$

The total heat transfer from a parallel plates channel is $\phi = \int_A q(x, y)\, dA$ over the whole channel heat transfer area. In turbulent flow, the heat transfer coefficient can be assumed constant $h(x) = h$ without losing accuracy in applications.

2.2.2 Natural convection between parallel plates

Elenbaas [47] was the first to experimentally study heat transfer in vertical isothermal parallel plates (see Fig. 4) in natural convection in the 1940s. From measured results, he obtained a correlation for the mean Nusselt number [48]

$$\mathrm{Nu} = \frac{hd}{k_f} = \frac{1}{24}\mathrm{El}\left[1 - \exp\left(-\frac{35}{\mathrm{El}}\right)\right]^{3/4} \quad, \quad \mathrm{El} = \frac{g\beta(T_w - T_\infty)d^3}{\nu^2}\mathrm{Pr}\frac{d}{L} \tag{2.11}$$

where El (-) is the Elenbaas number, β (K^{-1}) the thermal expansion coefficient (for gas $\beta = 1/T_\infty$), and d (m) the distance between parallel plates.
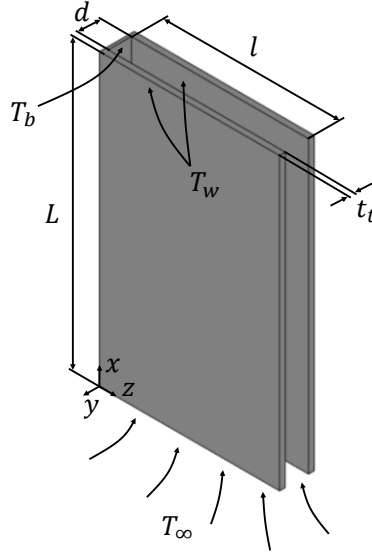
Figure 4. Single channel.

Later Bar-Cohen et. al. [29] used an approximate composite relation technique developed by Churchill and Usagi [49] to correlate the experimental data obtained by Elenbaas into an easy-to-use formula. This technique requires only two limiting asymptotic solutions to form a smooth and continuous fit for the intermediate Nusselt number values. A fully developed channel flow asymptote, d/L small, and a vertical isothermal plates asymptote, d/L large, are

$$\mathrm{Nu_a} = \frac{hd}{k_f} = \begin{cases} \dfrac{1}{24}\mathrm{El} & \text{fully developed channel flow,} & d/L \text{ small} \\ 0.59\mathrm{El}^{1/4} & \text{vertical isothermal surface,} & d/L \text{ large} \end{cases} \quad, \tag{2.12}$$

where $\mathrm{Nu_a}$ (-) is the asymptotic Nusselt number. The generalized Nusselt number relation becomes

$$\mathrm{Nu} = \left[\left(\frac{1}{24}\mathrm{El}\right)^{-n} + \left(0.59\mathrm{El}^{1/4}\right)^{-n}\right]^{-1/n} \tag{2.13}$$

where Bar-Cohen et al. [29] optimized the exponent $n \approx 2$ to fit the experimental data, and the resulting correlation is

$$\mathrm{Nu} = \frac{hd}{k_f} = \left(\frac{576}{\mathrm{El}^2} + \frac{2.873}{\sqrt{\mathrm{El}}}\right)^{-1/2} \tag{2.14}$$

The total heat transfer rate of an isothermal channel in Fig. 4 where $T_w = T_b$ is

$$\phi_i = 2hLl(T_w - T_\infty) \tag{2.15}$$

An interesting detail is that the vertical isothermal surface limit in Eq. (2.12) is not the same as that of an isothermal vertical plate, which is [50]

$$\mathrm{Nu} = \frac{hL}{k_f} = 0.68 + \frac{0.670\,\mathrm{Ra}_L^{1/4}}{\left[1 + \left(\frac{0.492}{\mathrm{Pr}}\right)^{9/16}\right]^{4/9}} \qquad \mathrm{Ra}_L = \frac{g\beta\Delta T L^3}{\nu^2}\mathrm{Pr} \le 10^9. \tag{2.16}$$

In the above equation, Ra_L (-) is the Rayleigh number, and the Nusselt number constant 0.68 takes into account conduction without convective heat transfer. This constant is usually added to the Nusselt number formula to give values at low Rayleigh numbers. Equation (2.16) gives for air (Pr = 0.7)

$$\mathrm{Nu} = 0.68 + 0.513\,\mathrm{Ra}_L^{1/4} \qquad \mathrm{Ra}_L \le 10^9, \tag{2.17}$$

where the result $0.513\,\mathrm{Ra}_L^{1/4}$ is the solution of boundary layer equations.

To compare Eqs. (2.12) and (2.17) they are first written in a slightly different way. If the characteristic length in the Nusselt number formula from Eq. (2.12) is changed the formula becomes $\mathrm{Nu} = hL/k_f = C\,\mathrm{Ra}_L^{1/4}$. The value of coefficient C from Eq. (2.12) is now C = 0.59. If Eq. (2.17) is written as $\mathrm{Nu} = hL/k_f = C\,\mathrm{Ra}_L^{1/4}$, the value of coefficient C would vary between 0.55 and 0.515 depending on the value of Ra_L. The reason for the difference between a single vertical surface channel from Eq. (2.17) and a channel flow from Eq. (2.12) is called the chimney effect. It is discussed in Chapter 4.

2.2.3 Natural convection in rectangular channels

Heat transfer from isothermal channels with shapes other than parallel plates, such as a rectangular channel in Fig. 5, can be treated with the model proposed by Aihara [51]. In a natural convection case, short fins may change the aspect ratio of the channel (defined as $\alpha = longer\ wall/shorter\ wall$) so noticeably that the parallel plates result becomes inadequate.
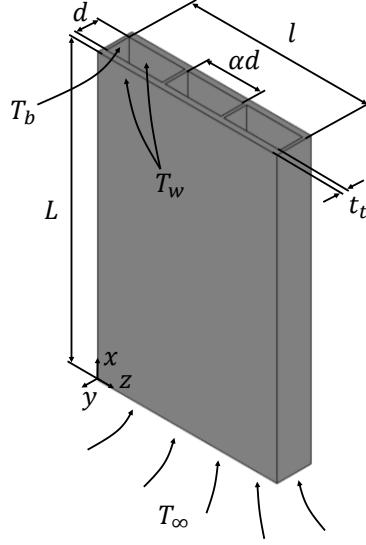
Figure 5. Natural convection heat transfer in rectangular channels.

The heat transfer rate of a single isothermal channel where $T_w = T_b$ in Aihara's method is calculated from

$$\phi = hA(T_w - T_\infty) \tag{2.18}$$

where the heat transfer area is $A = 2dL(1 + \alpha)$ (m^2), and heat transfer coefficient h (Wm^{-2}K^{-1}) is obtained from

$$h = \frac{\mathrm{Nu}_\xi k_f}{\xi} \tag{2.19}$$

where the Nusselt number correlation is

$$\mathrm{Nu}_\xi = \mathrm{Ra}_\xi \left(1 - \exp\left\{-\left(2\mathrm{Ra}_\xi\right)^{-0.75}\right\}\right) \tag{2.20}$$

The Rayleigh number is defined as

$$\mathrm{Ra}_\xi = \frac{g\beta\Delta T\xi^3}{\nu^2}\mathrm{Pr}\frac{\xi}{L} \tag{2.21}$$

and the characteristic length ξ (m) is

$$\xi = \frac{\alpha}{(1 + \alpha)(f\mathrm{Re})^{1/3}}d, \tag{2.22}$$

where $f\mathrm{Re} = 24(1 - 1.3553\alpha^{-1} + 1.9467\alpha^{-2} - 1.7012\alpha^{-3} + 0.9564\alpha^{-4} - 0.2537\alpha^{-5})$ [44].

2.3   Heat conduction in a solid

In a steady state case without volumetric heat sources the governing heat conduction equation for a base plate and fins is

$$\frac{\partial^2 T}{\partial x^2} + \frac{\partial^2 T}{\partial y^2} + \frac{\partial^2 T}{\partial z^2} = 0. \tag{2.23}$$

It can be solved analytically for fins with different cross-sections, if the heat transfer coefficient is constant everywhere. The literature [11, 52] contains results also for more complex cases, which take into account the changing fin surface temperature distribution in the calculation of the heat flux distribution.
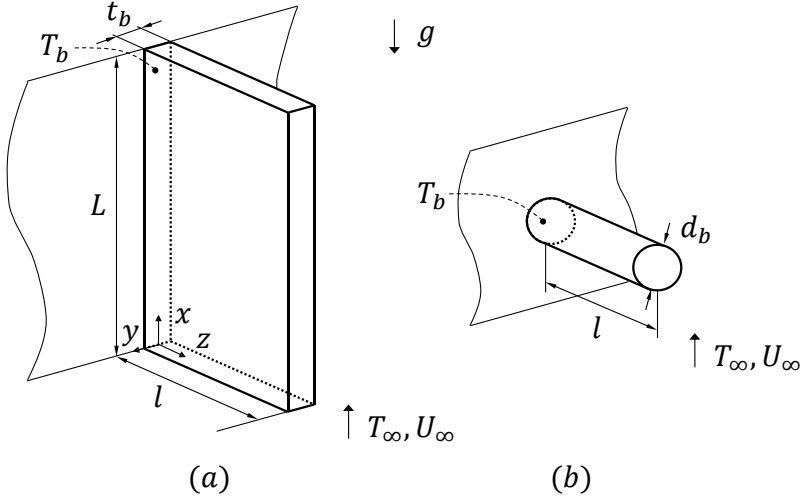

Figure 6. Schematics of a rectangular (a) and pin fin (b).

2.3.1 Single fin with an isothermal base

In Fig. 6, single fins with constant thickness ($t_b = t_t$) can be approximated as thin bodies, where the diffusion term in the fin thickness direction ($\partial^2 T/\partial y^2$) can be ignored. The temperature of the surroundings is constant $= T_\infty$ as is also the fin base temperature $= T_b$. If the surface heat transfer coefficient is also constant, $\partial^2 T/\partial x^2$ can also be ignored. After these simplifications, we have only one temperature diffusion term in Eq. (2.23). By using the temperature excess $\theta = T - T_\infty$ (K) and by assuming a constant convective heat transfer coefficient h at the fin surface, we get the classical one-dimensional fin equation for a rectangular fin in Fig. 6a

$$\frac{\partial^2 \theta}{\partial z^2} - \frac{2h}{k_s t_b}\, \theta = 0, \tag{2.24}$$

where k_s (Wm^{-1}K^{-1}) is the thermal conductivity of solid, t_b (m) the fin thickness, and h (Wm^{-2}K^{-1}) is the heat transfer coefficient. The above assumptions are, in fact, a subset of so-called Murray-Gardner assumptions [3 p. 10]. Equation (2.24) is solved when the fin tip is assumed insulated

$$\frac{\theta}{\theta_b} = \frac{\cosh\big(m_c(l-z)\big)}{\cosh(m_c l)}, \tag{2.25}$$

where $\theta_b = T_b - T_\infty$ (K) is the temperature excess at the fin base (z = 0), l (m) is the fin height, z (m) is the coordinate, and the fin constant m_c (m^{-1}) is defined in Eq. (2.26). Solution (2.25) is also valid for a pin fin in Fig. 6b, when the constant m_c of a pin fin in Eq. (2.26) is used:

$$m_c = \begin{cases} \sqrt{\dfrac{2h}{k_s t_b}} & \text{rectangular fin} \\[4mm] \sqrt{\dfrac{4h}{k_s d_b}} & \text{cylindrical pin fin} \end{cases}, \qquad (2.26)$$

Total heat transfer is obtained by integrating local heat flux over both fin surfaces, or by taking the derivative from Eq. (2.25) $\phi = k_s t_b L \, d\theta/dz|_{z=0}$. For a rectangular fin, we obtain

$$\phi = m_c k_s t_b L \tanh(m_c l)\theta_b \qquad (2.27)$$

where ϕ (W) is the fin heat transfer rate. We can present the same result using fin efficiency by comparing the heat transfer of an actual fin to an isothermal fin of equal size, where $T(z) = T_b$

$$\phi = \eta \phi_i, \qquad (2.28)$$

where η (-) is the fin efficiency and $\phi_i = 2hLl(T_b - T_\infty)$ (W) is the heat transfer rate from an isothermal fin at the fin base temperature. The fin efficiency of a rectangular fin and that of a pin fin is

$$\eta = \frac{\tanh(m_c l)}{m_c l} \qquad (2.29)$$

The fin efficiency concept in Eq. (2.29) is used also for shapes other than rectangular or pin fin. As mentioned in Ref. [3], Harper and Brown originally proposed a method, in which the fin tip area is added to the total fin height as an imaginary extension while the tip is still considered insulated. For instance, the fin efficiency of a trapezoidal fin in Fig. 7 is

$$\eta = \frac{\mu_b}{2K^2 l_e} \frac{K_1(\mu_a)I_1(\mu_b) - I_1(\mu_a)K_1(\mu_b)}{I_0(\mu_b)K_1(\mu_a) + I_1(\mu_a)K_0(\mu_b)} \qquad (2.30)$$

where extended fin height $l_e = l + t_t/2$, and I_n and K_n are the modified Bessel functions of the first and second kind, respectively. The coefficients μ_a (-) and μ_b (-) are defined as

$$\mu_a = 2K \left[\frac{t_t(1 - \tan\alpha)}{2\tan\alpha}\right]^{1/2}$$
$$\mu_b = 2K \left[l_e + \frac{t_t(1 - \tan\alpha)}{2\tan\alpha}\right]^{1/2} \qquad (2.31)$$

where $K = (h/(k_s \sin\alpha))^{1/2}$ (m$^{-1/2}$). The triangular fin is a special case of a trapezoidal fin ($t_t = 0$), and the result is

$$\eta = \frac{I_1(2m_c l)}{(m_c l)I_0(2m_c l)}, \qquad (2.32)$$

where m_c is the same as for the rectangular fin in Eq. (2.26). Next, single fin results are extended to an isothermal base fin array.
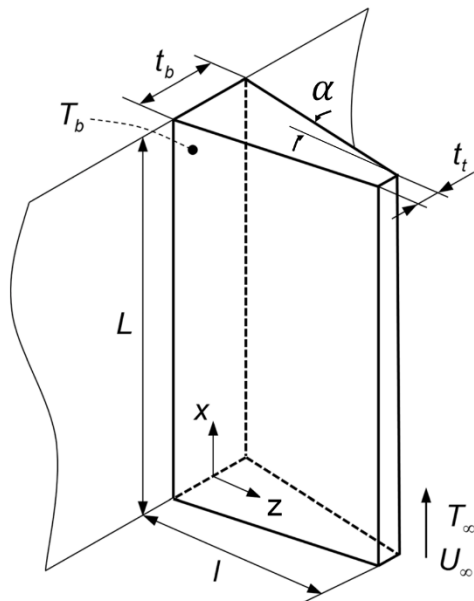

Figure 7. Schematics of trapezoidal fin.

2.3.2 Fin array with an isothermal base

To study a fin array with an isothermal base, we must first understand the performance of *an isothermal fin array*. The fin array in Fig. 8 is composed of multiple fins attached to the same base plate. In an isothermal array, both the base plate and fins are isothermal at temperature $= T_b$, and its total heat transfer can be obtained by calculating only a single fin (or channel) and multiplying the result with the number of fins.
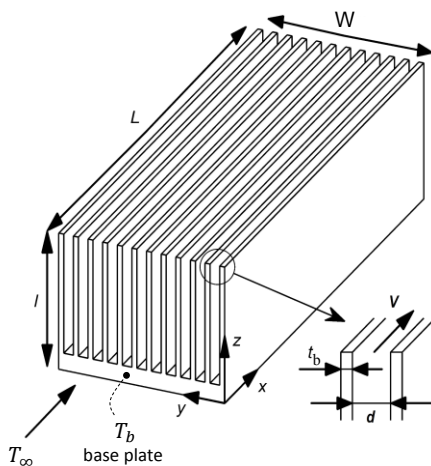
Figure 8. Forced convection heat sink with isothermal base plate.

In natural convection, calculation is straightforward because the varying mixed mean temperature is already included in the heat transfer coefficient with the result of $\phi_i = 2Llh(T_b - T_\infty)$. In forced convection, the heat transfer coefficient is expressed usually using the temperature difference between the wall and the flow mixed mean temperature, as in Eq. (2.10). The solution of a single channel heat transfer can be presented using the energy balance of flowing air

$$\phi_i = \rho V dl c_p (T_m(L) - T_\infty), \tag{2.33}$$

where $T_m(L)$ is the mixed mean temperature at the channel outlet. This temperature $T_m(L)$ can be calculated using Eq. (4.5) by substituting the length of a channel for L instead of Δx, and using the heat transfer coefficient from Eq. (2.8). Noting that $T_m(L) - T_\infty = (T_b - T_\infty) - (T_b - T_m(L))$ and combining the results above, the forced convection heat transfer from a single fin in an isothermal fin array is calculated as

$$\phi_i = \rho V dl c_p (T_b - T_\infty) \left[1 - \exp\left(-\frac{2hL}{\rho V c_p d} \right) \right] = 2Llh_{eff}(T_b - T_\infty), \tag{2.34}$$

where heat transfer coefficient h is obtained from Eq. (2.8), and h_{eff} (Wm^{-2}K^{-1}) is an effective heat transfer coefficient, which takes into account the decreasing temperature difference in the flow direction

To calculate *an isothermal base plate fin array with non-isothermal fins*, we can use the model presented by Teertstra et al. [37]. The model exploits the result for a single fin in Eq. (2.28) but modifies the heat transfer coefficient inside the fin coefficient m_c in Eq. (2.26) by employing ambient temperature as a reference temperature. In forced convection, an effective heat transfer coefficient h_{eff} (Wm^{-2}K^{-1}), must be introduced to change the reference temperature. In natural convection, the heat transfer coefficient already uses ambient temperature as a reference and $h_{eff} = h$. In forced convection, h_{eff} it is obtained from Eq. (2.34), and the result is

$$h_{eff} = \begin{cases} h & \text{nat. conv. } h \text{ from Eq. (2.11)} \\ \dfrac{\rho c_p V d}{2L}\left(1 - \exp\left(-\dfrac{2hL}{\rho c_p V d} \right) \right) & \text{forc. conv. } h \text{ from Eq. (2.8).} \end{cases} \tag{2.35}$$

The heat transfer rate from an *isothermal base plate fin array* is obtained by multiplying the result of a single fin Eq. (2.28) by the number of fins N and by using h_{eff} from Eq. (2.35) in Eq. (2.26) instead of h

$$\phi = N\eta\phi_i \tag{2.36}$$

Interesting limits in an isothermal base plate cooling with forced convection are a very short and wide channel ($L \to 0$ and $d \to \infty$), and a very long and narrow channel ($L \to \infty$ and $d \to 0$). By introducing a new variable for ratio $r = L/d$, the first case above approaches the limit $r \to 0$, and the latter $r \to \infty$. At the short and wide channel limit $r \to 0$, the flowing air mean temperature at the outlet approaches the ambient temperature, and the effective heat transfer coefficient approaches the channel heat transfer coefficient value $h_{eff} \to h$. Practically this means that the mixed mean temperature is not changing in the channel, because it is short and wide. On the other hand, the very long and narrow channel, $r \to \infty$, has the effective heat transfer coefficient

approaching $h_{eff} \rightarrow 0$. This means that the mixed mean temperature of flowing air has already heated up to its maximum value, the same as with the base plate T_b, and adding any extra length to the heat sink does not improve the overall thermal performance.

Chapter 3

Multi-objective optimization

Optimization is defined by the Merriam-Webster dictionary [53] as "*an act, process, or methodology of making something (as a design, system, or decision) as fully perfect, functional, or effective as possible; specifically: the mathematical procedures (as finding the maximum of a function) involved in this*".

The methods of single objective optimization are well known and have been used for decades as long as modern computers have been available [54]. However, many practical cases benefit from the simultaneous optimization of multiple objective functions. In the case of a fin array, e.g., optimizing only the heat transfer rate does it at the expense of pressure loss or material weight. One option in optimization is to constrain the other quantities, such as pressure loss, that the result still has practical value. The main drawback here is that it is often difficult before optimization to decide on adequate constraining limits. In multi-objective optimization, we need not decide on the constraining limits a priori, because we can obtain an infinite number of mathematically equally good compromises between all the important criteria. In the present thesis, we use multi-objective optimization as a tool to minimize heat sink material weight by minimizing their maximum temperature or outer volume simultaneously.

As a general note about practical optimization, we must remember that our calculation model is based on several assumptions and is thus approximate. In addition, evaluating the thermal properties of air at a slightly different temperature can affect the optimal geometry dimensions. The goal of practical industrial optimization cases is, therefore, to obtain an optimal geometry within limited time resources as accurately as it is reasonable with the calculation model, and to cut down any further objective function evaluations because of the diminishing return. Next, we discuss some key concepts of general optimization not given in Publications.

3.1 Background concepts

3.1.1 Multi-objective optimization problem

Multi-objective optimization (MOO) is an extension of single objective optimization (SOO). In both, the design variables, which are presented as the design variable vector $x = (x_1, x_2, ..., x_n)^T$, are subject to improvement during optimization in order to find a better design. In a typical fin array case, these design variables are the geometrical dimensions of the base plate and fins, component locations, and the number of fins. In a SOO problem, the goodness of the design is calculated with the chosen objective function $f(x)$, also known as criterion, which is evaluated for each candidate design variable vector in search for an optimum combination. In a typical fin array case, the objective function is the maximum temperature of an array, array weight, or array outer volume. The difference between SOO and MOO problems is that, instead of just one criterion in

SOO problems, MOO problems have at least two conflicting criteria, which are minimized simultaneously. The general formulation of an MOO problem is to

find $\qquad \boldsymbol{x} = (x_1, x_2, \ldots, x_n)^T \in \Omega$

where $\qquad \Omega = \{\boldsymbol{x}_l \leq \boldsymbol{x} \leq \boldsymbol{x}_u : g_i(\boldsymbol{x}) \leq 0, i = 1,2,\ldots,n_{ie}; h_j(\boldsymbol{x}) = 0, j = 1,2,\ldots,n_{ec}\}$ $\qquad$ (3.1)

to minimize $\quad \boldsymbol{f}(\boldsymbol{x}) = \big(f_1(\boldsymbol{x}), f_2(\boldsymbol{x}), \ldots, f_m(\boldsymbol{x})\big)^T$

where Ω is the feasible region, $\boldsymbol{x}_l$ and $\boldsymbol{x}_u$ are the lower and upper bound for design variable space, $\boldsymbol{g}(\boldsymbol{x})$ is a vector of inequality constraints, and $\boldsymbol{h}(\boldsymbol{x})$ is a vector of equality constraints. Because of an increased number of criteria in MOO problems, the goodness or optimality of a design variable vector $\boldsymbol{x}$ must be defined in a way different from that with SOO problems, where it was adequate to find the minimum value of only one objective function. The extension of optimality concept in MOO problems is called Pareto optimality.

3.1.2 Pareto optimality

Optimality is the most important concept of optimization, and the generalization of optimality to multiple conflicting objectives is called Pareto optimality. The term derives from the French-Italian economist Vilfredo Pareto [55], though Edgeworth [56] discussed the concept earlier in his text on economical calculus. Because not all criteria can achieve minimum values with same design variable vector $\boldsymbol{x} \in \Omega$, the result of a multi-objective optimization is a set of mathematically equally good compromises called the Pareto optimal set. The Pareto optimal solution vector is defined mathematically as follows: the design variable vector $\boldsymbol{x}^* \in \boldsymbol{\Omega}$ is Pareto optimal only if no other vector $\boldsymbol{x} \in \Omega$ exists to satisfy the conditions

$$
\begin{aligned}
&f_i(\boldsymbol{x}) \leq f_i(\boldsymbol{x}^*) \quad \text{for all } i = 1, \ldots, m \text{ and} \\
&f_i(\boldsymbol{x}) < f_i(\boldsymbol{x}^*) \quad \text{for at least one } i = 1, \ldots, m.
\end{aligned}
\qquad (3.2)
$$

An equal verbal expression is that if any criterion cannot be improved without worsening at least one other criterion, the solution is Pareto optimal. In practical heat sink optimization, e.g., if you cannot lower the maximum temperature of the heat sink without adding any extra mass, the solution is Pareto optimal, as noted in Publication IV. Fig. 9 below shows Pareto optimal solutions in a criteria space in a bold line. The design variable vector can also be weakly Pareto optimal if no other feasible vector exists that improves all the objective functions simultaneously.

3.1.3 Feasible region

The feasible region Ω, defined in Eq. (3.1), is a subset of the design variable space confined by the design variable vector bounds and constraint functions. The image of the feasible region $\boldsymbol{f} : \mathbb{R}^n \to \mathbb{R}^m$ to an objective space, shown in Fig. 9, is called the feasible objective region [57], and it is a subset of the objective space $\mathbb{R}^m$. The best compromise solutions, i.e., the Pareto optimal set, are shown at the boundary of feasible region in bold line. During multi-objective optimization, so-called Ideal and Nadir vectors are used to normalize the values of objectives to assure their equal treatment in multi-objective optimization, as discussed in Publications II and IV. Practical examples of Pareto optimal sets are shown in Chapter 5, where the objective functions f_1 and f_2 are the heat sink material weight and maximum temperature.
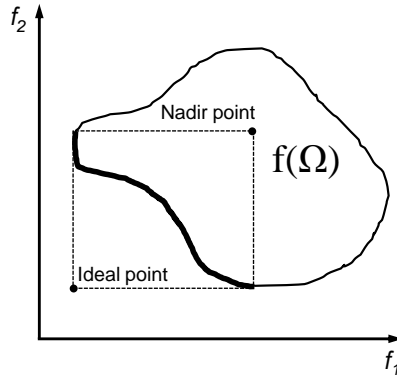
Figure 9. Pareto-optimal set shown in bold line and the feasible objective region f(Ω) in a criteria space with the Nadir and Ideal point.

3.1.4 Pareto front and dominance

In optimization, we expect to find no Pareto optimal solutions immediately at the first time steps, but only at the end. During optimization, we obtain the constantly updating Pareto front, which so far consists of best-found compromises. This Pareto front then advances during optimization towards the actual Pareto optimal set shown in Fig. 9 in bold line. The update rule for the Pareto front at every time step is to compare all solution candidates, new and pre-existing ones, against each other and remove the dominated candidates from this set. Pareto dominance is defined in objective space as [58]

vector $\boldsymbol{u} = (u_1, \ldots, u_m)^T$ is said to dominate $\boldsymbol{v} = (v_1, \ldots, v_m)^T$ if and only if

$$\forall i \in \{1, \ldots, m\}, u_i \leq v_i \land \exists i \in \{1, \ldots, m\}: u_i < v_i$$

(3.3)

which put verbally says that the vector $\boldsymbol{u}$ must be at least partially less than vector $\boldsymbol{v}$ in the criteria space to dominate it.

3.1.5 Decision maker and analyst

Multi-objective optimization results in a set of mathematically equally good compromises. However, we usually need a final solution when dealing with industrial problems. The decision maker, with some preferences, is responsible for a final solution among all the possible compromises. Usually, the decision maker is a person or a group with a better understanding of and insight into the problem than outsiders [57]. The decision maker's preferences can be taken into account, e.g., directly by weighting the objective functions and setting the constraint bounds appropriately, or after the optimization by identifying the preferable final solution from the Pareto-optimal set. Unlike the decision maker, an analyst is a person or computer program responsible for the mathematical side of the multi-objective optimization problem.

For example, in the present thesis, solutions to multi-objective optimization problems are given as Pareto optimal sets. The reader can see and judge from the figures how different Pareto optimal solutions correspond to the given objective functions but does not know the actual geometry of these solutions. The author is the decision maker who selects certain Pareto optimal solutions for

detailed presentation of their geometry in separate figures for the reader. In this case, the author's preference is to demonstrate that by optimizing different heat sinks, the material used can be significantly reduced without affecting performance. The role of the analyst is taken care of by the computer aided optimization algorithm, chosen by the author. In industry, the decision maker may have additional considerations, such as, the effect of manufacturability on the final solution.

3.1.6 External penalty function

In Publications II and IV, a constrained optimization problem can be converted to an unconstrained optimization problem by using an exterior penalty function. The evaluation of the object function $f_i(\boldsymbol{x})$ is replaced by $F_i(\boldsymbol{x})$ [59]:

$$F_i(\mathbf{x}) = \begin{cases} f_i(\mathbf{x}) & \mathbf{x} \in \Omega \\ f_{\max} + \sum_{i=1}^{n_{ie}} \max[0, g_i(\mathbf{x})] & \text{otherwise} \end{cases}. \tag{3.4}$$

In Eq. (3.4) only the inequality constraints are summed, because a common practice is to convert the equality constraints into new inequality constraints as $g_{j+n_{ie}} \equiv |h_j(\boldsymbol{x})| - \sigma \leq 0$, where σ is a small number [59]. Using the exterior penalty function allows us to treat the vectors outside the feasible region as if they were inside the region. If at least one constraint is violated, the vector is not feasible, and the evaluated value $f_i(\mathbf{x})$ is changed into a large number $f_{\max}$, to which we add the total constraint violation by summing up the values of all inequality constraints larger than zero. This constraint violation summing has the advantage that the solution gets worse if the total constraint violation gets larger. This property helps the optimization algorithm to find a direction towards the feasible area by generating the necessary gradient from the total summation of constraint violation.

3.2 Optimization methods

Multi-objective optimization can be performed with several different methods as mentioned in Publications IV and V. Traditional methods convert a multi-objective optimization problem to a single objective one. Examples of these are the weighted sum and the ε-constraint method [60, 61, and 62]. These methods are still popular today, but especially the weighted sum method has its drawbacks. It rarely produces an even distribution of Pareto optimal solutions [63] and may not find all Pareto optimal solutions unless the problem is convex [57]. However, most problems presented in the literature have a convex Pareto-optimal solutions surface [64], though exceptions are not rare (see, e.g., [65, 66]). The greatest drawback with both of the above traditional methods is that they produce only one Pareto optimal solution per one optimization run. This leads to a large number of total objective function evaluations, which in turn makes these methods computationally time consuming. The bright side is that these Pareto optimal points are usually fully optimized because of the great effort put in their finding. The ε-constraint method is used to optimize forced convection heat sinks in Publication III.

Over the past decades, more advanced methods have emerged. These are multi-objective versions of the genetic algorithm (GA) or particle swarm optimization (PSO), which can be used to find all the Pareto optimal solutions in one optimization run and compared to traditional methods, save

CPU-time in multi-objective optimization [67]. Some examples of effective multi-objective GAs are the "nondominated sorting genetic algorithm" NSGA, introduced in 1994 [68], and its popular successors NSGA-II in 2002 [67] and NSGA-III in 2014 [69].

Some comparisons between GA and PSO have been made in Aho's thesis [22], where he found that PSO appeared to perform a broader search in the design space and find the optimum with less computational effort than GA. Similar performance tests between GA and PSO was performed in [70], in which PSO also outperformed GA. In addition, PSO algorithms are usually simpler to implement. For these reasons, in this thesis, multi-objective versions of PSO algorithms were chosen to perform optimization in Publications II and IV. These algorithms generate new Pareto optimal candidates at each iteration, which are checked for Pareto dominance, and dominated vectors are sorted out from the current Pareto front. Another extra benefit is that these algorithms can deal with discrete variables with no added problems.

It must be noted that evolutionary multi-objective algorithms, such as PSO algorithms, are not guaranteed to find Pareto optimal solutions, but only a set of non-dominated solutions. Due to the partially random nature of the algorithms, they also give slightly different results in each optimization run.

3.2.1 ε-Constraint method

The ε-constraint method was introduced by Haimes et. al in 1971 [62]. In the method, one objective function $f_u(\boldsymbol{x})$ is chosen to be optimized, and all the other objectives functions $f_i(\boldsymbol{x})$ $(i \neq u)$ are treated as constraints. The multi-objective optimization problem is now an ordinary constrained single objective problem:

$$
\begin{aligned}
\text{minimize} \quad & f_u(\boldsymbol{x}) \\
\text{subject to} \quad & f_i(\boldsymbol{x}) \leq \varepsilon_i \quad \text{for all} \quad i = 1, \dots, m, \quad i \neq u \quad\quad (3.5) \\
& \boldsymbol{x} \in \Omega.
\end{aligned}
$$

With this method, one Pareto-optimal solution can be obtained at a time with all of them accessible regardless of the convexity of the problem [57]. However, the analyst must pay attention to the selection of constraint ε_i values, because improper selection can lead to a situation with no feasible solutions [71]. This method is used in Publication III to optimize forced convection heat sinks.

3.2.2 Particle Swarm Optimization

In nature, swarming of, e.g., bird flocks and fish schools, has given an evolutionary advantage for many species. In his book, Wilson [72] suggests that, theoretically at least, flocks offer protection from predators, improve feeding ability, help energy conservation, and facilitate reproduction. Kennedy and Erbhart [73] were inspired by this swarming phenomenon and sought to model flying bird flocks by using a few simple rules that each bird follows, and a real-like swarming behavior emerged. In simulating flock movements, the developers discovered accidentally that the algorithm could be used to optimize nonlinear problems. It proved to be an effective method for a variety of difficult functions. This optimization version of the algorithm was named Particle swarm optimization (PSO), later known as the standard PSO (sPSO). For

SOO problems, the algorithm itself is simple. A swarm has N members and at initialization, the swarm members occupy the feasible search space randomly

$$\boldsymbol{x}_{i,k=0} = \boldsymbol{x}_l + \boldsymbol{r}_i(\boldsymbol{x}_u - \boldsymbol{x}_l), \quad i = 1, \dots, N$$
$$V_{i,k=0} = \boldsymbol{r}_i, \quad i = 1, \dots, N,$$

(3.6)

where $\boldsymbol{x}_{i,k=0}$ is the location vector (design variable vector) for a swarm member i at the initial time step $k = 0$, $\boldsymbol{r}_i$ is a random number vector between 0 and 1, and $\boldsymbol{x}_l$ and $\boldsymbol{x}_u$ are the lower and upper bound of the design variable space, respectively. The swarm member initial velocity vector is $V_{i,k=0}$, which is set as a new random number vector $\boldsymbol{r}_i$. In the sPSO – algorithm, the velocity update rule for subsequent time steps $(k + 1)$ is

$$\boldsymbol{x}_{i,k+1} = \boldsymbol{x}_{i,k} + \boldsymbol{V}_{i,k+1}$$
$$\boldsymbol{V}_{i,k+1} = c_1\boldsymbol{r}_{i,1}\big(\text{pbests}[i] - \boldsymbol{x}_{i,k}\big) + c_2\boldsymbol{r}_{i,2}\big(\text{gbest} - \boldsymbol{x}_{i,k}\big) + c_3\boldsymbol{V}_{i,k}$$

(3.7)

where $\boldsymbol{r}_{i,1}$ and $\boldsymbol{r}_{i,2}$ are random number vectors between 0 and 1, pbests$[i]$ is the location vector of the best result found by the individual swarm member i, gbest is the location vector of the global optimum found by the whole swarm, and $\boldsymbol{V}_{i,k}$ is the velocity vector of the swarm member i at the time step k. These three components of the velocity update rule in Eq. (3.7) are known as cognitive, social, and momentum components, respectively. In the sPSO algorithm, the values of $c_1 = c_2 = 2$ and $c_3 = 1$ were used. Shi and Erbhart [74] improved this algorithm by modifying the inertia weight coefficient c_3 by proposing that its initial value be equal to 1.4, and that it be decreased during optimization run to a final value of about 0.5. The explanation for the decreasing value was that by having a changing inertia weight coefficient, the relative importance between the exploration phase of the search space and the fine-tuning phase of finding the final optimum could be adjusted during optimization run. The high value at the beginning of optimization puts more weight on the exploration of the search space, and the low value at the end focuses the search on the best candidate. Later they suggested that a constant value of about $c_3 = 0.8$ will generally work better [75]. Clerc and Kennedy suggested a formula from which optimal coefficient values can be calculated [76]. The paper is a somewhat difficult to follow, but after a careful reading, the resulting values $c_1 = c_2 = 1.4962$ and $c_3 = 0.7298$ can be obtained. These values have been used in several versions of PSO [77].

To perform a multi-objective optimization run, we need a modified version of the algorithm. The most famous multi-objective PSO, called MOPSO, was introduced by Coello Coello et. al [58], where the current Pareto front design variable vectors (non-dominated solutions) are stored in repository called REP. In the present thesis, a modified version of this algorithm was used. In optimization, the target for each swarm member i in the beginning (for example first 25 % of the time steps) is selected to be the second nearest repository point from REP measured by the Euclidian norm in the design variable space, which sets the swarm for initial exploration of design space. In later phase, the target is changed to be the nearest repository point. Details and some previous optimization cases performed with the algorithm can be found in Ref. [78]. The norm $d_{i,h}$ is calculated between each particle i and each repository point h in normalized design variable space in respect of its upper and lower bounds from

$$d_{i,h} = \sqrt{\sum_{j=1}^{n} \left[\frac{REP[h]_j - x_{i,j}}{x_{u,j} - x_{l,j}} \right]^2},$$ (3.8)

where REP is the repository of the current Pareto front. After each time step, Pareto dominance is checked, and dominated solutions are removed from the Pareto front. In Publication II, Eqs. (3.6), (3.7) and (3.8) were used (In (3.7) gbest is replaced with REP[h]) with the coefficient values $c_1 = c_2 = 2$, and $c_3 = 1.4$ in the beginning and decreasing during optimization run to 0.5.

However, in Publication IV the algorithm was updated. The idea for update was taken from the Bonyadi et al. [77] LcRiPSO algorithm. The actual target coordinates of a swarm member (pbest or repository point) are replaced by a Gaussian distributed hyper-sphere. In this modification, a swarm member i does not aim exactly at a repository point, but at a random location near it. This adds some randomness to the algorithm and, at the same time, removes some problems associated with the sPSO algorithm [77]. One problem is stagnation or dimensional stagnation, whereby particles are stuck in some dimensions without any improvement. Other problems, which this modification solves, are bad performance with small swarms, local convergence issues, and rotational variance. Rotational variance means that if we rotate a design variable space, the performance of the optimization algorithm changes. Optimization is initialized as before with Eq. (3.6), but the velocity update rule is now

$$x_{i,k+1} = x_{i,k} + V_{i,k+1}$$
$$V_{i,k+1} = c_1 r_{i,1} \left(\text{NDR} \left(\text{REP[h]}, H_k^2 (x_{i,k}, \text{REP[h]}) \right) - x_{i,k} \right)$$
$$+ c_2 r_{i,2} \left(\text{NDR} \left(\text{pbests[i]}, H_k^2 (x_{i,k}, \text{pbests[i]}) \right) - x_{i,k} \right) + c_3 V_{i,k}$$ (3.9)

where pbests[i] is the current personal Pareto optimal solution found by a swarm member. Variables $c_1 = c_2 = 1.4962$, $c_3 = 0.7289$, $r_{i,1}$, and $r_{i,2}$ are random number vectors in the range of [0, 1], and NDR(x, $\sigma^2 I$) is the normally distributed random number with mean value of x, variance σ^2, and identity matrix I. In this case, the mean value in NDR is the target (REP[h] or pbests[i]) in Eq. (3.9), and the variance is calculated for time step k using squared value of H_k function, which is defined as

$$H_k(y_k, z_k) = \begin{cases} l_t |y_{k-1} - z_{k-1}|, & \text{if } |y_k - z_k| = 0 \\ l_t |y_k - z_k|, & \text{otherwise,} \end{cases}$$ (3.10)

where $l_t = 0.4641/(N^{0.21} n^{0.58})$, N is the swarm size, and n is the number of design variables. In practice, Eq. (3.10) calculates the Euclidian distance between particle i (y_k in Eq. (3.10)) and target point (z_k in Eq. (3.10)), and multiplies the result with constant l_t, which is determined case specifically. In addition, if the current location of particle i is the same as REP[h] or pbests[i] value, the distance from previous time step k - 1 is used. The variance is, therefore, larger if the distance between the particle and the target is larger, which is the case in the exploration phase of optimization. Later, when the particles settle down and these distances get smaller, the variance also settles down and the fine-tuning phase of the optimization is performed. Details considering Eqs. (3.9) and (3.10) is presented in Ref. [77].

Chapter 4

Optimization method

This chapter introduces a method for multi-objective optimization of forced and natural convection fin arrays. The method combines a multi-objective optimization algorithm and a calculation model for a heat sink temperature field. This method can be used to find an optimal heat sink geometry with an arbitrary number of heat dissipating components, which must be maintained within a temperature limit they can withstand. A typical heat sink optimization case in industry consists of several hundred different geometry evaluations in order to find the optimum one. However, if new heat sink designs are to be optimized frequently, these evaluations must be accomplished in short time, a requirement that in practice limits the use of general purpose CFD because of its too long CPU –time consumption to evaluate one temperature field. A key part of the present method is a fast calculation model, developed to replace CFD solutions in optimization. The new model is a combination of analytical and numerical solutions, and it reduces the required CPU -time significantly. The validity of the model to give a maximum temperature value is tested with suitable test cases. Several multi-objective optimization cases are presented to demonstrate the usefulness of the calculation model as a part of multi-objective optimization.

4.1   Calculation model

The calculation model cuts down on the CPU –time needed to predict the heat sink maximum temperature at least by a factor of one thousand when compared to CFD, as mentioned in Publications IV and V. This speedup is achieved by limiting the use of full numerical 3D solution only to solid and by solving the fluid mean temperature as a system of individual 1D solutions, which are then coupled at the solid-fluid interface with convective heat transfer coefficients obtained from analytical correlations. These steps in the calculation model are the same for both forced and natural convection flows. For forced flow, a constant mean velocity value can be used, which is solved from the fan and system characteristic curves. With natural flow, coupling of velocity with the fluid temperature distribution must be taken into account. The coupling equation is obtained from the force balance between the driving buoyant force in a channel and the opposing shear stress from the channel walls. These solutions are then calculated sequentially until convergence is achieved.

4.1.1   Calculation of a solid temperature field

The heat sink temperature field requires a full 3D solution for the base plate to accurately capture the most important result, i.e., the maximum temperature of the heat sink. For fins, a 2D solution is adequate because they are thin structures with no significant temperature gradient existing in the direction of their thickness. Several methods can be used to obtain the solution, e.g., the

analytical method presented by Lehtinen [4], which solves Eq. (2.23) with truncated Fourier series. It is a computationally inexpensive method but suitable only for rectangular fins. The method used in the present thesis is the finite volume method (FVM), which is flexible for arbitrary fin cross-sectional shapes. Another principle advantage of the FVM is that global conservation is inherently part of the model, because of the integral form of conservation equation for each control volume [79 p. 72].

Heat conduction is mathematically a diffusion phenomenon. When using central difference scheme the FVM and finite difference methods give the same algebraic equations as a result. An example discretization is done in Publications I and II for an individual fin cell indexed (i,j) shown in Fig. 10.
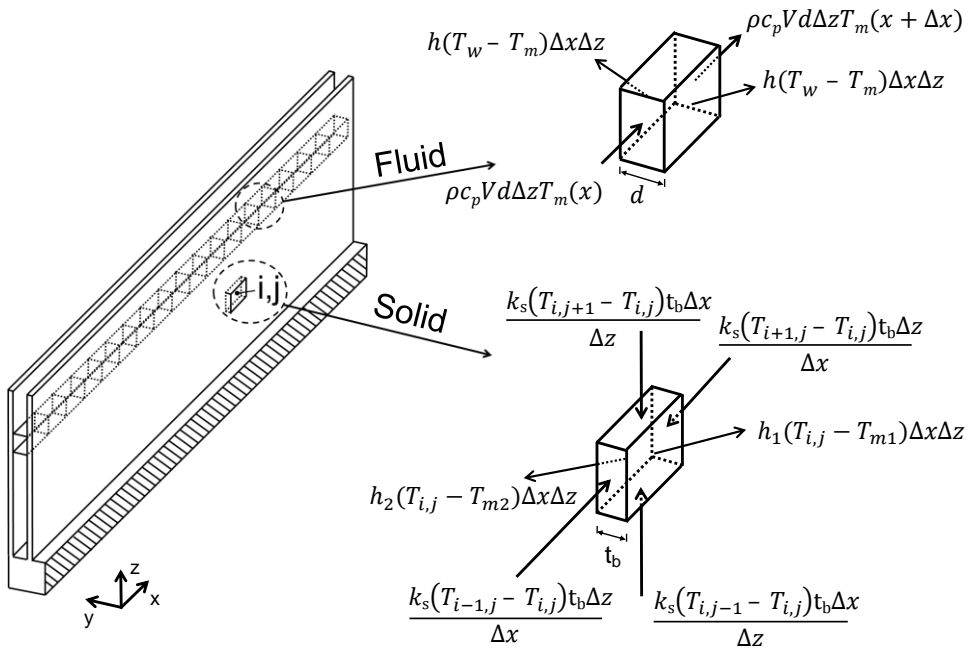
Figure 10. Discretization of single fin (Solid) and schematics of sub channel (Fluid) discretization.

The heat balance of a single discretized solid area cell from Fig. 10 is

$$
\begin{aligned}
&\frac{k_s}{\Delta z}\left(T_{i,j+1} - T_{i,j}\right)t_b\Delta x + \frac{k_s}{\Delta z}\left(T_{i,j-1} - T_{i,j}\right)t_b\Delta x + \frac{k_s}{\Delta x}\left(T_{i+1,j} - T_{i,j}\right)t_b\Delta z \\
&+ \frac{k_s}{\Delta x}\left(T_{i-1,j} - T_{i,j}\right)t_b\Delta z + h_1\left(T_{m1} - T_{i,j}\right)\Delta x\Delta z + h_2\left(T_{m2} - T_{i,j}\right)\Delta x\Delta z = 0.
\end{aligned}
\tag{4.1}
$$

Coupling of the heat flux between the local fin temperature $T_{i,j}$ (K) and the fluid mean temperatures T_{m1}, T_{m2} (K) from Fig. 10 is done with the local heat transfer coefficients h_1, h_2 (Wm^{-2}K^{-1}). Suitable heat transfer coefficients are calculated from Eq. (2.8) for a known mean

velocity by first calculating the Reynolds number and then the corresponding Nusselt number. Eq. (4.1) can then be rearranged to a standard algebraic system form

$$A_P T_{i,j} + A_N T_{i,j+1} + A_S T_{i,j-1} + A_W T_{i-1,j} + A_E T_{i+1,j} = Q_P \qquad (4.2)$$

where $A_N = A_S = k_s t_b \Delta x / \Delta z$ (WK^{-1}), $A_W = A_E = k_s t_b \Delta z / \Delta x$ (WK^{-1}), $A_P = -[2(A_N + A_W) + (h_1 + h_2)\Delta x \Delta z]$ (WK^{-1}) and $Q_P = -(h_1 T_{m1} + h_2 T_{m2})\Delta x \Delta z$ (W). Equations similar to Eq. (4.2) are obtained for each control volume inside the fins and the base plate. In the base plate, the Q_P term is the heat transfer rate from a local component, if the control volume surface touches it. Heat flux from component to base plate is assumed uniform. In the cells touching the base plate-fin interface shown in Fig. 11, the coefficients A_N and A_S in Eq. (4.2) are replaced with A_{b-f} (WK^{-1}), which takes into account the different cross-sections between the cells. From Fig. 11, the heat transfer rate ϕ (W) between cells 1 and 2 can be calculated as $\phi = A_{b-f}(T_1 - T_2)$, where

$$A_{b-f} = \frac{2k_s \Delta x}{\dfrac{\Delta z_1}{\Delta y} + \dfrac{\Delta z_2}{t_b}} \qquad (4.3)$$

Δz_1 (m) is the control volume height of the base plate, Δz_2 (m) the fin control volume height, Δy (m) the base plate control volume width, and t (m) the fin control volume thickness.
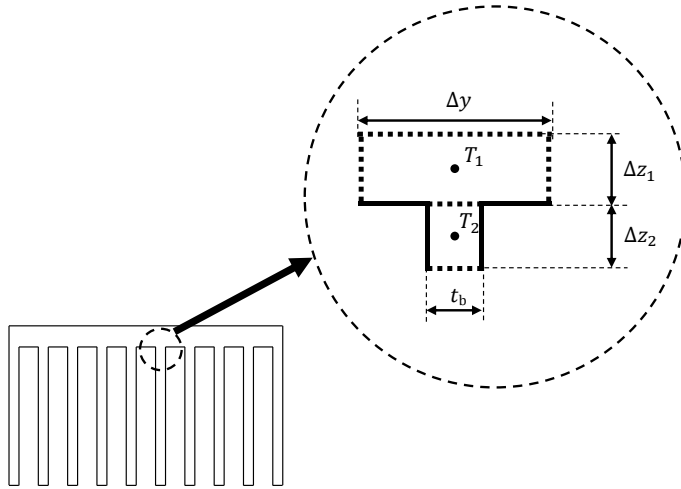

Figure 11. Interface between base plate and fin.

4.1.2 Calculation of fluid mean temperature

Using a general purpose CFD, the solution for fluid temperature and velocity distributions consumes most of the CPU calculation time because of the large number of control volumes necessary in a full heat sink calculation. In the present model, the greatest saving in CPU -time consumption is achieved by using 1D solutions for mean temperature and mean velocity distributions. Figure 10 shows one example how the calculation domain for the fluid region is discretized with the same number of control volumes as for the fins in the above solution of the solid region. For example, if fins are discretized using 30 volumes in the flow x -direction and 15

volumes in the fin height z -direction, the corresponding fluid side discretization is also 30 times 15 for every channel between two fins. This means that the control volume length Δx and height Δz are the same for both regions, and only the control volume width of the fin t is replaced with the channel width d on the fluid side, as is shown for one sub channel discretization in Fig. 10. One-dimensional solutions of forced channel flow are then applied to these control volumes. This requires a considerably smaller number of control volumes than a full 3D CFD solution, because we need to solve only the mean values of velocity and temperature.

$$2h(\mathrm{x})\mathrm{d}x(T_m(x) - T_w)$$

$$V \longrightarrow \quad \rho c_p V d T_m(x) \longrightarrow \quad \longrightarrow \rho c_p V d T_m(x) + \frac{\partial}{\partial x}\rho c_p V d T_m(x)\mathrm{d}x$$

$$T_\infty$$
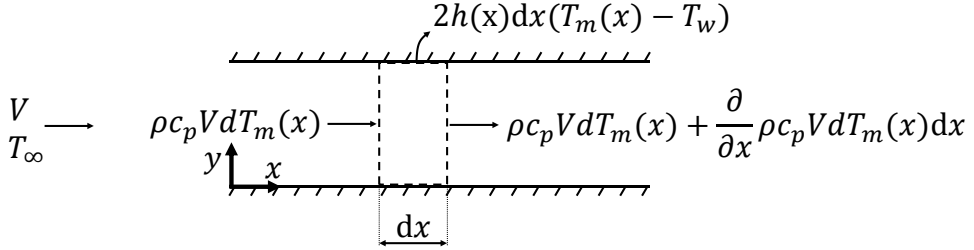
Figure 12. Heat balance in a differential element on the fluid side.

In the present model, we ignore axial heat conduction in the *x*-direction within the fluid, because in a typical heat sink the Peclet number $\mathrm{Pe} = \mathrm{RePr} \geq 100$, and in that case axial conduction is not important [80]. Another simplification is to ignore conduction and convection in air in the z-direction (see Fig. 10). In the model, fluid properties are assumed constant, and the wall temperature remains constant within one control volume. We obtain an equation for the fluid mean temperature by using the general fluid energy equation (2.3) in a steady flow situation. Because the problem is essentially one-dimensional, the governing equation can be easily derived from the heat balance in Fig. 12.

$$\rho c_p V d \frac{\partial T_m(x)}{\partial x} = 2h(x)\big(T_w - T_m(x)\big). \tag{4.4}$$

Integration of Eq. (4.4) for one control volume with a length Δx in the x-direction gives

$$\frac{T_m(x + \Delta x) - T_w}{T_m(x) - T_w} = e^{-\frac{2h\Delta x}{\rho c_p V d}}. \tag{4.5}$$

Equation (4.5) is the solution to a temperature change in a 1D-flow situation inside the control volume with a constant wall temperature (see Fig. 10). The local mean heat transfer coefficient in Eq. (4.5) is obtained from Eq. (2.8). The flow type, i.e., laminar or turbulent, is checked from the Reynolds number. In a laminar flow case, use of the isothermal wall Nusselt number from Eq. (2.8) is assumed in the calculation model, and its effect on total heat transfer is tested in Section 4.3.1. With turbulent flow, it is adequate to use isothermal Nusselt number from Eq. (2.8).

4.1.3 Calculation of fluid velocity

Mean velocity values are calculated in the same mesh as the mixed mean temperature discussed above. In the model, shear stress is ignored between air-air interfaces in the z-direction in Fig. 10, because channel walls cause virtually all the shear stress. In the case of ***forced convection*** heat sinks, where a fan creates the flow, the mean velocity V in the channels can be solved from

the operating point based on the fan and system characteristic curves. Alternatively, it can be given as a fixed value. The system characteristic curve is determined by the pressure loss equation for a channel of length L and hydraulic diameter $d_h = 2d$

$$\Delta p = \frac{1}{2} \rho V^2 \left[4f \frac{L}{d_h} + \sum_i K_i \right]. \tag{4.6}$$

In Eq. (4.6), f (-) is the Fanning friction factor presented in Eq. (4.7), and $\sum_i K_i$ (-) is the sum of minor losses, such as entrance and exit losses. The fan operating point is obtained at the intersection of the pressure drop curve in Eq. (4.6) and the fan characteristic curve. The mean friction factor for developing laminar [44] and turbulent flow between parallel plates is

$$f = \begin{cases} \dfrac{3.44(x^+)^{-0.5} + \dfrac{\frac{0.647}{4x^+} + 24 - 3.44(x^+)^{-0.5}}{1 + 0.000029(x^+)^{-2}}}{\mathrm{Re}} & \text{laminar flow} \\[2em] 0.0791 \left(\frac{2}{3} \mathrm{Re} \right)^{-0.25} & \text{turbulent flow,} \end{cases} \tag{4.7}$$

where the dimensionless length $x^+ = x/(\mathrm{Re}\, d_h)$ (-). For turbulent flow, results of a fully developed flow can be used, such as the above Blasius correlation. The hydraulic diameter is replaced with the effective diameter of $2/3 d_h$ to improve accuracy [81].

In the trapezoidal fin case, mean velocities are evaluated individually for each sub channel in the z-direction by setting the total pressure loss in the x-direction the same in each sub channel. In the case of natural convection only (see Fig. 13), we have a different mean velocity in every sub channel in the z-direction even for rectangular fins, because the mean velocity is not driven by a uniform pressure gradient but by a buoyant force. The results are presented in Publications I, II, IV and V.
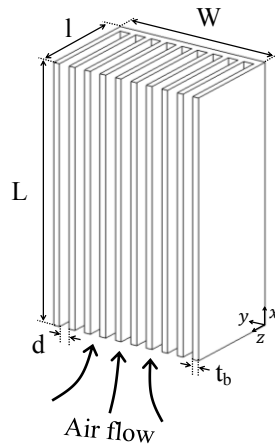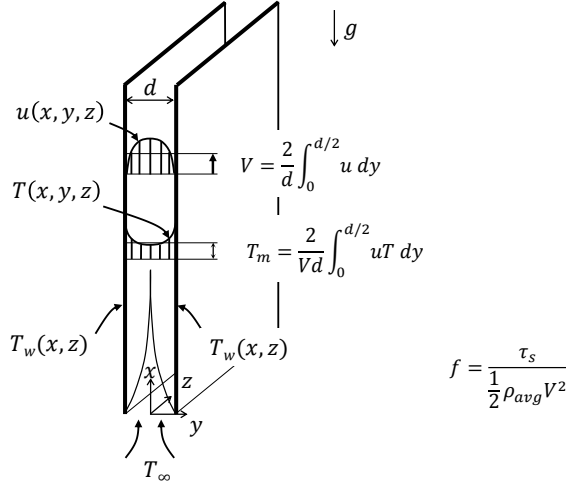

Figure 13. Natural convection fin array.

Figure 14. Velocity and temperature profiles in a channel.

In **natural convection** channel in Fig. 14, we need the mean velocity. One way to derive equation for mean velocity is to assume that the fluid average temperature in a channel creates the driving force for buoyancy, and the forced convection friction factor is used to calculate friction from the channel wall shear stress. Using the Boussinesq approximation, i.e., the density change of air is taken into account only in the channel, we get from the force balance in a channel

$$-\rho_{avg}dg - 2\tau_s + \rho_\infty dg = 0 \tag{4.8}$$

where ρ_{avg} is the average air density in a channel, calculated from the equation of state using the fluid average temperature defined in Eq. (4.10). The surface shear stress τ_s is calculated using the friction factor $f = \frac{\tau_s}{1/2\rho_{avg}V^2}$ from Eq. (4.7).

By introducing the Reynolds number $\mathrm{Re} = Vd_h/\nu$ and by combining the above equations, as is done in Publication IV, we obtain

$$V = \frac{g\beta d_h^2}{2\nu\, fRe}\left(T_{avg} - T_\infty\right), \tag{4.9}$$

where the thermal expansion coefficient $\beta = 1/T_\infty$. This is the solution to mean velocity in a 1D sub channel when the air average temperature in the channel T_{avg} (K) is

$$T_{avg} = \frac{1}{L}\int_0^L T_m\, dx. \tag{4.10}$$

The average temperature in Eq. (4.10) is integrated from the fluid mean temperature distribution in the channel, which is obtained from numerical 1D calculations. As a side note, Eq. (4.9) is also used in the literature [82] in the case of isothermal channels when T_{avg} is replaced with T_w, which is true for long channels, and also in [31] where average temperature T_{avg} is the total volume average fluid temperature of the channel in the case of constant heat flux base plate.

4.2 Accuracy of the calculation model

The presented calculation model is tested against experimental, analytical, and CFD solutions in some cases. In the model, it is assumed that the heat transfer coefficient is obtained from the Nusselt number correlations of an isothermal wall channel in forced flow, and that shear stress is calculated from the forced channel flow friction factor correlation. These assumptions are used also for natural convection, in which case it is also assumed that the buoyancy term is calculated using the average fluid temperature in a channel, and that any extra flow from the fin tip area is ignored.

Because the validity of a calculation model is the key part in multi-objective optimization, its accuracy is tested. In practice, the fins are not isothermal, and the use of an isothermal wall Nusselt number may affect the results noticeably. For some idea of accuracy, some test cases are presented in the natural convection case of linearly varying wall temperature.

In addition, the chimney effect mentioned in Chapter 2 is discussed, because the present calculation model is partly verified against the analytical Bar-Cohen solution in Eq. (2.14), where the chimney effect is present.

4.2.1 Test cases for forced convection

Analytical test case: The forced convection model is first tested in an isothermal base plate case against the analytical model presented by Teertstra [37]. The test covers 15 cases, and the total heat transfer rate ϕ (W) is compared to analytical results. The cases are shown in Table 2, and the dimensions are the same as in Fig. 8, the flow mean velocity is V and the base temperature of the fin is constant T_b.

Table 2. Geometrical and temperature values of tested isothermal base plate cases

Case number	d [mm]	t_b[mm]	l [mm]	L [mm]	T_b [K]	T_∞ [K]	V [m/s]
1	3	1	40	100	313	293	10
2	3	1	40	100	313	293	20
3	3	1	40	100	353	293	10
4	3	1	40	100	353	293	20
5	3	1	40	200	313	293	10
6	3	1	40	200	313	293	20
7	3	1	40	200	353	293	10
8	3	1	40	200	353	293	20
9	3	1	80	100	313	293	10
10	3	1	80	100	313	293	20
11	3	1	80	100	353	293	10
12	5	2	80	200	353	293	20
13	5	2	80	200	353	293	10
14	5	2	80	200	313	293	20
15	5	2	80	200	313	293	10

CFD test case: The forced convection model is also compared in Publication I with CFD results of an isothermal base plate in Fig. 8, where the base plate temperature is T_b = 373 K. The other

values are t_b = 2 mm, d = 3 mm, l = 110 mm, T_∞ = 300 K, Re = 10000. Now the fins are not isothermal. Thermal properties of air are taken at 308 K, and k_s = 200 (Wm⁻¹K⁻¹). The grid independency of the solution was checked. Details are given in Publications I and II.

Experimental test case: The experimental validation case from industry (in Publication I) is illustrated in Fig. 15. It differs from test cases above that now a heat generating component is mounted on the base plate. The component generates a constant heat transfer rate ϕ = 1200 W, and is located 50 mm from the leading edge in the x-direction. The component's length is 104 mm and its width is the same as the base plate width, W = 132 mm. The array contains 27 fins with height l = 110 mm and a base plate of thickness b = 20 mm and length L = 300 mm. Temperature was measured with thermocouples at the base plate center line, 3 mm under the surface, where the component is mounted. The volumetric airflow in the measurements was 0.16 m³s⁻¹, which produced a Reynolds number of Re = 7100 in the channels, when the inlet air temperature was T_∞ = 24 °C. In the experiments, an inverter controlled fan was used. The flowrate was measured using an IRIS - flange with an estimated accuracy of ±2 %. The fin array was inserted in a channel with equal cross-sectional area thereby blocking all bypass flow.
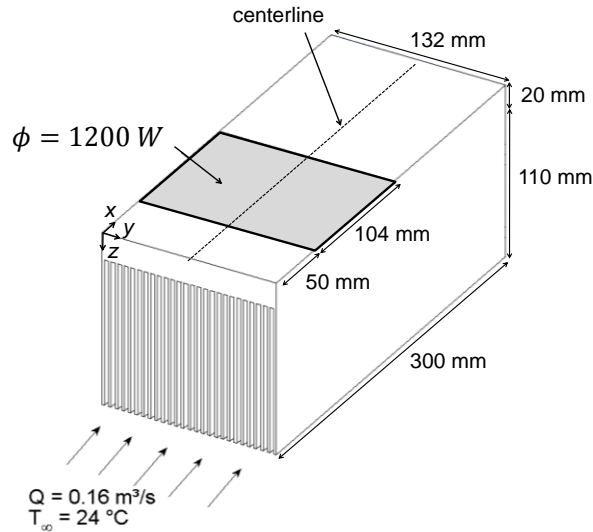

Figure 15. Schematic of experimental test case.

4.2.2 Test cases for natural convection

In the natural convection case, the model is tested in several different cases for isothermal channel, isothermal base plate, and also for full 3D heat sink.

Isothermal channel test: The isothermal channel is compared using the Bar-Cohen Eq. (2.14) and CFD in 144 different cases in Publication IV. All the variations of channel dimensions, ambient T_∞, and wall temperatures T_w appear in Table 3. CFD calculations were performed using OpenFOAM with a buoyantPimpleFoam solver for compressible flow with ideal gas law. Calculations made use of 2D laminar flow, the Sutherland viscosity law, Pr = 0.7, and a constant c_p = 1006 J/kgK.

36

Table 3. Dimensions and temperatures of tested isothermal 2D channels

Variable	Value	Unit
L	50; 100; 200; 400	mm
d	5; 7.5; 10; 15	mm
T_w	310; 320; 330	K
T_∞	280; 290; 300	K

Isothermal base plate test: These test cases were originally presented in Ref. [83]. The first test case is a single channel with isothermal fins and the second a single channel with an isothermal base plate. The fin height l was selected to be relatively large in comparison to the channel width d to ensure non-isothermal fins. In calculations, the channel width d was varied between 1 and 20 mm. Dimensions and temperatures were $L = 250$ mm, $l = 200$ mm, $T_w = 320$ K, and $T_\infty = 300$ K. In the case of an isothermal base plate, dimensions are the same, but, in addition, the fin thickness $t_b = 2$ mm and the heat conductivity of solid $k_s = 200$ Wm^{-1}K^{-1}. Calculation are compared with the results of an analytical Teertstra's model and with CFD. CFD solutions were calculated with the commercial Ansys Fluent.
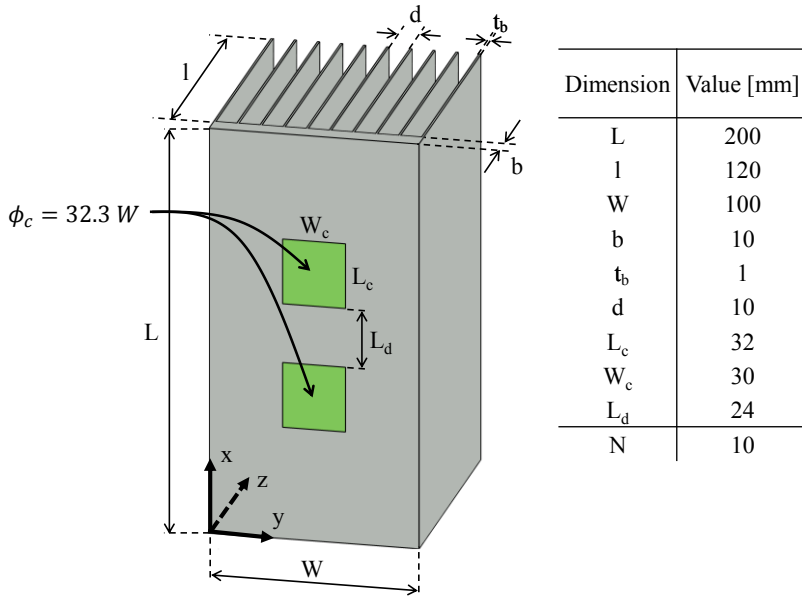

Dimension	Value [mm]
L	200
l	120
W	100
b	10
t_b	1
d	10
L_c	32
W_c	30
L_d	24
N	10

Figure 16. Reference array in full 3D test case in natural convection.

Full 3D test: A full 3D reference heat sink in Fig. 16 was calculated with the present model. The comparison solution was calculated with CFD using an OpenFOAM chtMultiRegionFoam solver, which can solve conjugated heat transfer. For a conjugated solution, fluid and solid region temperature fields must be calculated and coupled at the fluid-solid interface. In the solid region,

the mesh had about $5 \cdot 10^4$ cells and in the fluid region about 10^6 cells. The solution was laminar, and the Sutherland viscosity law in Eq. (2.5) was used. Transient approach was selected to help the solution being stable. A coupled transient solution takes a long time to achieve a steady state temperature distribution in the solid region because of the large thermal capacity of an aluminum array. Therefore, an assumption was made to use a low value of the thermal capacity ρc_p in the solid region to significantly reduce the CPU -time of CFD solution. Inspecting the transient energy equation (4.11) below

$$\rho_s c_p \frac{\partial T}{\partial t} = k_s \nabla^2 T, \qquad (4.11)$$

reveals us that the thermal capacity of solid ($\rho_s c_p$ term) does not affect to the spatial temperature distribution term $k_s \nabla^2 T$. The author decided to decrease the value of $\rho_s c_p$ by a factor of one thousand, which helped to achieve a steady state distribution of the solid region temperature field in 3 seconds in transient CFD calculations. Without a modification of the $\rho_s c_p$ value, the required time t is many orders of magnitude larger.

4.3   Special features of natural convection

Natural convection flows have special features that are absent in forced convection flows. Such features are caused by buoyancy-induced flow and the way in which natural convection arrays are installed for cooling. Because natural convection arrays are usually installed in an open space instead of tightly fitted ventilation channels of forced convection, the open space allows the flow to enter from all sides. When flow patterns are carefully studied in CFD calculations, flow has been found to come mainly from the open bottom with a small portion of it entering from the fin tip area. However, as noted in Publication V, the additional flow from the open fin tip area has only a small effect on the results, such as the maximum temperature of the array. In the calculation model, the fin tip area is thus assumed closed, and all flow is assumed to be in a vertical direction. However, the non-isothermal channel wall and the effect of parallel channels, namely the chimney effect, can affect the results.

4.3.1   Non-isothermal channels

The calculation of convective heat transfer is based on the Nusselt number correlations. In forced convection, flow is usually turbulent, and using a constant heat transfer coefficient is adequate, because the value of the coefficient is not sensitive to the boundary condition at the walls. In natural convection, where flow is usually laminar, the use of a heat transfer coefficient based on the isothermal wall correlations is only approximatively correct. In Publication IV, some tests were made to compare the use of the isothermal wall correlation Eq. (2.8). An exact solution to the arbitrarily varying wall temperature (2.9) was also used, when the wall temperature changed linearly in the flow direction $T(x) = T_0 + x/L(T_L - T_0)$, where T_0 (K) is the wall temperature at $x = 0$, and T_L at $x = L$. These tests gave some idea of the accuracy of the present model. The tested cases are shown in Table 4, and detailed solutions and results appear in Publication IV.

Table 4. Dimensions and temperature pairs of a tested non-isothermal 2D channel with the wall temperature distribution $T_w(x) = T_0 + x/L(T_L - T_0)$

Dimension	Values	Unit
L	100	mm
d	5; 10	mm
$[T_0, T_L]$	[300, 320]; [300, 350]; [320, 300]; [350, 300]	K
T_∞	280	K

4.3.2 Chimney effect

Enhancement of heat transfer in fin array channels, when compared to a single vertical surface or channel, is called the chimney effect. This means that the total heat transfer of an array is greater than heat transfer from a similar number of single channels. In addition, the total heat transfer of a single channel is also greater than heat transfer from two vertical surfaces. Heat transfer enhancement caused by the chimney effect can be more than 10 % over that of vertical surfaces. Some test cases with a varying number of channels N_{ch}, shown in Table 5, were studied numerically with CFD using OpenFOAM.

Table 5. Isothermal channel test cases for the chimney effect

L [mm]	T_s [°C]	T_∞ [°C]	d [mm]	N_{ch} [-]
100	80	20	10	1
100	80	20	10	3
100	80	20	10	5
100	80	20	10	7
100	80	20	10	9
100	80	20	10	11
100	80	20	10	13
100	80	20	10	15
100	80	20	20	1
100	80	20	20	3
100	80	20	20	5
100	80	20	20	7
100	80	20	40	1
100	80	20	80	1
100	80	20	160	1
100	80	20	∞	single surface

4.4 Heat sink optimization

A single heat sink can be modeled efficiently with sophisticated models, such as CFD. However, when performing an optimization, which requires hundreds or thousands of different geometries to be evaluated using an optimization algorithm, CFD becomes too time consuming. A solution proposed here is to combine the presented new calculation model with a state-of-the-art multi-objective optimization algorithm to form an effective optimization method for practical industrial heat sinks. An example of saving CPU -time is the optimization case in Section 4.4.3 below, which required thousands of temperature field evaluations, but took only about two hours to

perform it with a new method running on a laptop (Intel i-7-3520M @ 2.90 GHz processor with 8 GB of RAM). Two hours is also approximately the minimum required CPU -time for a single CFD case calculation of natural convection cooling with the same computer (saving of CPU - time is discussed more in Publications IV and V). The optimization cases discussed here were first presented in Publications II, III, IV, and V. Some additional information is given below.

4.4.1   Forced convection case I

A multi-objective optimization case in Publication II is optimized with a slightly modified MOPSO algorithm in Section 3.2.2. The reference array shown in Fig. 17 consists of two 100x100 mm² components with heat dissipation rates of 550 and 450 W. In optimization, components are clustered together in in-line arrangement with a 50 mm distance between them. The component cluster is shown in a dashed line in Fig. 18 below. In optimization, this component cluster is treated as one entity composed of two components. It generates two new design variables for optimization, its locations X and Y. The velocity boundary condition was given using a fan curve $\Delta p = -1000Q + 400$ (Pa), where Q (m³s⁻¹) is the volumetric flow. Optimization was performed for the rectangular and triangular fins separately. This multi-objective optimization problem is written formally as (See Eq. (3.1))

find $\qquad \boldsymbol{x} = (L, W, b, N, t_b, t_t, l, X, Y)^T \in \Omega$

to minimize $\qquad \boldsymbol{f}(\boldsymbol{x}) = \big(m(\boldsymbol{x}), T_{max}(\boldsymbol{x})\big)^T$

subject to

$\Omega = \{\boldsymbol{x} \in \mathbb{R}^9 \mid \boldsymbol{x}_l \leq \boldsymbol{x} \leq \boldsymbol{x}_u \ ; \ g_i(\boldsymbol{x}) \leq 0, i = 1,2,\dots,7\}$

$\boldsymbol{x}_l = \big(L_{min}, W_{min}, b_{min}, N_{min}, t_{b\,min}, t_{t\,min}, l_{min}, X_{min}, Y_{min}\big)^T$

$\boldsymbol{x}_u = \big(L_{max}, W_{max}, b_{max}, N_{max}, t_{b\,max}, t_{t\,max}, l_{max}, L_{max} - L_C, W_{max} - W_c\big)^T$

$g_1 = LWb\rho_s + NLl\rho_s \dfrac{t_b + t_t}{2} - m_{max} \leq 0$

$g_2 = -\left(LWb\rho_s + NLl\rho_s \dfrac{t_b + t_t}{2} - m_{min}\right) \leq 0$

$g_3 = b + l - l_{max} \leq 0$

$g_4 = d_{min} - \dfrac{W - Nt_b}{N - 1} \leq 0$

$g_5 = d_{min} - \dfrac{W - Nt_t}{N - 1} \leq 0$

$g_6 = X + L_C - L \leq 0$

$g_7 = Y + W_C - W \leq 0$

with dimensions shown in Figs. 17 and 18. The used solid density $\rho_s = 2700$ kgm⁻³. The inequality constraints g_i, where i = 1,…,7 are expressed in words in Table 6 below. The reference was originally presented in Lehtinen's thesis [4] except that the distance between the components was 60 mm and the thickness of fins was 1 mm. Moreover, in the original case, the Reynolds number was held constant, 2000, and the flow was laminar.
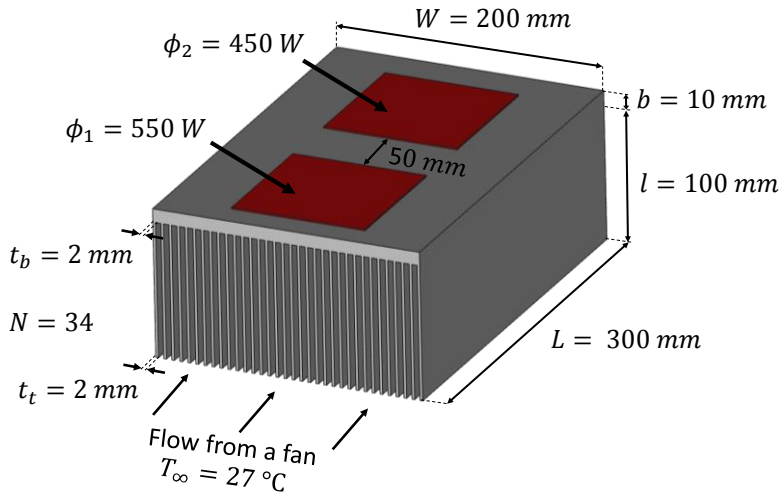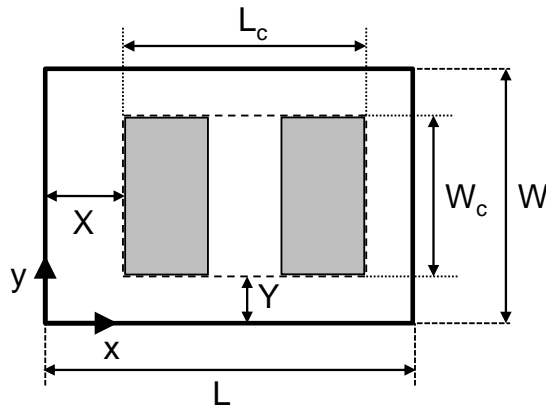
Figure 17. Reference geometry in optimization.

Figure 18. Location of component cluster on the base plate.

Table 6. Inequality constraints

Inequality constraint	Expression in words
g_1	heat sink mass m $\leq$ m$_{max}$
g_2	heat sink mass m $\geq$ m$_{min}$
g_3	heat sink total height $\leq$ l$_{max}$
g_4 and g_5	distance between adjacent fin surfaces $\geq$ d$_{min}$ at every z-location
g_6	component cluster must be located on the base plate in x-direction
g_7	component cluster must be located on the base plate in y-direction

4.4.2 Forced convection case II

This multi-objective optimization case and its results are presented in detail in Publication III. The reference array, an existing industrial heat sink, is shown in Fig. 19, and the details of nine components are given in Table 7. In optimization, the Reynolds number was fixed to a value of 3300, and the flow was turbulent.

Table 7. Component details

Component	Size (mm²)	Heat dissipation (W)
1-3	94×48	450
4-6	93×20	150
7-8	29×69	15
9	34×94	0
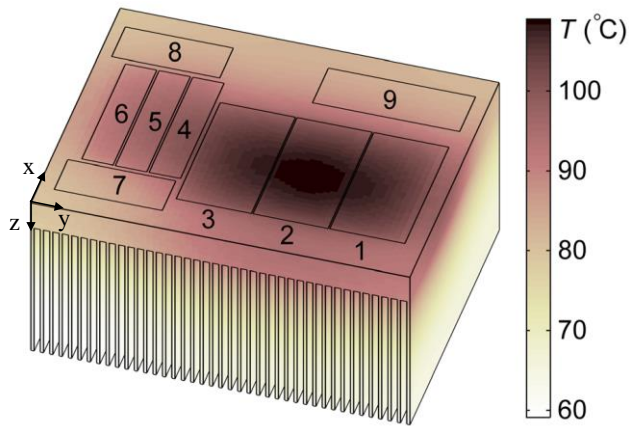
Figure 19. Reference array (m = 6.65 kg).

The resulting temperature field in Fig. 19 for the reference case was calculated using two different calculation models. The model in this thesis gave the heat sink a maximum temperature of 109.6 °C. The other method was that of Lehtinen [4], presented also briefly in Publication III. With Lehtinen's method, the maximum temperature was 109.1 °C. A different numbers of discretized control volumes in calculations and pressure loss evaluation probably caused this small difference between the models. As mentioned in Publication III, the multi-objective optimization was performed with a Matlab's fmincon algorithm and the ε-constraint method presented in Section 3.2.1. The multi-objective optimization problem is (see Eq. (3.1))

find $\qquad \boldsymbol{x} = (N, V, d, L, b, t_b, t_t, l, d_{LE})^T \in \boldsymbol{\Omega}$

to minimize $\qquad \boldsymbol{f(x)} = \big(m(\boldsymbol{x}), T_{max}(\boldsymbol{x})\big)^T$

subject to

$P = 6\ W$

$Re = 3300$

$W = 242\ mm$

$d_{LE} + 156\ mm \le L$

$156\ mm \le L \le 220\ mm$

$1.5\ mm \le t_b \le 3\ mm$

$0.3\ mm \le t_b \le 3\ mm$

$6\ mm \le b \le 26\ mm$

$4\ mm \le d_{LE} \le 45\ mm$

$N \in [38, 39, \dots, 55]$

The case was optimized for each fin number N between 38 and 55. In the ε-constraint method, the mass was kept as constraint, and T_{max} was subjected to optimization because mass can be calculated relatively quickly, and if its constraint is violated, no evaluation for T_{max} need to be performed. By using $Re = 3300 = V2d/\nu$, $P = 6 = (N-1)ldV\Delta p$, $\Delta p = 0.5\rho V^2 \left[K_{in} + \frac{4fL}{2d} + K_{out} \right]$, and $d = (W - Nt_b)/(N-1)$, we can eliminate almost half the design variables. In the rectangular fin heat sink case, the remaining design variables in optimization are L, b, t_b, d_{LE} and in the trapezoidal fin case additionally fin thickness at its tip t_t (see Fig. 7). The total number of function evaluations is large with this approach, and optimization consumed considerably more CPU-time in this optimization case when compared with other optimization cases presented in this thesis.

4.4.3 Natural convection case III

In Publication IV, the natural convection heat sink in Fig. 16 was optimized with the multi-objective optimization algorithm "updated MOPSO", mentioned in Section 3.2.2. Here the components were not treated as a component cluster, as in Fig. 18, but as independent heat sources capable of moving individually. Each component generates two additional design variables, which are the coordinates in the x- and y-direction. They also create an extra constraint, because two components are not allowed to occupy the same space. The optimization problem of the case in Publication IV is defined as

find $\qquad \boldsymbol{x} = (L, W, b, l, t, N, \boldsymbol{X_c}, \boldsymbol{Y_c})^T \in \boldsymbol{\Omega}$

to minimize $\qquad \boldsymbol{f(x)} = \big(m(\boldsymbol{x}), T_{max}(\boldsymbol{x})\big)^T$

subject to

$g_1 = b + l - l_{max} \le 0$

$g_2 = d_{min} - \dfrac{W - Nt_b}{N-1} \le 0$

In addition, a constraint was used for overlapping components based on the calculation of the overlapping areas. If overlapping areas exists, the constraint is violated. In this optimization case,

the reference array, shown in Fig. 16, is the same as was used in the testing of natural convection calculation model in Section 4.2.2.

4.5   Developed software

The method to optimize forced convection heat sinks with the presented calculation model is implemented as standalone software for commercial use. Implementation is done using Matlab, because it enables the use of fast linear algebra matrix calculation operations based on the FORTRAN lapack libraries [84]. In the software, the user first fills the heat sink dimensions, component locations, heat dissipation rates, and the fan curve for volumetric flow in the GUI. The software then calculates the temperature field of the heat sink based on these values. The user can also optimize the heat sink for a given set of heat dissipating components by choosing the optimization module in the software. In the optimization module, user gives the upper and lower bound values for different design variables and constraining limit values for minimum channel width, heat sink maximum height, and heat sink mass. The software then performs multi-objective optimization of the heat sink using the maximum temperature and heat sink mass as optimization criteria. The optimization algorithm is the MOPSO algorithm described in this thesis. Optimization is generally complete in a couple of hours and the user can see the results on the screen.

4.6   Summary of the method

The developed multi-objective optimization method for forced and natural convection heat sinks is summarized in Fig. 20. The method consists of a calculation model for a heat sink and a multi-objective optimization algorithm. The calculation model is composed of a numerical finite volume solution of solid and fluid temperature fields and an analytical solution of convective heat transfer coefficients and friction factors for channel flow. These equations are written in a linear system in matrix notation and solved using MATLAB implementation. The calculation model was first applied to a forced convection heat sink in Publication I. Later, the calculation model was expanded to a natural convection case in Publication IV. The model was tested with experimental and CFD results, which are shown in Publications I, II and IV. Forced convection results were also compared to those obtained by Lehtinen's method [4, 21] in Publication III.
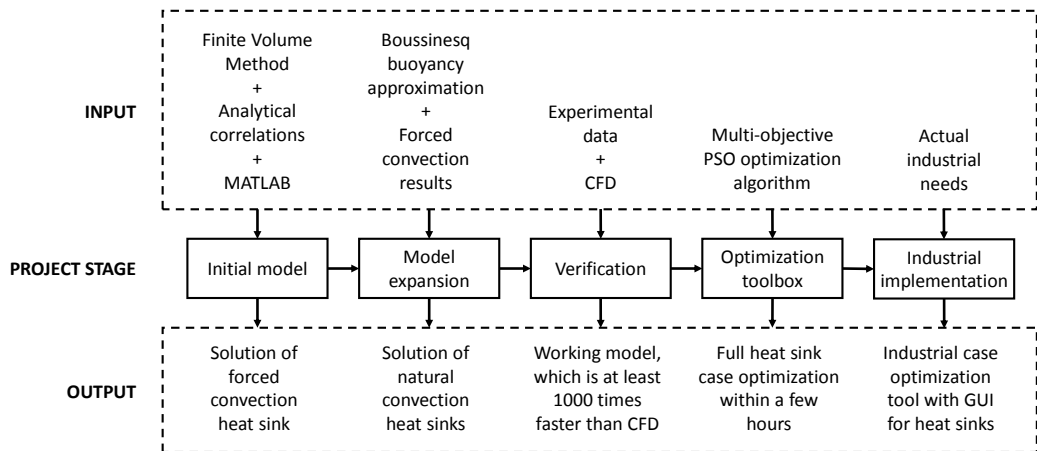
Figure 20. Overview of method.

According to the test cases, the calculation model worked within engineering accuracy, and it is well suited for calculating the heat sink temperature field in optimization. The main advantage of the present calculation model is its relatively fast calculation time over CFD. As pointed out in Publications IV and V, savings in CPU -time are many orders of magnitude over CFD solutions. Multi-objective optimization has been performed with different algorithms, as discussed in Publications II, III, and IV. Furthermore, the method is implemented as standalone software for use in an industrial predesign process.

Chapter 5

Results and discussion

This Chapter compares the results on the test cases in Chapter 4 with the experimental, analytical, or numerically calculated CFD results in 2D and 3D cases. These tests were run because the accuracy of the calculation model constitutes the essential part of heat sink optimization. After its accuracy is tested, the model is used in multi-objective optimization of test cases presented in Chapter 4. All these results have been reported in Publications I, II, III, IV and V, but some additional results on the chimney effect are given here.

5.1 Accuracy of the calculation model

The accuracy of the calculation model is tested in cases of forced and natural convection, all of them originally reported in Publications I, II, IV, and V. Chapter 4 summarized the tested geometries and details, and the key results are given below.

5.1.1 Forced convection tests

Analytical test case: The first test case is an isothermal base plate heat sink cooled by forced convection. This is the simplest test case of fin array heat transfer, because its mean flow velocity is fixed and the base plate remains at a constant temperature. Results of the calculation model are compared with analytical results obtained with the model presented by Teertstra, described in Section 2.3.2. The dimensions and temperatures of the tested cases are given in Table 2. Results on comparison of calculations are shown in Table 8, testifying to an excellent agreement. The greatest deviation is less than 1.2 % with most of them within 0.5 % as shown in Table 8, where the present calculation model results are shown with ϕ_m and those of the Teertstra model with ϕ_T.

CFD test case: One CFD test case with isothermal base plate was also compared with CFD in Publication I (see Section 4.2.1). The flow mixed mean temperature and the pressure loss in the channels were the main items compared and results of them are given in Table 9 below. These results differ slightly from those in Publication I, because now a somewhat more accurate temperature integration was used. In Table 9, the result on the mean temperature difference of air is about 5 % and that on pressure loss about 8 % between the calculation model and CFD. Additional result was also calculated with the Teertstra analytical model, which gave $\Delta T = 18.52$ K, to confirm that they all are approximately similar. CFD result was calculated using the k-ε model with enhanced wall functions with Ansys Fluent. If k-ω SST had been used as a turbulence model, the CFD result may have been slightly different and probably closer to analytical results.

Table 8. Heat transfer results of test cases from Table 2, present calculation model (ϕ_m), and the Teertstra model (ϕ_T).

Case number	ϕ_m [W]	ϕ_T [W]	difference [%]
1	7.51	7.52	-0.17
2	12.00	12.01	-0.08
3	22.21	22.34	-0.58
4	35.71	35.86	-0.41
5	12.60	12.60	0.024
6	20.75	20.72	0.14
7	36.86	37.28	-1.13
8	61.37	61.78	-0.67
9	9.56	9.57	-0.09
10	13.55	13.58	-0.18
11	28.50	29.59	-0.3
12	102.44	102.76	-0.31
13	69.65	69.96	-0.44
14	34.32	34.35	-0.08
15	23.43	23.45	-0.08

Table 9. Mean temperature difference $\Delta T = T_m(L)$ - T_∞, and pressure loss of a heat sink in CFD test case.

Quantity	CFD	Calculation model	Teertstra model
ΔT [K]	19.96	18.92	18.52
Δp [Pa]	1099	1013	-

Experimental test case: An experimental heat sink was also presented in Publication I with a component dissipating 1200 W. The component is mounted on a 20 mm thick base plate 50 mm from the leading edge of the heat sink. Experimental results are obtained by measuring seven spatial temperatures with thermocouples in the base plate centerline, 3 mm under the surface. The calculated temperature distribution is shown in Fig. 21 and its comparison with experiments in Fig. 22.
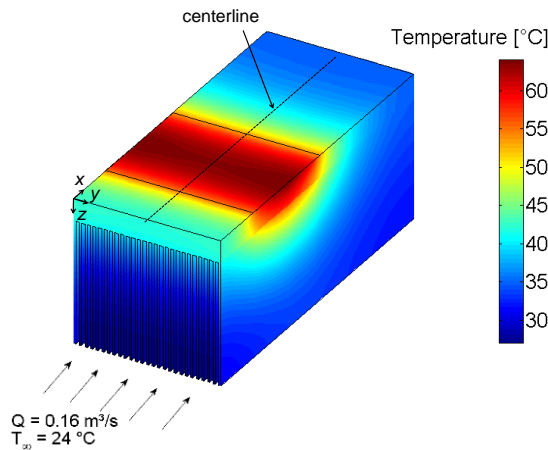
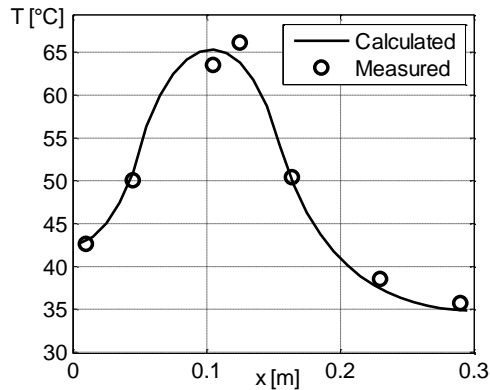
Figure 21. Calculated temperature distribution.

Figure 22. Centerline temperature distribution, 3 mm under surface in Fig. 21.

The calculated temperature distribution on the centerline in Fig. 22 agrees reasonably well with measurements. The difference at one point may be a measurement error. However, the pressure loss calculation differed from the measured data. The measured value was 435 Pa, but calculation gave a value of 501 Pa, probably because velocity was not uniformly distributed before the test section.

Concluding forced convection tests: Based on the above test results, we can conclude that the calculation model is in good agreement in all cases tested in forced convection cooling, especially in the isothermal base plate tests. This is not surprising, since the Gnielinski Nusselt number correlation in Eq. (2.8) for convective heat transfer is very accurate in the channel flow, as is the numerical finite volume solution for heat conduction in the solid. The largest uncertainty in the industrial forced convection calculations with the fan curve is probably due to the uncertainty taking into account the laminar / turbulent transition point of the flow in low Reynolds numbers, and the prediction of the pressure loss to solve accurately the fan operating point from the characteristic curves of the fan and the system.

5.1.2 Natural convection tests

Isothermal channel test: The present model was tested in the case of isothermal 2D channels with CFD and the Bar-Cohen correlation Eq. (2.14). The combinations for calculations are given in Table 3 with only some results shown in Fig. 23.
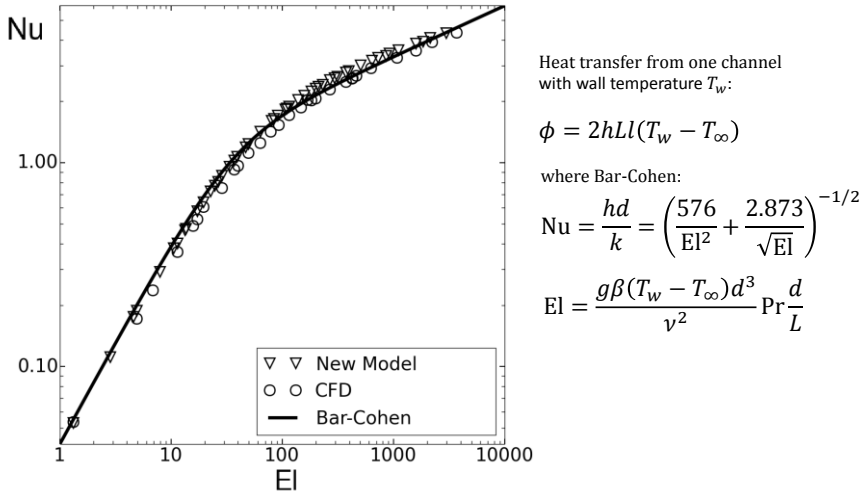
Heat transfer from one channel
with wall temperature T_w:

$$\phi = 2hLl(T_w - T_\infty)$$

where Bar-Cohen:

$$\text{Nu} = \frac{hd}{k} = \left(\frac{576}{\text{El}^2} + \frac{2.873}{\sqrt{\text{El}}}\right)^{-1/2}$$

$$\text{El} = \frac{g\beta(T_w - T_\infty)d^3}{v^2}\text{Pr}\frac{d}{L}$$

Figure 23. Results of different methods in isothermal 2D channel.

The results between the calculation model, CFD, and the Bar-Cohen equation are in good agreement as a function of the Elenbaas number. An interesting finding is that in each case the results obtained with CFD gave slightly lower Nusselt number values.

Isothermal base plate case: Comparison is made between the results of the new calculation model, CFD, and the results obtained with the Bar-Cohen and Teertstra models in Chapter 2. These results were originally published in [83]. The heat transfer rate ϕ is shown in Fig. 24 as divided by the channel width d. We can see that the results of different models agree well in the isothermal channel (Case 1 in Fig. 24) as well as in the isothermal base plate case (Case 2 in Fig. 24). We can observe that if L and l are fixed, the optimal channel width d to maximize the heat transfer of a fin array is about 10 mm and 9 mm in the isothermal channel and the base plate case, respectively.
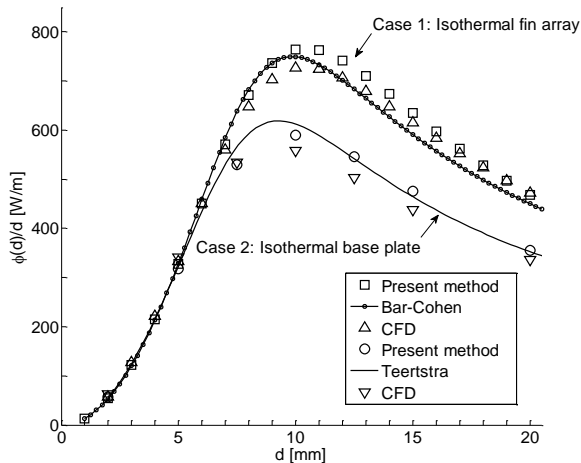
Figure 24. Results of different methods when $L = 0.25$ m, $l = 0.2$ m, $T_b = 320$ K, and $T_\infty = 300$ K, $t_b = 2$ mm and $k_s = 200$ W/mK.

Full 3D case: The model was tested also in a practical 3D case with two heat dissipating components. The test case is discussed in Section 4.2.2 in Fig. 16, and the results are shown in Fig. 25. The results of the 3D heat sink agree well in Fig. 25, and the maximum and minimum temperature excess is given in Table 10.
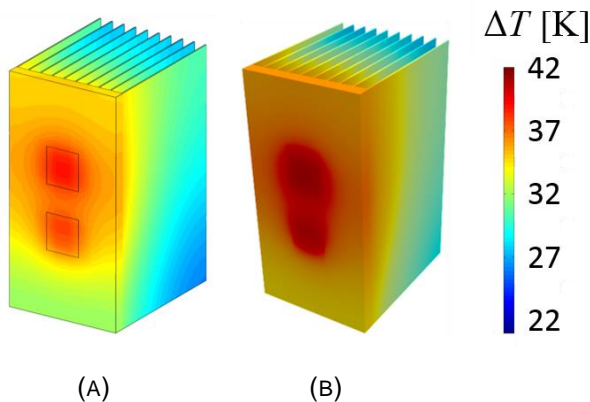

Figure 25. Temperature fields calculated with the new model (A) and CFD (B).

Table 10. Minimum and maximum temperature difference $\Delta T = T_w - T_\infty$ in Fig. 25

	CFD	Model	Difference
ΔT_{min}	23.5	21.4	-8.9 %
ΔT_{max}	41.7	38.9	-6.7 %

Concluding natural convection tests: The above analytical equations, which were used in comparison, are based on experimental results, and all CFD results were for laminar flow, where no turbulence model is used. This means that these comparison results are generally of high quality and can be used for comparison with confidence. Later, CFD results, which were also tested with these 2D solutions, were used for comparison in full 3D cases. From the overall results presented in this Section, we can conclude that in isothermal 2D channels, non-isothermal 3D channels and full 3D cases, the calculation model works well. These tests were important, because the natural convection model included several assumptions discussed in Chapter 4. Interesting side note is that the results obtained for the heat transfer rate with the present calculation model tend to be slightly higher in all cases compared to those obtained with CFD.

5.1.3 Discussion about model accuracy

The difference between the results obtained with the calculation model and the comparison results obtained by analytical solutions, CFD or experimental results, were less than 10 % in each case tested. This is a good result, because often heat transfer correlations include uncertainty in the same order of magnitude. As a tool in industrial optimization, this accuracy is sufficient because typically in heat sink case optimization a plenty of room for improvement exists. If only minor improvements (less than 10 %) were available, the accuracy of the model should be improved. However, in practice, the potential for improvement is of the order of 50 %, for which the current accuracy is sufficient.

5.2 Tests of special features in natural convection

5.2.1 Non-isothermal wall effect

The calculation model uses the Nusselt number correlation of an isothermal wall, which is a good approximation in forced convection cooling, where the flow is mainly turbulent. However, in natural convection, the flow is usually laminar, and the temperature distribution on the wall affects the heat transfer coefficient. In Publication IV, a test was carried out in which the temperature on the channel walls varied linearly in the flow direction. Different test combinations are given in Table 4 and heat transfer results in Table 11. The channel wall temperature distribution is $T(x) = T_0 + x/L \times (T_L - T_0)$.

We can generally conclude from the results in Table 11 that the model works quite well in the case of an increasing wall temperature ($\nearrow$). This is the case in a typical cooling array, because the cooling air flows in at the bottom of the array, and because the heat dissipating components cause the wall temperature to increase in the flow direction. In the case of a decreasing wall temperature ($\searrow$), the model is not so accurate. In that case, using the superposition principle in Eq. (2.9), which takes into account the varying surface temperature, improves results, as can be seen in Table 11.

Overall, the results obtained with the superposition principle were better than with the isothermal correlation, as shown in Publication IV. However, in the case of an increasing wall temperature, the results of the current model were acceptable.

Table 11. Heat transfer of different channels with varying wall temperature from Table 4; $T_\infty = 280$ K, ϕ'_p solutions of the new model, ϕ'_{CFD} with CFD, and ϕ'_{sp} based on Eq. (2.9). (Increasing wall temperature ($\nearrow$), decreasing wall temperature ($\searrow$))

L	d	T_0	T_L	$T(x)$	ϕ'_{CFD}	ϕ'_p	difference	ϕ'_{sp}	difference
[mm]	[mm]	[K]	[K]	change	[W/m]	[W/m]	to CFD [%]	[W/m]	to CFD [%]
100	5	300	320	$\nearrow$	22.7	23.3	2.7	23.5	3.8
100	5	300	350	$\nearrow$	46.2	47.6	3.0	48.7	5.4
100	5	320	300	$\searrow$	14.6	15.9	9.0	15.5	5.9
100	5	350	300	$\searrow$	23.4	27.5	17.7	25.8	10.5
100	10	300	320	$\nearrow$	42.8	41.9	-2.2	43.5	1.5
100	10	300	350	$\nearrow$	74.4	68.7	-7.7	74.5	0.2
100	10	320	300	$\searrow$	36.6	42.1	14.9	37.9	3.6
100	10	350	300	$\searrow$	58.1	71.5	23.2	60.2	3.7

5.2.2 Chimney effect

An isothermal vertical channel can be solved analytically in two limiting cases, if we have a long and narrow or a very short and wide channel. The solution of a wide isothermal channel should be the same as that of vertical isothermal surfaces $Nu \approx 0.52 \, Ra^{1/4}$. However, the coefficient 0.52 does not correlate well with experimental data in channels. For example in the Bar-Cohen Eq. (2.14), the asymptote of an isothermal wide channel was selected as $Nu = 0.59 \, Ra_L^{1/4}$, which correlates better with data obtained by Elenbaas [30]. This enhancement of heat transfer is called the chimney effect.

For example, Raithby and Hollands mention the chimney effect [85], that a channel has higher heat transfer than isolated plate, and quote Miyatake and Fuijii [86] as having claimed *"because the chimney effect is important, even at large spacing"*. In analytical solution, the asymptotic value of the coefficient C in the Nusselt number $\mathrm{Nu} = C\mathrm{Ra}_L^{1/4}$ is $C = 0.55$ [85]. However, Raithby and Hollands discovered that Elenbaas experimental data fits better when the value of C is about 0.60. Different research groups have fitted the same coefficient. For instance, Miyatake and Fuijii discovered that the constant C should be 0.613. Martin et al. [82] proposed $C = 0.62$, which correlates best with the data of Augn [87].

The CFD calculations in the present thesis give the coefficient C a value of 0.528 for a single vertical surface and variations between 0.53 … 0.65 for channels. Solutions are shown in detail in Table 12. Heat transfer is likely to increase for two reasons. First, in a single vertical surface case, the surrounding air is stagnant, but in the case of a channel, the centerline velocity is not zero. This lower velocity gradient decreases shear stress and allows the mean velocity to increase. Secondly, after the channel outlet, the buoyant plume is not exposed to stagnant air but to other plumes next to it as seen in Fig. 26. This reduces shear and mixing above the channel outlets and allows warmer air to flow higher as a coherent entity. These two factors increase the mean velocity in channels compared to a single surface and thus increase the total heat transfer.
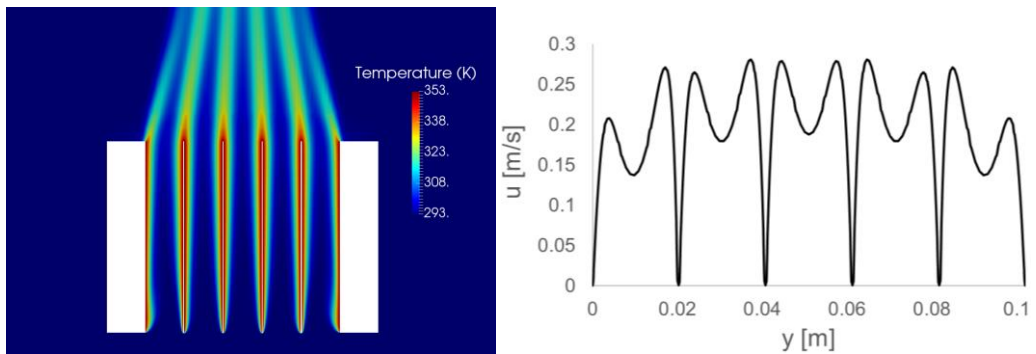

Figure 26. Temperatures of five parallel channels and corresponding velocity profiles at channel outlets ($x = 0.1$ m).

Table 12. Results of coefficient $C = Nu/Ra^{1/4}$ for a different channel number N_{ch}

d [mm]	N_{ch} [-]	ϕ/N_{ch}	C
10	1	44.8	0.584
10	3	46.1	0.601
10	5	47.0	0.612
10	7	47.3	0.617
10	9	47.6	0.620
10	11	48.1	0.627
10	13	49.4	0.644
10	15	49.6	0.646
20	1	43.8	0.572
20	3	45.0	0.587
20	5	45.7	0.596
20	7	45.9	0.599
40	1	42.0	0.548
80	1	41.3	0.538
160	1	41.0	0.534
∞	1	40.9	0.533
vertical surface	1	40.5	0.528

The following observation was made from the results in Table 12. Many channels exhibit larger heat transfer than a single channel, which also again has larger heat transfer than two vertical surfaces. These solutions explain better why different values have been proposed for the coefficient C in the literature. It all depends on the number of fins in tested heat sinks.

5.3   Optimization results

In the optimization cases in Section 5.3.1 and 5.3.3, the size of 30 and 40 swarms were used in the modified MOPSO algorithm with 100 and 150 rounds of iterations. These different optimization parameter combinations yielded the same results within good accuracy in both cases (at maximum a few percentage deviations between the runs). It was a good observation because it means that these optimization problems are not highly sensitive to selected parameter values. Because the main importance of optimization results is to demonstrate how much room for improvement exists in a typical heat sink case, results of one representative optimization run was selected for presentation in each case. In Section 5.3.2, the fmincon algorithm of MATLAB was used with ε-constraint method and optimization runs were repeated with many different fin numbers for one constrained mass value. This vastly larger number of total function evaluations yielded results that are probably slightly closer to actual Pareto optimums than in the case of the MOPSO algorithm.

5.3.1   Forced convection optimization: Case I

The first calculation model in multi-objective optimization was done for the reference heat sink in Fig. 17 in Section 4.4.1, a heat sink consisting of two heat dissipating components. In optimization, the components were considered as a component cluster, and their relative position was fixed. The heat sink is cooled by forced convection with a given fan curve of $\Delta p = -1000Q + 400$ (Pa), where Q (m³/s) is the volumetric flow. Criteria in multi-objective optimization were the maximum temperature of the heat sink and its material weight. Pareto

optimal solutions of rectangular and triangular fins are shown in Fig. 27. They are compared in detail with the same maximum temperature as in the reference solution. These solutions appear in Fig. 27 in the line of maximum allowed temperature with their geometrical details shown in Fig. 28. Detailed dimensions of the original reference case and optimized heat sinks are shown in Table 13.
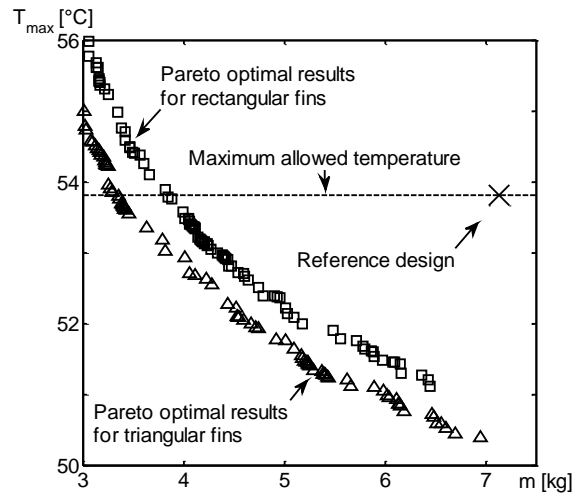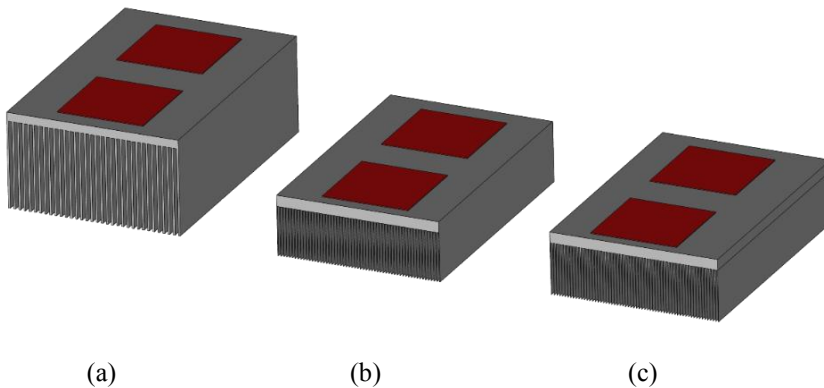

Figure 27. Pareto-optimal results.

| (a) | (b) | (c) |

Figure 28. Reference design (a) and selected Pareto-optima with rectangular (b) and triangular fins (c) from Fig. 27.

Table 13. Dimensions of heat sinks in Fig. 28.

	Original design	Optimized design	
		Rectangular	Triangular
T_{max} (°C)	**53.8**	**53.8**	**53.8**
m (kg)	**7.13**	**3.85**	**3.35**
L (mm)	300	288.8	286.5
W (mm)	200	189.1	195.9
b (mm)	10	12.8	12.4
N (mm)	34	58	62
t_b (mm)	2	0.77	1.04
t_t (mm)	2	0.77	0
l (mm)	100	56.4	59.4
X (mm)	20	14.4	12.7
Y (mm)	50	42.4	53.9

In Fig. 27, we can see that the mass criterion can be improved significantly from the reference design. Results show that in optimal cases, triangular fins with a smaller mass perform the same as rectangular fins. However, the total mass reduction between a rectangular and a triangular optimum (about 13 %) is not as significant as one would expect from the results of single fin optimization, as discussed in Publication II.

The main reason for the above is that about half the mass is in the base plate, which enables heat to spread effectively into fins. In the single fin case, all mass is concentrated in the fin. However, fin mass drops by about 25 % between a rectangular and a triangular optimum (from 1.96 kg to 1.47 kg). Additionally, the flow is not evenly distributed in array channels. In a channel, flow velocity is highest in the fin tip area, which is the coldest. In a single fin case, the flow is uniform over the fin surface.

5.3.2   Forced convection optimization: Case II

The original array mass in Fig. 19 is 6.65 kg. Its maximum temperature and mass were subjected to multi-objective optimization with the Reynolds number kept at a constant value of 3300. The ε-constraint method was used with MATLAB's fmincon algorithm and details about optimization can be found in Publication III. Results are shown in Fig. 29 with two optimal geometries from the Pareto optimal set shown in Figs. 30 and 31. The optimal geometries are rectangular and triangular in cross section in Fig. 29, respectively. In Fig. 29, the optimal solution of rectangular fins, shown with a circle, and optimal solution of trapezoidal fins, shown with square, have the same maximum temperature as the reference solution but significantly lower mass. With rectangular fins, heat sink mass was reduced about 51 % and with trapezoidal fins by about 59 %.
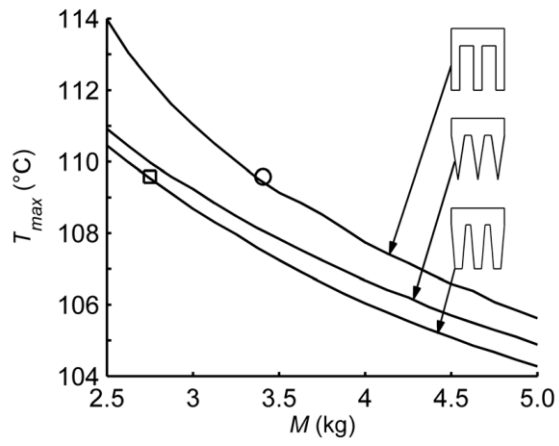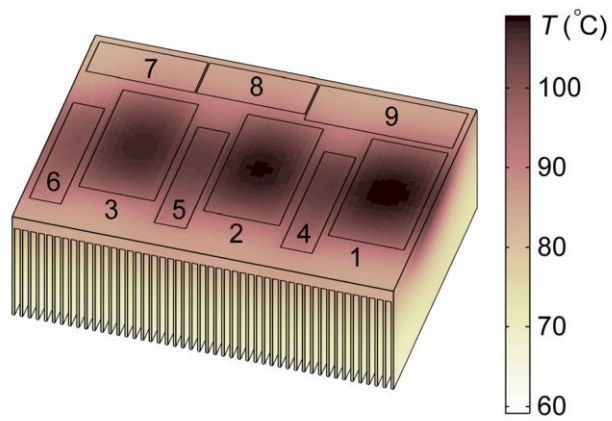
Figure 29. Pareto-optimal solutions.

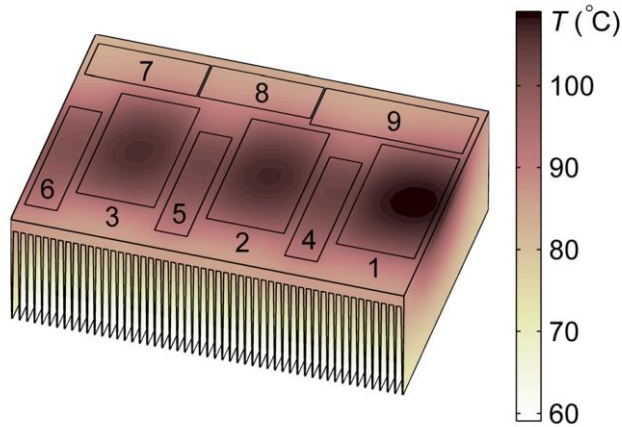**Figure 30.** Optimal heat sink with rectangular fins (m = 3.41 kg).

Figure 31. Optimal heat sink with trapezoidal fins (m = 2.75 kg).

The most interesting result, mentioned in Publication III, is that the trapezoidal fin array, in fact, performs better than a triangular one. The result is different for a single fin, where triangular was better than trapezoidal, as mentioned in Publication III. The reason is flow distribution. In the array, flow is distributed unevenly with the highest volumetric flow at the tip of the fin where the channel is at its widest. Consequently, the fin tip cools too much, lowering the efficiency of the fin. In the trapezoidal case, the thickness of the fin tip still enables sufficient conduction.

5.3.3 Natural convection optimization: Case III

In the natural convection case, a reference fin array shown in Fig. 16 was the subject of multi-objective optimization. In Publication IV, optimization was performed with two different sets of criteria, because the first selection of maximum temperature and mass gave inconveniently large arrays as an optimal result. A second optimization was performed whose criteria were fin array mass and outer volume with the components' maximum temperature held as a constraint in optimization. The constraining value was equal to 38.9 °C, which was the value of the reference design. One possibility could also have been that all the three criteria would have been optimized simultaneously. However, this approach was simplified here by changing the maximum temperature criterion as a constraint, since it provides sufficient information on the amount of mass that can be reduced by maintaining the same heat sink performance.

In the original reference, the array data is shown in Fig. 16, and the components are located symmetrically in the center. Results of multi-objective optimization are shown in Fig. 32, where mass and outer volume of the array constituted the criteria. The dimensions of one selected Pareto optimum, which is believed to represent a good comparison point (marked #1 in Fig. 32), and where mass was reduced by about 50 % and outer volume by about 40 % are $N = 36$, $t_b = 0.54$ mm, $L = 68$ mm, $W = 256$ mm, $b = 6$ mm, $l = 82$ mm; component locations are shown in Fig. 33.
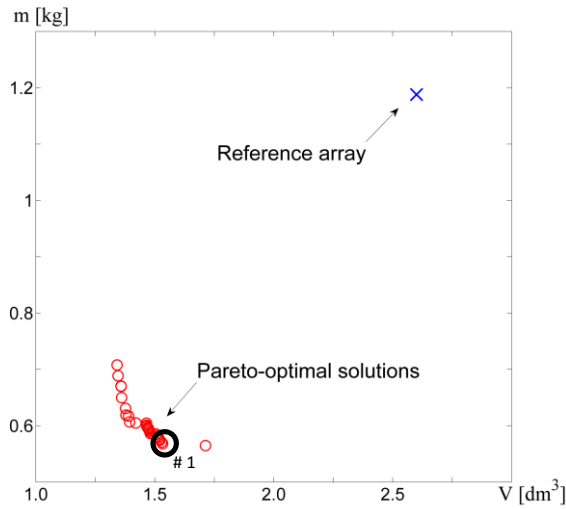
m [kg]

1.2

×

Reference array

1

0.8

Pareto-optimal solutions

0.6

1

1.0   1.5   2.0   2.5   V [dm^3]

Figure 32. Pareto-optimal results.

ΔT [K]

37

33

29

25

21

Reference
m = 1.19 kg
V = 2.6 dm³
ΔT_{max} = 38.9 K

1
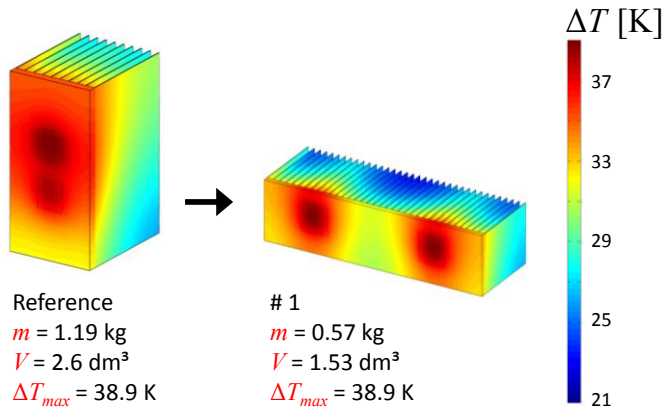m = 0.57 kg
V = 1.53 dm³
ΔT_{max} = 38.9 K

Figure 33. Selected solution.

The reference and final cases in Fig. 33 were also calculated using CFD. When the CFD results were compared with those in Fig. 33, the maximum temperature of components differed by less than 10 %. However, the lowest CPU -time consumption was about 1 hour with the CFD (with two CPUs) and with the calculation model less than 5 seconds (with single CPU). Based on these numbers, it is safe to say that the model is more than one thousand times faster than the CFD approach. In addition, preprocessing time was not included in the numbers above. It makes the model even faster in comparison because, with the CFD approach, considerable time is used to mesh the domain and choose the appropriate boundary conditions, whereas with the model, only a few numerical parameters are modified and the calculations are ready to operate.

5.4   Discussion

In the case of isothermal wall and isothermal base plate tests, the new calculation model accurately predicted the heat transfer rate of the channel. In the complete 3D heat sink cases with discrete components, the prediction of the maximum temperature was almost precise in the experimental case of forced convection, and acceptable in cases of natural convection. In forced convection, all the constituent parts of the calculation model are as accurate as are the Nusselt number and friction factor correlations used, and thus the obtained results are excellent. In natural convection, the error is greater because the mean flow velocity is calculated from the equilibrium of forces using assumptions, such as the average fluid temperature in the channel to predict buoyancy, and forced convection friction factor for shear stress. In addition, the flow is laminar and the effect of the wall temperature distribution must be taken into account when calculating the wall heat flux distribution. However, this was simplified in the model by using isothermal wall Nusselt number since, as indicated in Section 5.2.1, its use has only a minor effect on the total heat transfer rate if the wall temperature increases in the flow direction. In practice, this is the case in a typical industrial heat sink.

In this thesis, the comparing solutions from the literature were mainly analytical solutions for the cases of isothermal channels and isothermal base plates. These analytical solutions of Bar-Cohen and Teertstra (see Chapter 2) are based on experiments or they have been validated experimentally. In addition, a comparison was made in the case of a heat sink with nine components between the Lehtinen's model and the present calculation model in Publication III, and no significant difference was found between the models. However, no other relevant data in the literature has been found for discrete components cases than those of Lehtinen and Lindstedt [4, 21]. The rare cases encountered by the author concerned other liquids and were not suitable for comparison. Because of the rare data, CFD was used as a main comparison tool in 3D calculations, and its feasibility was confirmed in the same analytical tests that were performed for the present calculation model.

After testing the model, it was used in several different multi-objective optimization cases, where it demonstrated that significant material savings are realized when optimization is performed. In a typical case presented in this thesis, about 50% of the total mass was reduced in result of optimization without affecting the performance of the heat sink. In conclusion, the optimization cases presented in this thesis show that existing heat sinks have generally too thick fins. The optimum thicknesses of the fins was found to be a rather thin, of the order of 1 mm and 0.5 mm respectively, in the cases of forced and natural convection. The exact dimensions are influenced by the components and the operating conditions and, therefore, these figures should not be taken in general. Another interesting finding was that in the case of heat sinks, the trapezoidal fins are more efficient than the triangular fins, which is not predictable on the basis of single-fin analysis.

Chapter 6

Summary & Conclusions

This thesis introduces a new model to calculate the heat sink temperature distribution in forced and natural convection cooling. This presentation is based on that in Publication V, which combines the separate models for forced and natural convection in Publications I and IV, respectively. The main advantage of the new model is that it significantly reduces CPU calculation time over CFD. The speedup is achieved by replacing the slow 3D -solution of air velocity and temperature distributions in CFD with 1D -solutions of air mean velocity and temperature distributions in the channels, where the convective heat transfer and friction is calculated from analytical correlations. Numerical solution is performed only for the temperature field of the solid.

The calculation model was tested for its accuracy in many test cases, and the results obtained were compared with those with CFD and analytical solutions: the maximum temperature difference was within 10 % between the solutions. This is important, because in optimization the maximum temperature of the components constitutes the most important quantity. However, the modifications mentioned above make the new model at least a thousand times faster than CFD. This holds true even after the transient natural convection CFD solutions were made faster by modifying the thermal capacity (ρc_p –value) of the aluminum array. Thermal capacity value was reduced to one thousandths of the original, which allowed temperature distribution to reach the steady state levels in a relatively short time, as mentioned in detail in Publication IV.

The main advantage of the new model is in its ability to calculate quickly many completely different heat sink geometries. This allowed the new calculation model being used in multi-objective optimization, because it helps us to arrive at the best compromise solutions, called the Pareto optimal set, with in practical time period. In optimization, the chosen criteria are usually components' maximum temperature, and mass or outer volume of the heat sink. The multi-objective optimization version of the PSO algorithm was chosen as the optimization algorithm, because it is effective and simultaneously capable of dealing with both discrete (the number of fins) and continuous (all geometrical dimensions) variables.

The suitability of the model in optimization was demonstrated in several cases in the thesis. The chosen optimization cases, originally published in Publications II, III, and IV, are common, e.g., in the power electronics industry. These examples showed that multi-objective optimization helps to reduce the mass of a heat sink significantly, as long as optimization criteria and constraints are chosen carefully. The new method thus benefits optimization in industrial use, where time consumption in pre-design is an important consideration. In fact, as a demonstration of the achieved speedup, one multi-objective optimization using the new model consumes typically fewer CPU -resources than one heat sink CFD -solution.

The method can be easily implemented as a stand-alone software package. It needs a suitable programming platform such as MATLAB or Python, which supports the fast linear algebra solution libraries. The calculation model has already once been implemented and is currently being used in industry.

In summary, the main contributions of this thesis are to

- present the calculation model for forced convection, which combines effectively analytical and numerical solutions.
- extend the calculation model for natural convection by utilizing the average fluid temperature and forced convection friction factor results in channel flow.
- use the calculation model as a part of a multi-objective optimization method and show how it can benefit heat sink design process by helping to find efficient geometries with significantly fewer material used.

Chapter 7

Future work

In this thesis, the calculation model constitutes a key element of the optimization method. However, it has many built-in assumptions, some of which were tested here. Yet some other assumptions, e.g., the impact of radiation heat transfer on the model's accuracy should be tested in future work. In this thesis, it was assumed that all the heat sink surfaces are made of bright aluminum, whose emissivity is about ≈ 0.05, a rather low value, which in the case of forced convection has no significant impact on the total heat transfer rate. In a natural convection case in Ref. [30], it was also concluded that in the case of an isothermal heat sink the thermal radiation had typically only a small effect on total heat transfer. However, the issue should still be examined in a case of many hot discrete components.

A further important topic for future studies is to investigate enhancement of heat transfer with pin fins and other alternative fin structures, a subject that was briefly studied in Publication V. For example, fins cut in the flow direction break the developing temperature boundary layers and increase mixing and turbulence in the cutoff section, resulting in an increased heat transfer coefficient. On the other hand, cutting shortens the heat transfer area, because of removed material. However, previous studies [38] suggest that there is an optimal cutting length to maximize heat transfer in the array, a topic that should be studied.

Yet another important topic for future studies is to determine optimal layout patterns and heat sink dimensions for different sets of components. It would be ideal to find some non-dimensional variables that would immediately indicate how to size the heat sink dimensions and arrange component locations for maximum performance. A possible correlation need not be perfect to be helpful. Such guidelines could then be used in pre-design without running actual optimization, or at least, they could serve as a good starting point for actual optimization.

References

[1]   Bar-Cohen A, Holloway C A, Thermal science and engineering – from macro to nano in 200 years. Proceedings of the IHTC-15, August 10 – 15, 2014, Kyoto, Japan.

[2]   Wang P, McCluskey P, Bar-Cohen A (2013) Two-Phase Liquid Cooling for Thermal Management of IGBT Power Electronic Module. Journal of Electronic Packaging 135:021001-1 – 11. http://dx.doi.org/10.1115/1.4023215

[3]   Kraus A D, Aziz A, Welty J (2001) Extended surface heat transfer. New York, Wiley

[4]   Lehtinen A (2005), Analytical Treatment of Heat Sinks Cooled by Forced Convection. Doctoral thesis, Tampere University of Technology, Tampere, Finland.

[5]   Copper / Aluminum price ratio, Charts & Data for mining industry, InfoMine, web page (referenced 4th January 2018): www.infomine.com

[6]   Ahmadi M, Pakdaman M F, Bahrami M (2015) Pushing the limits of vertical naturally-cooled heatsinks; Calculations and design methodology. International Journal of Heat and Mass Transfer, 87, 11-23. http://dx.doi.org/10.1016/j.ijheatmasstransfer.2015.03.086

[7]   Iyengar M, Bar-Cohen A (2003) Least-Energy Optimization of Forced Convection Plate-Fin Heat Sinks. IEEE Transactions on components and packaging technologies, 26(1). http://dx.doi.org/10.1109/TCAPT.2003.811484

[8]   Elkerbout M, Egenhofer C (2017) The EU ETS price may continue to be low for the foreseeable future – Should we care? CEPS Policy Insight No 2017/22, June 2017. http://aei.pitt.edu/id/eprint/88047

[9]   European Council (23 and 24 October 2014) Conclusions, EUCO 169/14, CO EUR 13, CONCL 5, Brussels, 24 October 2014.

[10]   Karvinen R, Karvinen T (2010) Optimum geometry of fixed volume plate fin for maximizing heat transfer. International Journal of Heat and Mass Transfer 53:5380-5385. http://dx.doi.org/10.1016/j.ijheatmasstransfer.2010.07.018

[11]   Karvinen R, Karvinen T (2012) Optimum Geometry of Plate Fins. ASME Journal of Heat Transfer, August 2012, 134, 081801-1 – 7. http://dx.doi.org/10.1115/1.4006163

[12]   Bejan A, Sciubba E (1992) The optimal spacing of parallel plates cooled by forced convection. International Journal of Heat and Mass Transfer, 35(12), 3259-3264. https://doi.org/10.1016/0017-9310(92)90213-C

[13]   Mereu S, Sciubba E, Bejan A (1993) The optimal cooling of stack of heat generating boards with fixed pressure drop, flowrate or pumping power. International Journal of Heat and Mass Transfer, 36(15), 3677-3686. https://doi.org/10.1016/0017-9310(93)90047-A

[14]   Bejan A, Morega Al M (1994) The optimal spacing of a stack of plates cooled by turbulent forced convection. International Journal of Heat and Mass Transfer, 37(6), 1045-1048. https://doi.org/10.1016/0017-9310(94)90228-3

[15] Muzychka Y S (2005) Constructal design of forced convection cooled microchannel heat sinks and heat exchangers. International Journal of Heat and Mass Transfer, 48, 3119-3127. http://dx.doi.org/10.1016/j.ijheatmasstransfer.2005.02.014

[16] Lindstedt M, Karvinen R (2012) Optimization of isothermal plate fin arrays with laminar forced convection. Journal of Enhanced Heat Transfer, 19(6):535-547. http://dx.doi.org/10.1615/JEnhHeatTransf.2012006003

[17] Ryu J H, Choi D H, Kim S J (2002) Numerical optimization of the thermal performance of a microchannel heat sink. International Journal of Heat and Mass Transfer, 45, 2823-2827. http://dx.doi.org/10.1016/S0017-9310(02)00006-6

[18] Kim D-K, Kim S J (2007) Closed-form correlations for thermal optimization of microchannels. International Journal of Heat and Mass Transfer, 50, 5318-5322. http://dx.doi.org/10.1016/j.ijheatmasstransfer.2007.07.034

[19] Kim D-K, Jung J, Kim S J (2010) Thermal optimization of plate-fin heat sinks with variable fin thickness. International Journal of Heat and Mass Transfer, 53, 5988-5995. http://dx.doi.org/10.1016/j.ijheatmasstransfer.2010.07.052

[20] Biswal L, Chakraborty S, Som S K (2009) Design and Optimization of Single-Phase Liquid Cooled Microchannel Heat Sink. IEEE Transactions on components and packaging technologies, 32(4). http://dx.doi.org/10.1109/TCAPT.2009.2025598

[21] Lindstedt M (2013), Modeling and Optimization of Plate Fins and Plate Fin Heat Sinks. Doctoral thesis, Tampere University of Technology, Tampere, Finland.

[22] Aho T (2008), Multiobjective Placement Optimization of Heat Generating Components on Printed Wiring Board. Doctoral thesis, Tampere University of Technology, Tampere, Finland.

[23] Bejan A (1995) Entropy Generation Minimization: The Method of Thermodynamic Optimization of Finite-Size Systems and Finite-Time Processes. CRC Press, October 20, 1995.

[24] Chen Q, Liang X-G, Guo Z-Y (2013) Entransy theory for the optimization of heat transfer – A review and update. International Journal of Heat and Mass Transfer, 63, 65-81. http://dx.doi.org/10.1016/j.ijheatmasstransfer.2013.03.019

[25] Herwig H (2014) Do We Really Need "Entransy"? A Critical Assessment of a New Quantity in Heat Transfer Analysis. ASME Journal of Heat Transfer, 136, 045501-1 – 4. http://dx.doi.org/10.1115/1.4026188

[26] Bejan A (2014) "Entransy," and Its Lack of Content in Physics. ASME Journal of Heat Transfer, 136, 055501-1 – 6. http://dx.doi.org/10.1115/1.4026527

[27] Kostic M M (2017) Entransy concept and controversies: A critical perspective within elusive thermal landscape. International Journal of Heat and Mass Transfer, 115, 340-346. http://dx.doi.org/10.1016/j.ijheatmasstransfer.2017.07.059

[28] Culham J R, Muzychka Y S (2001) Optimization of Plate Fin Heat Sinks Using Entropy Generation Minimization. IEEE Transactions on components and packaging technologies, 24(2), 159-165. http://dx.doi.org/10.1109/6144.926378

[29] Bar-Cohen A, Rohsenow W M (1984) Thermally Optimum Spacing of Vertical, Natural Convection Cooled, Parallel Plates. Journal of Heat Transfer, 106(1), 116-123. http://dx.doi.org/10.1115/1.3246622

[30]   Bar-Cohen A, Iyengar M, Kraus A D (2003) Design of Optimum Plate-Fin Natural Convective Heat Sinks. Journal of Electronic Packaging, Transactions of the ASME, Vol 125, pp. 208-216. http://dx.doi.org/10.1115/1.1568361

[31]   Kim D-W (2012) Thermal optimization of plate-fin heat sinks with fins of variable thickness under natural convection. International Journal of Heat and Mass Transfer, 55(4). http://dx.doi.org/10.1016/j.ijheatmasstransfer.2011.10.034

[32]   Shen Q, Sun D, Xu Y, Zhao X (2014) Orientation effects on natural convection heat dissipation of rectangular fin heat sinks mounted on LEDs. International Journal of Heat and Mass Transfer, 75:462-469. http://dx.doi.org/10.1016/j.ijheatmasstransfer.2014.03.085

[33]   An B H, Kim H J, Kim D-K (2012) Nusselt number correlation for natural convection from vertical cylinders with vertically oriented plate fins. Experimental Thermal and Fluid Science, 41:59-66. https://doi.org/10.1016/j.expthermflusci.2012.03.010

[34]   Park K T, Kim H J, Kim D-K (2014) Experimental study of natural convection from vertical cylinders with branched fins. Experimental Thermal and Fluid Science, 54:29-37. https://doi.org/10.1016/j.expthermflusci.2014.01.018

[35]   Lee M, Kim H J, Kim D-K (2015) Nusselt number correlation for natural convection from vertical cylinders with triangular fins. Applied Thermal Engineering, 93:1238-1247. https://doi.org/10.1016/j.applthermaleng.2015.10.105

[36]   Yu X, Feng J, Feng Q, Wang Q (2005) Development of a plate-pin fin heat sink and its performance comparison with a plate fin heat sink. Applied Thermal Engineering, 25(2-3), 173-182. https://doi.org/10.1016/j.applthermaleng.2004.06.016

[37]   Teertstra P, Yovanovich M M, Culham J R (2000) Analytical forced convection modelling of plate fin heat sinks. Journal of Electronics Manufacturing, 10(4), 253-261. https://doi.org/10.1142/S0960313100000320

[38]   Ahmadi M, Mostafavi G, Bahrami M (2014) Natural convection from rectangular interrupted fins. International Journal of Thermal Sciences, 82:62-71. http://dx.doi.org/10.1016/j.ijthermalsci.2014.03.016

[39]   Ndao S, Peles Y, Jensen M (2009) Multi-objective thermal design optimization and comparative analysis of electronics cooling technologies. International Journal of Heat and Mass Transfer, 52, 4317-4326. http://dx.doi.org/10.1016/j.ijheatmasstransfer.2009.03.069

[40]   Bornoff R, Parry J, Wilson J, A (2016) Novel Approach to Heat Sink Mass Minimisation. Proceedings of Therminic 2016, 21 – 23 September, Budapest, Hungary.

[41]   Kays W, Crawford M, Weigand B (2004) Convective Heat and Mass Transfer. McGraw-Hill Education, 4th edition.

[42]   Winterton R H S (1999) Newton's law of cooling. Contemporary Physics, 40:3, 205-212. http://dx.doi.org/10.1080/001075199181549

[43]   Cheng K C, Fujii T (1998) Heat in history Isaac Newton and Heat Transfer. Heat Transfer Engineering, 19:4, 9-21. http://dx.doi.org/10.1080/01457639808939932

[44]   Shah R K, London A L (1978) Laminar Flow Forced Convection in Ducts. New York, Academic Press.

[45]   Gnielinski V (1975) Neue Gleichungen für den Wärme- und den Stoffübergang in turbulent durchströmten Rohren und Kanälen. Forsh. Ing. Wes., 41, Nr. 1. https://doi.org/10.1007/BF02559682

[46]   Graetz L (1882) Über die wärmeleitungsfähigkeit von Flüssigkeiten. Annalen der physik, 254(1), 79-94. http://dx.doi.org/10.1002/andp.18822540106

[47]   Elenbaas W (1942) Heat dissipation of parallel plates by free convection. Physica 9(1):665 – 671. https://doi.org/10.1016/S0031-8914(42)90053-3

[48]   Incropera F P, DeWitt D P, Bergman T L, Lavine A S (2006) Fundamentals of Heat and Mass Transfer. John Wiley & Sons, 6th edition.

[49]   Churchill S W, Usagi R (1972) A general expression for the correlation of rates of transfer and other phenomena. AIChE Journal, 18(6), 1121-1128. http://dx.doi.org/10.1002/aic.690180606

[50]   Churchill S W, Chu H H S (1975) Correlating equations for laminar and turbulent free convection from a vertical plate. International Journal of Heat and Mass Transfer, 18(11), pp. 1323-1329. https://doi.org/10.1016/0017-9310(75)90243-4

[51]   Aihara T, Maruyama S, Choi J S (1986) Laminar free convection with variable fluid properties in vertical ducts of different cross-sectional shapes. Proceedings of IHTC-8, 17-22 August, San Francisco, USA.

[52]   Lindstedt M, Karvinen R (2017) Conjugated heat transfer from a uniformly heated plate and a plate fin with uniform base heat flux. International Journal of Heat and Mass Transfer, 107, 89-95. https://doi.org/10.1016/j.ijheatmasstransfer.2016.10.079

[53]   Merriam-Webster dictionary, web page (referenced 5th March 2018): https://www.merriam-webster.com/dictionary/optimization

[54]   Deb K (2005) Optimization for Engineering Design Algorithms and Examples. Prentice-Hall of India, Eighth printing, July 2005.

[55]   Pareto V (1971) Manual of Political Economy. The MacMillan Press Ltd (the original edition in French in 1927).

[56]   Edgeworth F Y (1881) An essay on the application of mathematics to the moral sciences. Mathematical physics, C. Kegan Paul & CO, London. http://books.google.com/books?id=s7cJAAAAIAAJ&oe=UTF-8

[57]   Miettinen K (1999) Nonlinear Multiobjective Optimization. Kluwer Academic Publishers, Boston.

[58]   Coello Coello C, Pulido G, Lechuga M (2004) Handling multiple objectives with particle swarm optimization. IEEE Transactions on evolutionary computation, 8:(3). http://dx.doi.org/10.1109/TEVC.2004.826067

[59]   Deb K (2000), An efficient constraint handling method for genetic algorithms. Comput. Methods Appl. Mech. Engrg, 186 311-338. https://doi.org/10.1016/S0045-7825(99)00389-8

[60]   Gass S, Saaty T (1955) The Computational Algorithm for the Parametric Objective Function, Naval Research Logistics Quarterly 2, 39-45. http://dx.doi.org/10.1002/nav.3800020106

[61]   Zadeh L (1963) Optimality and Non-Scalar-Valued Performance Criteria, IEEE Transactions on Automatic Control 8, 59-60.

http://dx.doi.org/10.1109/TAC.1963.1105511

[62]   Haimes Y Y, Lasdon L S, Wismer D A (1971) On a Bicriterion Formulation of the
        Problems of Integrated System Identification and System Optimization, IEEE
        Transactions on Systems, Man, and Cybernetics 1, 296-297.
        http://dx.doi.org/10.1109/TSMC.1971.4308298

[63]   Das I, Dennis J E (1997) A closer look at drawbacks of minimizing weighted sums of
        objectives for Pareto set generation in multicriteria optimization problems. Struct.
        Optim., 14, 63–69. https://doi.org/10.1007/BF01197559

[64]   Das I, Dennis J E (1998) Normal-boundary intersection: a new method for generating
        the Pareto surface in nonlinear multicriteria optimization problems. SIAM J. Optim. 8,
        631–657. https://doi.org/10.1137/S1052623496307510

[65]   Koski J (1985) Defectiveness of weighting method in multicriterion optimization of
        structures. Commun. Appl. Numer. Methods, 1, 333–337.
        http://dx.doi.org/10.1002/cnm.1630010613

[66]   Stadler, W. 1995: Caveats and boons of multicriteria optimization. Microcomput. Civ.
        Eng. 10, 291–299. http://dx.doi.org/10.1111/j.1467-8667.1995.tb00291.x

[67]   Deb K, Pratap A, Agarwal S, Meyarivan T (2002), A Fast and Elitist Multiobjective
        Genetic Algorithm: NSGA-II, IEEE Transactions on evolutionary computation, Vol. 6,
        No. 2, 182-197. http://dx.doi.org/10.1109/4235.996017

[68]   Srinivas N, Deb K (1994) Multiobjective Optimization Using Nondominated Sorting
        in Genetic Algorithms. Journal of Evolutionary Computation, 2(3), 221-248.
        http://dx.doi.org/10.1162/evco.1994.2.3.221

[69]   Deb K, Jain H (2014), An Evolutionary Many-Objective Optimization Algorithm
        Using Reference-Point-Based Nondominated Sorting Approach, Part I: Solving
        Problems With Box Constraints. IEEE Transactions on evolutionary computation, Vol.
        14, No. 4, 577-601. http://dx.doi.org/10.1109/TEVC.2013.2281535

[70]   Wahde M (2008), Biologically Inspired Optimization Methods, WIT Press,
        Southampton.

[71]   Marler R T, Arora J S (2004) Survey of multi-objective optimization methods for
        engineers. Structural and Multidisciplinary Optimization, 26(6), 369-395.
        https://doi.org/10.1007/s00158-003-0368-6

[72]   Wilson E O (1975) Sociobiology, The abridged edition, 7th printing (printed 1998), The
        Belknap Press of Harvard University Press, USA.

[73]   Kennedy J, Eberhart R C (1995) Particle swarm optimization. Proc of IEEE
        International Conference on Neural Networks, 27th Nov. – 1st Dec., 1995, Perth, WA,
        Australia. http://dx.doi.org/10.1109/ICNN.1995.488968

[74]   Shi Y, Eberhart R C (1998) A modified particle swarm optimizer. Evolutionary
        Computation Proceedings, IEEE World Congress on Computational Intelligence, 4-9
        May 1998, Anchorage, AK, USA. http://dx.doi.org/10.1109/ICEC.1998.699146

[75]   Shi Y, Eberhart R C (1998) Parameter selection in particle swarm optimization. In:
        Porto V.W., Saravanan N., Waagen D., Eiben A.E. (eds) Evolutionary Programming
        VII. EP 1998. Lecture Notes in Computer Science, vol 1447. Springer, Berlin,
        Heidelberg. https://doi.org/10.1007/BFb0040810

[76]   Clerc M, Kennedy J (2002) The Particle Swarm – Explosion, Stability, and Convergence in a Multidimensional Complex Space. IEEE Transactions on evolutionary computation, Vol. 6, No. 1, February 2002. http://dx.doi.org/10.1109/4235.985692

[77]   Bonyadi M R, Michalewicz Z (2014) A locally convergent rotationally invariant particle swarm optimization algorithm. Swarm Intell 8:159-198. http://dx.doi.org/10.1007/s11721-014-0095-1

[78]   Lindstedt M (2010) Chip refiner flow fields and optimal design. Master's thesis, Tampere University of Technology, Tampere, Finland.

[79]   Ferziger J H, Peric M (2002) Computational Methods for Fluid Dynamics. 3rd edition, Springer-Verlag, Berlin, Heidelberg, New York, printed in Germany.

[80]   Weigand B (2004) Analytical Methods for Heat Transfer and Fluid Flow Problems. Springer, Berlin, Heidelberg. https://doi.org/10.1007/978-3-540-68466-4_5

[81]   Jones O C J (1976) An improvement in the calculation of turbulent friction factor in rectangular ducts. ASME Journal of Fluids Engineering, 98(2), 173-181. http://dx.doi.org/10.1115/1.3448250

[82]   Martin L, Raithby G D, Yovanovich M M (1991) On the low Rayleigh number asymptote for natural convection through an isothermal, parallel plate channel. Journal of Heat Transfer, Vol 113, 899-905. http://dx.doi.org/10.1115/1.2911219

[83]   Lampio K, Karvinen R (2015) A New Method to calculate natural convection heat transfer from a non-isothermal fin array. Proceedings of 7th Baltic Heat Transfer Conference, August 24-26, 2015, Tallinn, Estonia.

[84]   Matlab manual, web page (referenced 5th March 2018): https://se.mathworks.com/help/matlab/

[85]   Raithby G D, Hollands K G T (1975) in "Advances in Heat Transfer, edited by Irvine T.", A general method of obtaining approximate solutions to laminar and turbulent free convection problems, Academic Press, New York.

[86]   Miyatake O, Fujii T (1972) Free convection heat transfer between vertical plates – One plate isothermally heated and the other thermally insulated. Heat Transfer – Jpn., Res. 1, 30-38. http://dx.doi.org/10.1252/kakoronbunshu1953.36.405

[87]   Aung W, Fletcher L S, Sernas V (1972) Developing laminar free convection between vertical flat plates with asymmetric heating. International Journal of Heat and Mass Transfer, 15, 2293-2308. https://doi.org/10.1016/0017-9310(72)90048-8

Appendix: original papers

Publication I

Reijo Karvinen, Kaj Lampio

Combined numerical and analytical method for fin array heat transfer

Proceedings of CHT-12, July 1-6, 2012, Bath, England.

Reprinted with permission

COMBINED NUMERICAL AND ANALYTICAL METHOD
FOR FIN ARRAY HEAT TRANSFER

Reijo Karvinen, Kaj Lampio[§]
Tampere University of Technology, Finland
Department of Energy and Process Engineering, P.O. Box 589, 33101 Tampere, Finland
[§]Correspondence author. Email: kaj.lampio@tut.fi

ABSTRACT Fins and fin arrays are used for cooling heat generating components in electronics. Heat transfer composed of simultaneous convection and conduction can be solved numerically using commercial CFD codes but this is time consuming, especially if the goal is to optimize the geometry. A faster method is obtained by adopting analytical expressions for convection and solving only conduction numerically. In the paper this type of approach and equations are presented. The validity of the method is checked by comparing the results to measured data and to results obtained purely numerically. It was observed that the calculation time using the method presented is much shorter compared to that if velocity and temperature fields of the flow and solid are solved numerically. Thus, the method is a very suitable tool, for instance, in a multiobjective optimization where hundreds of solutions are required.

NOMENCLATURE

c_p	fluid specific heat
d	channel width
d_h	hydraulic diameter $d_h = 2d$
f	Fanning friction factor
f_{app}	apparent friction factor
G_n	eigenfunction
h	heat transfer coefficient
k_f	thermal conductivity of fluid
k	thermal conductivity of solid
l	fin height
L	fin length
L^*	dimensionless length, $L^* = L/(RePrd_h)$
Nu	Nusselt number
Pr	Prandtl number
$\dot{Q}$	heat rate
$\dot{q}$	heat flux
Re	Reynolds number, Vd_h/v
T	fin temperature
T_B	base plate temperature
T_m	fluid mean temperature
T_0	fluid inlet temperature
T_s	surface temperature

t	fin thickness
V	mean velocity in channel
x^+	dimensionless coordinate, $x^+ = x/(Red_h)$
x^*	dimensionless coordinate, $x^* = x/(RePrd_h)$
x, y, z	cartesian coordinates

Greek symbols

β	momentum velocity distribution factor
θ	temperature difference, $T(x,z) - T_0$
θ_0	temperature difference, $T_s - T_0$
λ_n	eigenvalue
μ	dynamic viscosity
υ	kinematic viscosity
ξ	dummy variable, Eq. (7)
ρ	density
σ	expansion ratio, $\sigma = d/(d + t)$

INTRODUCTION

Fins and fin arrays are used in the cooling of components in electronics. In Fig. 1 a typical array is shown, in which heat generating components are located on the lower surface of the base plate. When the heat release rate is known, the array should be designed in such a way that maximum temperatures are below the values which components can withstand without failure. In addition, the volume and mass of an array should be small and the pressure drop and fan power low. The flow in channels can be laminar or turbulent.

In principle, the solution of the convection-conduction problem in Fig. 1 can be obtained by solving numerically the partial differential equations governing fluid flow and temperatures. However, if the optimization of geometry is required, it takes much effort to approach the problem this way. Instead of employing a numerical approach, convection in channels can be treated very accurately using analytical expressions. This type of treatment also helps in finding non-dimensional variables from which the optimal geometry can be easily found.

Simultaneous use of analytical and numerical treatment has successfully been applied by Karvinen [2010] to find optimal geometries of fins. A similar type of approach can also be applied to fin arrays with isothermal fins [Lindstedt and Karvinen], and some new results have been obtained and found compared to those presented in the literature by Bejan et al. [1992]. Also non-isothermal fin arrays with a fixed temperature or heat flux in the base plate can be dealt with quite easily, as shown by Lindstedt and Karvinen [2011] and Lehtinen [2005]. An approximate analytical treatment of non-isothermal fin array with a constant base temperature by Teertstra et al. [2000] is also worthy of mention. Here they used the mean heat transfer coefficient of isothermal channel walls and the concept of fin efficiency.

Purely numerical solutions of non-isothermal arrays are also found. For example, Li and Peterson [2007] minimized the thermal resistance of a micro-channel fin array with a fixed base area for various values of pumping power. A fully developed laminar flow in the channel was assumed. This type of assumption is correct when the channel length is large compared to the channel width, and especially in the case of large Prandtl number fluids. In fact the governing equations are the same for micro scale and larger geometries. Many studies, such as those of Wang et al. [2011] and Ryu et al. [2002], have employed numerical modeling to optimize microchannel heat sinks.
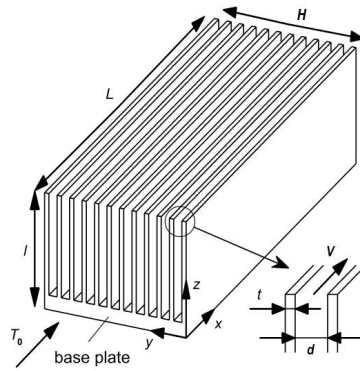
Figure 1. Plate fin array.

The present paper is based on a project in which the goal has been to develop a rapid method for the optimization of heat sinks in power electronics. Here convection in channels has been calculated using analytical expressions, and only conduction in fins and in the base plate is solved numerically. Very accurate expressions have been used that are based on the step change in a surface temperature and the superposition technique to take into account an arbitrarily varying surface temperature. For turbulent flow, even the assumption of a constant heat transfer coefficient is often accurate enough.

A comparison between the present solution and the purely numerical solution in the case of a turbulent flow in channels is shown concerning the calculation time. For laminar flow, the validity of the proposed model has already been presented in the literature by Lindstedt and Karvinen. It was observed that the calculation time was some orders of magnitude smaller compared to that of a purely numerical solution when use is made simultaneously of analytical expressions for convection and a numerical solution only for conduction. As for optimization, the results of a constant temperature base plate are a good starting point for multiobjective optimization, where the array volume and mass as well as the pressure drop or fan power are optimized simultaneously.

MODEL

Heat conduction in fin and base plate Temperature distributions $T(x,z)$ of fins differ according to the location of the heat generating components on the lower surface of the base plate shown in Fig. 1. Only if the base plate temperature is constant are they similar. In addition, the fluid mean temperature varies not only in the x- direction but also in the z- direction, depending on the fin temperature distribution. Thus, temperatures of fluid and fins are coupled together.

The temperature of a thin fin is assumed to be constant in the fin thickness direction and solved in the x- and z- directions. The edges of the fins and base plate in Fig.1 are insulated as is the lower surface of the base plate, except where the heat generating components are located. In these locations a known heat flux is given.

If heat transfer coefficients (h_1, h_2) and fluid mean temperatures (T_{m1}, T_{m2}) on both sides of the fin in Fig. 2 are known at the location (i,j), the equation for temperature $T_{i,j}$ taking into account convection and conduction using the finite difference method is
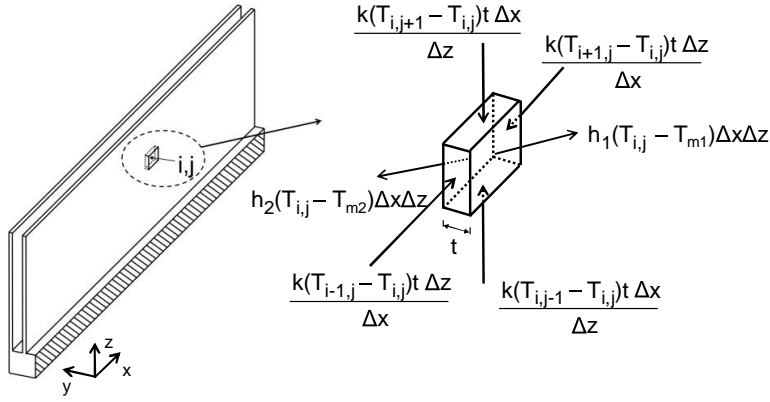
Figure 2. Heat balance of fin nodal point.

$$\frac{k}{\Delta z}\left(T_{i,j+1} - T_{i,j}\right)t\Delta x + \frac{k}{\Delta z}\left(T_{i,j-1} - T_{i,j}\right)t\Delta x + \frac{k}{\Delta \text{x}}\left(T_{i+1,j} - T_{i,j}\right)t\Delta z$$
$$+\frac{k}{\Delta \text{x}}\left(T_{i-1,j} - T_{i,j}\right)t\Delta z + h_1\left(T_{m1} - T_{i,j}\right)\Delta x\Delta z + h_2\left(T_{m2} - T_{i,j}\right)\Delta x\Delta z = 0 \tag{1}$$

In equation (1) above, heat transfer coefficients h_1 and h_2 are obtained from the analytical expressions given below. Conduction in the base plate is also treated with the 3D finite difference method.

If heat transfer coefficients and mean fluid temperatures are known everywhere in an array, the temperature distribution of fins and base plate is governed by the system of finite difference equations in matrix notation as $A\bar{T} = \bar{b}$, from which $\bar{T}$ can be solved. The calculation of mean temperatures and heat transfer coefficients are explained below.

Convective heat transfer   Heat transfer coefficients are needed in Eq. (1) in order to solve the fin temperature distributions. Because the heat transfer coefficient depends on the fin temperature especially in laminar flow, the use of an isothermal result yields errors in a non-isothermal channel. For example, the numerical values of heat transfer coefficients are different for constant surface temperature and heat flux boundary condition. Real fins are not isothermal, especially if the amount of material is optimized.

If a fully developed velocity profile is assumed, the local heat flux is obtained as a solution of the Graetz problem. For an isothermal parallel plate channel it is given by Shah et al. [1978] and Kays et al. [2005] as

$$\dot{q}(x,z) = \frac{4k_f\theta_0}{d_h}\sum_{n=0}^{\infty} G_n\exp\left(-2\lambda_n^2 x^*\right) \tag{2}$$

Table 1
Eigenvalues and functions for isothermal parallel plates

n	λ_n	G_n
0	3.885	1.717
1	13.09	1.139
2	22.32	0.952
> 2	$\dfrac{16}{\sqrt{3}}n + \dfrac{20}{3\sqrt{3}}$	$2.68\lambda_n^{-1/3}$

where eigenfunctions G_n and eigenvalues λ_n are given in Table 1. The non-dimensional distance in Eq. (2) is defined as

$$x^* = \frac{x}{RePrd_h} \tag{3}$$

In Eq. (3) the Reynolds number Re is defined using the hydraulic diameter $d_h = 2d$.

The solution (2), which is based on a fully developed velocity profile, is very accurate for high Prandtl number liquids. For small Prandtl numbers, Eq. (2) underestimates heat transfer near the inlet, but for long channels it is very accurate [Shah et al. 1978]. For air with $Pr \approx 0.7$, Eq. (2) gives an exact result when $x^* > 0.01$. A very accurate correlation of the mean Nusselt number for an isothermal channel is [Shah et al. 1978]

$$Nu_{m,T} = 7.55 + \frac{0.024(x^*)^{-1.14}}{1 + 0.0358(x^*)^{-0.64}\,Pr^{0.17}} \tag{4}$$

which also takes into account hydrodynamically developing velocity profile. Equation (4) is given because by using the mean heat transfer coefficient from Eq. (4), very good approximate results are obtained for the fin design. The heat transfer rate from an isothermal channel with wall temperatures T_s and the length L are obtained from equation

$$\dot{Q} = \rho c_p V d\,(T_s - T_0)\big(1 - \exp\big(-4L^* Nu_{m,T}\big)\big) = \rho c_p V d(T_m(x,z) - T_0) \tag{5}$$

where the non-dimensional length is defined

$$L^* = \frac{L}{RePrd_h} \tag{6}$$

Because the energy equation, the solution of which is Eq. (2), is linear for a fully developed velocity profile, the superposition principle can be used to derive the solution for arbitrarily varying surface temperature [Kays et al. 2005]

$$\dot{q}(x,z) = \frac{4k_f}{d_h} \sum_{n=0}^{\infty} G_n \left(\theta_0(0,z)\exp(-2\lambda_n^2 x^*) + \int_0^{x^*} exp\big(-2\lambda_n^2(x^* - \xi)\big)\frac{\partial\theta(\xi,z)}{\partial\xi}d\xi \right) \tag{7}$$

If the channel wall temperature $\theta = T(x,z) - T_0$ is known, the local heat flux is obtained from Eq. (7). The total heat transfer from the channel wall to the flow is also obtained from Eq. (7) by integrating it as a function of distance. The mean fluid temperature is obtained as

$$T_m(x,z) - T_0 = 2 \int_0^x \dot{q}(x,z)dx/(\rho c_p V d) \tag{8}$$

Now, the wall and mean fluid temperatures are known and heat transfer coefficients can be calculated everywhere

$$h(x,z) = \dot{q}(x,z)/\big(T(x,z) - T_m(x,z)\big) \tag{9}$$

When these are substituted into heat conduction Eq. (1), we obtain the equations which give the new temperature of the fin array. If the result from the solution $\bar{T} = A^{-1}\bar{b}$ is not the same as the original temperature distribution, new heat fluxes are solved from Eq. (7) and the process is repeated.

For **turbulent flow**, a similar type of solution as that for the laminar one exists, but the eigenvalues and eigenfunctions depend on the Reynolds number. In many cases an assumption of a constant heat transfer coefficient obtained, for instance, from the Gnielinski correlation [Hewitt 1998]

$$Nu_m = \frac{\left(\frac{f}{2}\right)(Re - 1000)Pr}{1 + 12.7\sqrt{\frac{f}{2}}(Pr^{2/3} - 1)}\left[1 + (d_h/x)^{2/3}\right] \tag{10}$$

can be used. In Eq. (10), f is the friction factor of a fully developed turbulent flow. For turbulent flow, heat transfer coefficients are calculated from Eq. (10) and substituted into Eq. (1), as in the laminar case.

Pressure drop   If the pressure drop across the array is the focus of interest, it consists of three parts: inlet loss, friction loss in a channel and exit loss. The apparent friction factor caused by the wall friction and velocity profile development can be solved for laminar flow using the correlation [Shah et al. 1978]

$$f_{app}Re = 3.44(x^+)^{-1/2} + \frac{\frac{0.674}{4x^+} + 24 - 3.44(x^+)^{-1/2}}{1 + 0.000029(x^+)^{-2}} \tag{11}$$

where

$$x^+ = \frac{x}{Red_h} \tag{12}$$

In addition to friction above, losses are also caused at the channel inlet and outlet. The inlet losses are especially difficult to evaluate because they depend on the shape of the inlet geometry, i.e., is there flow separation. If it is assumed that there are no losses at the inlet, the overall pressure drop can be expressed as

$$\Delta p = \frac{1}{2}\rho V^2(4x^+ f_{app}Re + \sigma^2 - 2\sigma\beta + 1) \tag{13}$$

In Eq. (13), $\sigma = d/(d + t)$ is the contraction ratio and β the correction factor of momentum. For fully developed velocity profile when $L^+ \geq 0.015$, its value is 1.2. Details concerning the evaluation of inlet and exit losses are found in the literature [Webb 2006].

For turbulent flow $\beta \approx 1$ at the exit and the flow development is very rapid in the inlet region. Thus, the first assumption is to use the friction factor of a fully developed turbulent flow

$$f = \frac{1}{4} (1.82 \log_{10} Re - 1.64)^{-2} \tag{14}$$

A slightly more accurate result for a parallel plate channel flow is obtained if, in the equation above, the Reynolds number is calculated using $0.64d_h$ as a characteristic length instead of d_h [White 1986].

RESULTS

The validity of the method presented above has already been tested for laminar flows. Next, some results of the proposed approach for turbulent flows concerning calculation times are compared to those needed in purely numerical solutions. Problems in numerical modeling are also discussed. Only one channel with an isothermal base plate is modeled when a comparison between the present method and numerical modeling is made. In addition, the results for the same array when a heat generating component is located on the base plate is compared to measured data.

Test case 1 The test case is an aluminum array shown in Fig.1 with dimensions $t = 2$ mm, $d = 3$ mm, $l = 110$ mm and $L = 300$ mm. Other values in the calculations were: $T_B = 373$ K, $T_0 = 300$ K and constant thermal properties $\rho = 1.14$ kg/m^3 , $k_f = 0.0274$ W/mK , $\mu = 1.886 \times 10^{-5}$ Pas, $k = 200$ W/mK and $c_p = 1005$ J/kgK.

For numerical modeling a commercial computer code Fluent was used. Since the base plate temperature is constant, only one half of the channel and fin needs to be considered. The grid was refined in the flow direction near the channel inlet and also after the channel exit. The number of control volumes affects the result, which is shown in Fig. 3. Grid independence for heat transfer and pressure loss was examined by calculating the same case with different grids and comparing the mean temperature rise, i.e., the temperature distribution integrated over the channel exit area in an array $\Delta T = T_{m,out} - T_0$ and the total pressure loss Δp. The smallest grid contained 4410 control volumes and the largest one 1008000. It can be seen that when the number of control volumes is greater than $5 \cdot 10^5$ we have a grid-independent result.

It was also noticed that in the standard k-epsilon method, an enhanced wall treatment [Chen et al. 1988] was required in order to get the solution to converge. If use is made of standard wall functions, the increase in control volumes does not give convergence. As a matter of fact, it is very difficult to know what theories commercial codes are using.

In the proposed model only 450 control volumes were needed in a fin; 30 control volumes in the x-direction and 15 control volumes in the z-direction. Table 2 shows a comparison between different methods for the temperature change and pressure drop in the channel. Corresponding fin temperature distributions are also shown in Fig. 4.

Table 2.
Results of purely numerical solution and proposed model

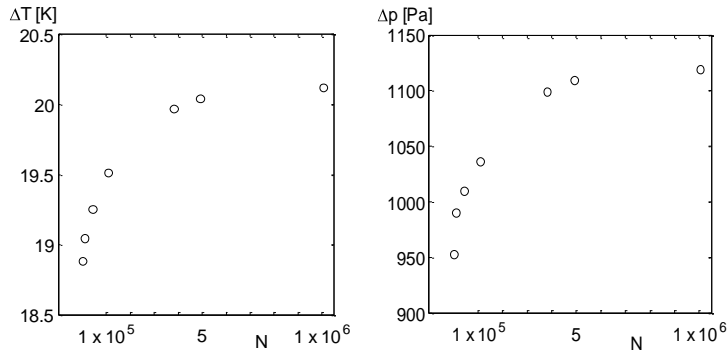| Quantity	numerical	Current Method	Difference
ΔT [K]	19.96	19.19	$-3.9\,\%$
Δp [Pa]	1099	1013	$-7.8\,\%$

Figure 3. Effect of control volumes on outlet temperature (left) and pressure loss (right).
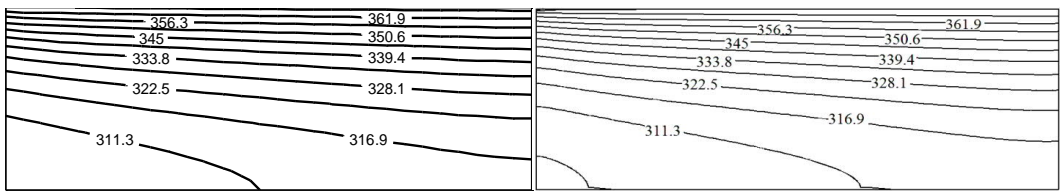

Figure 4. Fin temperature distribution of test case. Current method (left) and numerical solution (right).

On the basis of Table 2 and Fig. 4, it can be concluded that the proposed model is accurate enough for practical design purposes. It should also be noted that the results of numerical modeling depend very much on the type of turbulence model adopted. As regards time consumption, the current method is several orders of magnitude faster than purely numerical modeling.

Test case 2 The results of the present method are also compared to measurements made with a real heat sink. The geometry of the array was the same as in Test Case 1. The component, which generates constant heat flux of $\dot{Q} = 1200\text{ W}$ was located on the base plate, 50 mm from the leading edge in Fig 1. The component length was 104 mm and its width was the same as the base plate width, 134 mm. Altogether the array contained 27 fins and the base plate, the thickness of which was 20 mm. Temperature was measured with thermocouples in the base plate at its center line, 3 mm under the lower surface. The Reynolds number in the measurements was $Re = 7100$ and the inlet air temperature $T_0 = 24\ ^\circ\text{C}$.

The calculated temperature distribution at the center line in Fig. 5 is in reasonable agreement with the measurements. There is one point that differs but this may be due to a measurement error. However, the pressure loss calculation differed from the measured data. The measured value was 435 Pa but the calculation gave a value of 501 Pa. The reason for this may be that the velocity distribution before the test section was not uniform.
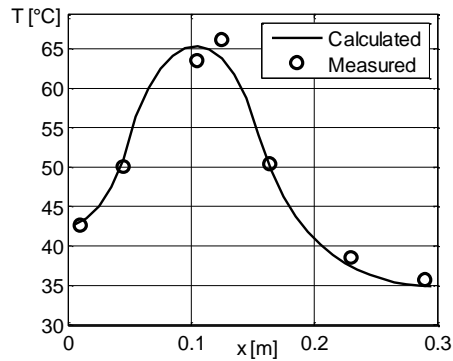
Figure 5. Measured and calculated temperature at center line of base plate.

CONCLUSIONS

In the paper a method is presented in which analytical solutions for fluid flow and forced convection are applied simultaneously with the numerical calculation of conduction in a solid. The solution procedure of conjugated convection and conduction problem is given. The method is suitable for laminar and turbulent flows. An essential advantage of the method presented is that the solution time of a three dimensional problem is very small. Thus, it is very suitable for multiobjective optimization where heat transfer, pressure drop, the amount of material or array volume must be simultaneously optimized.

It is important to note that the results obtained by using the simple method presented in the paper do not differ much from the results obtained with CFD modeling. It should also be noted that in the case of a turbulent flow, numerically obtained results are also very sensitive to the turbulence model adopted. Differences of the same magnitude may be obtained using different values for thermal properties in practical calculations. CFD calculations require much more time. This means that purely numerical modeling is an impractical tool for optimization. In practical fin arrays the temperature field is three dimensional and every fin and the base plate must be modeled, which entails very many control volumes, depending on the size of fin array. In such cases the overall design time of industrial fin array applications is long because optimization involves calculating hundreds of solutions in order to achieve good results. The method presented here can also be used in transient cases by assuming a quasi-static treatment in which the heat capacity of fluid is ignored. This type of assumption is valid especially for gases [Karvinen 1988].

REFERENCES

Bejan, A., Sciubba, E. [1992], The optimal spacing of parallel plates cooled by forced convection, *Int. J. of Heat and Mass Transfer*, Vol. 35, No. 12, pp 3259-3264.

Chen, H. C., Patel, V. C. [1988], Near-Wall Turbulence Models for Complex Flows Including Separation, *AIAA Journal*, Vol. 26, No. 6, pp 641-648.

Hewitt, G. F. [1998], *Heat Exchanger Design Handbook*, Begell House.

Kays, W., Crawford, M., Weigand, B. [2005], *Convective Heat and Mass Transfer 4th edition*, McGraw Hill, NY.

Kays, W., London, A. L. [1964], *Compact heat exchangers*. McGraw-Hill.

Karvinen, R. [1988], Transient Conjugated Heat Transfer to Laminar Flow in a Tube or Channel, *Int. J. Heat and Mass Transfer*, Vol. 31, No. 6, pp. 1326-1328.

Karvinen, R., Karvinen T. [2010], Optimum geometry of fixed volume plate fin for maximizing heat transfer, *Int. J. Heat and Mass Transfer*, Vol. 53, No. 23-24, pp. 5380-5385.

Li, J., Peterson, G.P. [2007], 3-Dimensional numerical optimization of silicon-based high performance parallel microchannel heat sink with liquid flow, *Int. J. of Heat and Mass Transfer*, Vol. 50, pp. 2895-2904.

Lindstedt, M., Karvinen, R., 2011. Optimization of fin arrays. Proc. of BHTC2011, 6th Baltic Heat Transfer Conference, Aug. 24-26 2011 Tampere, Finland.

Lindstedt, M., Karvinen, R., Optimization of isothermal plate fin array with laminar convection. *Journal of Enhanced Heat Transfer*, in print.

Lehtinen, A. [2005], Analytical Treatment of Heat Sinks Cooled by Forced Convection, *PhD. Thesis*, TUT Publication 579, Tampere University of Technology, Tampere.

Ryu, J.H., Choi, D.H., Kim, S.J. [2002], Numerical optimization of the thermal performance of a microchannel heat sink, Int. *J. Heat and Mass Transfer*, Vol. 45, pp. 2823-2827.

Shah, R. K., London, A. L. [1978], *Laminar flow Forced Convection in ducts*, Academic Press, NY.

Teertstra, P., Yovanovich, Culham, J.R. [2000], Analytical forced convection modeling of plate fin heat sinks, *J. Electronics Manufacturing*, Vol. 10, No. 4, pp. 253-261.

Wang, Z.-H., Wang, X.-D., Yan, W.-M., Duan, Y.-Y., Lee, D.-J., Xu, J.-L. [2011], Multi-parameters optimization for microchannel heat sink using inverse problem method, *Int. J. Heat and Mass Transfer*, Vol. 54, pp. 2811-2819.

Webb, R. [2006], Entrance and Exit Losses for Developing Flow in Parallel Plate Channels, *Heat transfer Eng*., Vol. 27, No. 10, pp. 30-35.

White, F. [1986], *Fluid Mechanics*, McGraw-Hill.

Publication II

Reijo Karvinen, Kaj Lampio

Multi-objective optimization of electronics heat sink geometries

Proceedings of IWHT 2013, October 18-21, 2013, Xi'an, China. Invited lecture.

IWHT2013-003

Multi-objective optimization of electronics heat sink geometries

Reijo Karvinen*, Kaj Lampio

Tampere University of Technology, Finland.
P.O. Box 589, 33101 Tampere, Finland

(*Corresponding Author: reijo.karvinen@tut.fi)

Abstract

Fins and fin arrays, which are used to enhance heat transfer, should be small in weight and volume, and the fans, which create flow, should consume little energy. Furthermore, to prevent failure, component temperatures during operation should be below limiting values. These are conflicting requirements, and in designing optimum cooling equipment, multi-objective tools are often needed. This paper introduces and shows use in optimization of an efficient method that combines analytical treatment of convection and numerical calculation of conduction. It discusses the principles of multi-objective optimization and applies a special algorithm to find optimum geometries for cooling fin arrays in power electronics. Only turbulent flow is considered because especially if the mass or volume of the array is minimized, the flow must be turbulent.

Keywords: Fin array, Heat sink, Multi-objective optimization, Turbulent flow

1 Introduction

Heat dissipation from electronics components has increased significantly during recent years. A typical heat sink used for cooling is shown in Fig. 1, where components are located on the lower surface of the base plate. The amount of material, compact size, and power required by the fan are the most important factors in industrial design. Limiting factors in optimization are the temperature the components can withstand and the fan power, which should be low to reduce operational costs. In practical applications, components with different heat dissipation rates are located on the base plate. Thus in many cases, simple boundary conditions such as isothermal base or constant heat flux on the base plate fail to describe the problem. In addition, if the amount of material is minimized, the fins are not isothermal, and no analytical solutions are then available for this type of problem.

Numerical solutions exploiting commercial codes can be used to optimize heat sinks with many heat generating components located in arbitrary locations on the base plate. Thus the temperature field in a fin array is three-dimensional. In modeling practical designs, the whole system must be modeled because one cannot use symmetry and solve the flow and temperature fields only in one channel. Whole system modeling therefore produces a truly time-consuming optimization problem because typically at least several hundred individual cases must be solved to obtain a solution approaching the desired optimum.

An efficient method by Karvinen and Lampio [1] to evaluate heat transfer in fin arrays combines analytical treatment of convection and numerical treatment of conduction. In the present paper, the method is adopted for multi-objective optimization to find an optimal array geometry. A similar approach was applied to optimizing single fins by Karvinen and Karvinen [2] and designing an isothermal array with laminar flow by Lindstedt and Karvinen [3]. The present paper focuses on the treatment of an isothermal 3D array.
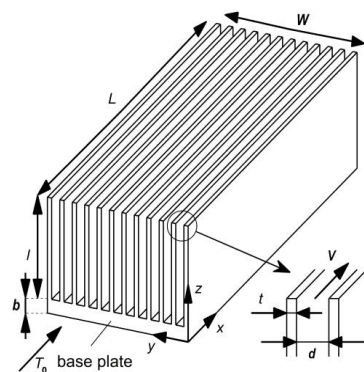

Fig. 1 Plate fin array

Many authors have proposed methods to calculate and optimize heat sinks. For example, Bejan and Sciubba [4] optimized heat transfer in an isothermal fin array with laminar flow and Bejan and Morega [5] with turbulent flow when the pressure drop and fin array width were fixed. Mereu et. al [6] showed optimal fin spacing results for an isothermal fin array, keeping pressure loss, mass flow, or pumping power as constants. Later, Kim and Kim [7] reported closed-form analytical optimization results for non-isothermal micro channel fin arrays with laminar flow, whose Reynolds number was low and whose ratios of channel width to height and fin material conductivity to fluid material conductivity were high.

Numerical optimization using analytical correlations has been the subject of many studies. Liu and Garimella [8] presented five approximate analytical methods to optimize micro channel heat sinks and compared the results with those obtained using a CFD model. Lindstedt and Karvinen [9] introduced optimal solutions for a non-isothermal fin array with an isothermal base plate, whose thermal resistance was minimized using a fin efficiency model for fin arrays with an isothermal base plate. The possibility to adopt the fin efficiency concept for designing fin arrays was originally presented by Teertstra et. al [10]. However, the basic idea is difficult to grasp on the basis of that paper. Lehtinen [11] introduced an analytical method for a non-isothermal fin array with discrete heat sources on the base plate, where 3D heat conduction in the base plate and 2D in the fins were solved simultaneously using a truncated Fourier series expression for temperature. Purely numerical calculations and optimization results of heat sinks have been proposed by many authors, for example, Ryu et. al [12], Wang et. al [13], and Li et. al [14].

In the present paper, the model in [1] was used to optimize typical fin arrays in industrial applications. Basically, convection was here treated with analytical equations and only conduction in the array was solved numerically. Solution was very rapid compared to a purely numerical solution of flow and temperature distributions in the channel. As an example, the method was applied to two industrial cases where the maximum temperature and sink mass were minimized. Because of two simultaneously minimized criteria, a multi-objective optimization method was adopted using the modified MOPSO optimization algorithm. The fan power was kept constant.

The first case was a single 1200 W heat source with the same width as the base plate. The second case consisted of two 100×100-mm discrete heat sources of 550 W and 450 W, which were smaller than the base plate, yielding a 3D problem. The cross-sections of the fins were either straight rectangular or triangular. A straight rectangular shape was easiest to manufacture, but a triangular shape may also be used in special applications. Thanks to optimization, significantly less material was required.

Nomenclature

a_0	Constant in fan curve Eq. (16) [Pas/m³]
b	Base plate thickness [m]
C	Constant in fan curve Eq. (16) [Pa]
c_1	Uniform random number in range [0, 2]
c_2	Uniform random number in range [0, 2]
c_3	Inertia coefficient
c_p	Specific heat of fluid [J/kgK]
d	Channel width [m]
d_h	Hydraulic diameter $d_h = 2d$ [m]
$d_{i,h}$	Euclidian norm between members i and h
f	Fanning friction factor $f = \tau_s/(\frac{1}{2}\rho V^2)$
$f(\mathbf{x})$	Objective function
f_{max}	Constant in external penalty function
$\mathbf{g}(\mathbf{x})$	Vector of inequality constraints
h	Heat transfer coefficient [W/m²K]
$\mathbf{h}(\mathbf{x})$	Vector of equality constraints
k	Thermal conductivity of solid [W/mK]
k_f	Thermal conductivity of fluid [W/mK]
L	Length of fin array [m]
l	Height of fin [m]
L_c	Length of component cluster [m]
m	Mass of heat sink [kg]
N	Number of fins
Nu_m	Average Nusselt number
PBESTS[ ]	Vector of personal Pareto optimal solutions of swarm members
Pr	Prandtl number $Pr = \nu / \alpha$
Re	Reynolds number $Re = Vd_h / \nu$
REP[ ]	Repository vector for Pareto optimal solutions
t	Fin thickness [m]
T_0	Temperature [°C]
T_∞	Temperature of environment [°C]
t_b	Fin thickness at base plate [m]
$T_{i,j}$	Temperature at location i,j [°C]
T_m	Fluid mixed mean temperature [°C]
T_{max}	Maximum temperature of heat sink [°C]
t_t	Fin thickness at fin tip [m]
V	Average Velocity [m/s]
$\mathbf{V}_{i,k}$	Velocity of swarm member i at time step k
W	Width of base plate [m]
W_c	Width of component cluster [m]
x	Streamwise coordinate [m]
$\mathbf{x}$	Vector of design variables
X	Distance of component cluster from x = 0 [m]
$\mathbf{x}_{i,k}$	Location of swarm member i at time step k
$\mathbf{x}_l$	Lower boundary values of design space
$\mathbf{x}_u$	Upper boundary values of design space
Y	Distance of component cluster from y = 0 [m]
y, z	Cartesian coordinates (Fig 1.)
α	Thermal diffusivity $\alpha = k_f/\rho c_p$ [m²/s]
Δp	Pressure loss [Pa]
$\Delta x, \Delta y, \Delta z$	Lengths of control volumes [m]
ν	Kinematic viscosity [m²/s]
ρ	Density of fluid [kg/m³]
ρ_b	Density of the material in the base plate [kg/m³]
ρ_f	Density of the material in the fin [kg/m³]
Φ	Heat dissipation [W]
Ω	Feasible area

2 Calculation model

2.1 Calculation of heat transfer and pressure drop

The details of the model combining analytical and numerical solutions can be found in [1]. Heat conduction in the base plate and fins was solved numerically using a 3D and a 2D finite difference method, respectively. The finite-difference equation governing the fin temperature $T_{i,j}$ at the location (i,j) in Fig. 2 is as follows

$$\frac{k}{\Delta z}\left(T_{i,j+1}-T_{i,j}\right)t\Delta x+\frac{k}{\Delta z}\left(T_{i,j-1}-T_{i,j}\right)t\Delta x$$
$$+\frac{k}{\Delta x}\left(T_{i+1,j}-T_{i,j}\right)t\Delta z+\frac{k}{\Delta x}\left(T_{i-1,j}-T_{i,j}\right)t\Delta z \qquad (1)$$
$$+h_1\left(T_{m1}-T_{i,j}\right)\Delta x\Delta z+h_2\left(T_{m2}-T_{i,j}\right)\Delta x\Delta z=0,$$

where T_{m1} and T_{m2} are the mixed mean temperatures of fluid, and h_1 and h_2 heat transfer coefficients.
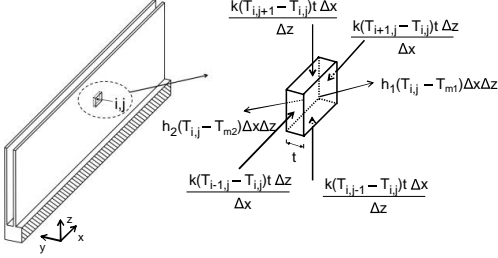
Fig. 2 Heat balance in fin

A similar equation was obtained for the base plate, but now the y-conduction term had to be included. In Eq. (1) above, heat transfer coefficients h_1 and h_2 are assumed to be known. In turbulent flow, they can be assumed to be independent of the fin temperature distribution and are obtained, e.g., from the Gnielinski correlation [15]

$$Nu_m=\frac{hd_h}{k_f}=\frac{\left(\frac{f}{2}\right)(Re-1000)Pr}{1+12.7\sqrt{\frac{f}{2}}\left(Pr^{2/3}-1\right)}\left[1+\left(d_h/x\right)^{2/3}\right]. \quad (2)$$

Heat dissipation from components was given as a boundary condition on the base plate surface, where the component was located. Other surfaces were insulated. The friction factor in Eq. (2), used also in pressure loss calculations, is [16]

$$\frac{1}{(4f)^{1/2}}=2.0\log_{10}\left(0.64\,Re_{d_h}\,(4f)^{1/2}\right)-0.8\,. \quad (3)$$

Since the heat transfer coefficients and mean fluid temperatures were known everywhere in an array, the temperature distribution of fins and base plate was governed by the system of finite difference equations (1), in matrix notation $\mathbf{AT}=\mathbf{b}$, from which $\mathbf{T}$ could be solved. The solution procedure started by assuming the fin temperature $T(x,z)$. An isothermal guess was a good starting point. After that fluid mean temperatures T_{m1} and T_{m2} needed in Eq. (1) were obtained by solving the energy balance equation in a channel.

When the fin temperature $T(x,z)$, heat transfer coefficient $h(x,z)$ and $T_m(x,z)$ were known, a new mean temperature T_m^n was obtained from equation

$$\rho c_p Vd\frac{\partial T_m^n}{\partial x}=q(x,z)\,, \quad (4)$$

where

$$q(x,z)=2h(x,z)(T(x,z)-T_m(x,z))\,. \quad (5)$$

In Eq. (5) above $T(x,z)$ is the mean value of channel wall temperatures.

In addition to the friction loss, the leading and trailing edges can also cause losses. Generally, the pressure drop needed to evaluate fan power is obtained from the equation

$$\Delta p=\frac{1}{2}\rho V^2\left(4x^+f_{app}\,Re+\sigma^2-2\sigma\beta+1\right), \quad (6)$$

where the leading edge loss is ignored. In Eq. (6), $\sigma=d/(d+t)$ is the contraction ratio and β the correction factor of momentum. For a fully developed laminar velocity profile, the latter value is $\beta=1.2$. Dimensionless length is defined as $x^+=x/(d_h\,Re)$, and f_{app} is the apparent mean friction factor, which takes into account the effects of surface shear stress and flow acceleration. Details about evaluating inlet and exit losses are found in the literature [17].

For a turbulent flow, $\beta\approx1$ at the exit and the developing length for flow is short in the inlet region. Thus for a turbulent flow, $f_{app}\approx f$ and the friction factor of a fully developed turbulent flow in Eq. (3) can be used. The above model is valid also for a laminar flow, but then heat transfer coefficients in Eq. (1) depend on the fin surface temperature and must be calculated for each point (i,j) individually.

2.2 Comparison of proposed model with CFD solution

The results of our method and a CFD solution were compared in an array with an isothermal base plate in [1]. The test case was an aluminum array in Fig. 1 with dimensions t = 2 mm, d = 3 mm, l = 110 mm, and L = 300 mm. Other values in the calculations were Re = 10000, T_B = 373 K, T_0 = 300 K, and constant thermal properties ρ = 1.14 kg/m³, k_f = 0.0274 W/mK, μ = 1.866 $\cdot 10^{-5}$ Pas, c_p = 1005 J/kgK and material properties for solid ρ_f = 2700 kg/m³ and k = 200 W/mK.

For a CFD solution, a commercial computer code Fluent was used. Since the base plate temperature was constant, only one half of the channel and fin needed to be considered. The grid was refined in the flow direction near the channel inlet and after the channel exit. The grid independence for heat transfer and pressure loss was examined by calculating the same case with different grids and by comparing the mean temperature rise $\Delta T = T_{m,out} - T_0$, i.e., the temperature distribution integrated over the channel exit area in an array and the total pressure loss Δp. The number of control volumes affected the results, as shown in Fig. 3. The smallest grid consisted of 4410 control volumes and the largest 1008000. We observed that when the number of control volumes was greater than $5\cdot10^5$, the solution became grid-independent.

In contrast, in the proposed model only 450 control volumes were needed in a fin: 30 control volumes in the x-direction and 15 in the z-direction. Fig. 4 shows the fin temperature distributions obtained with our model and those with the commercial Fluent code. The agreement is very good. The calculation time between the presented method and the CFD solution differed several orders of magnitude. The validity of the proposed model was also verified experimentally [1].
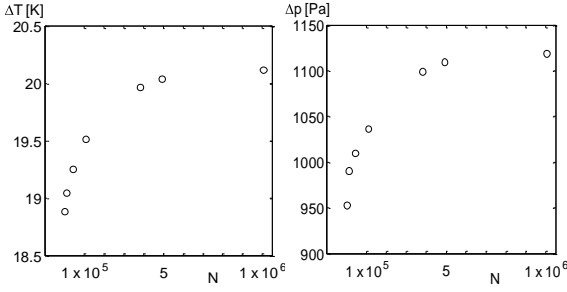
3

Fig. 3 Effect of number of control volumes on outlet temperature (left) and pressure loss (right) in CFD solution.
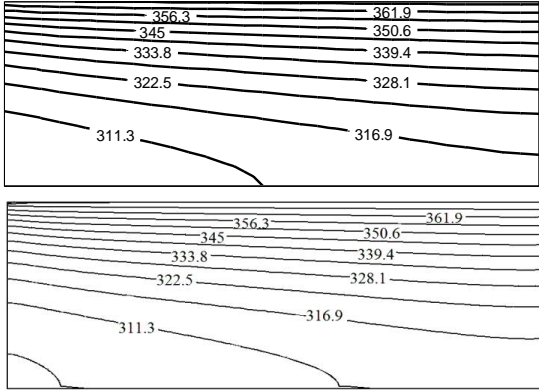

Fig. 4 Fin temperature distributions with proposed method (top) and CFD solution (bottom).

3 Optimization

3.1 Multi-objective optimization

Multi-objective optimization embraces at least two (usually) conflicting criteria, which are minimized simultaneously. A multi-objective optimization problem is in general formulated as follows

$$\text{minimize} \quad \mathbf{f}(\mathbf{x}) = \left(f_1(\mathbf{x}), f_2(\mathbf{x}),...,f_m(\mathbf{x})\right)^{\mathrm{T}}$$
$$\mathbf{x} = \left(x_1, x_2,...,x_n\right)^{\mathrm{T}} \in \Omega, \tag{7}$$

where $\mathbf{f}(\mathbf{x})$ is an objective function vector and $\mathbf{x}$ is the design variable vector. It differs from single objective optimization in that it comprises many objective functions whereas single objective optimization has only $f_1(\mathbf{x})$. A feasible region is defined as

$$\Omega = \{\mathbf{x}_l \le \mathbf{x} \le \mathbf{x}_u : g_i(\mathbf{x}) \le 0, i = 1,2,...,n_{ie};$$
$$h_j(\mathbf{x}) = 0, j = 1,2,...,n_{ec}\}, \tag{8}$$

where $\mathbf{g}(\mathbf{x})$ is a vector of inequality constraints, and $\mathbf{h}(\mathbf{x})$ is a vector of equality constraints.

In multi-objective optimization, a set of optimal solutions in a design space is called Pareto optimal solutions. The design variable vector $\mathbf{x}^* \in \Omega$ is Pareto optimal only if no other vector $\mathbf{x} \in \Omega$ exists to satisfy the conditions [18].

$$f_i(\mathbf{x}) \le f_i(\mathbf{x}^*) \quad \text{for all i} = 1,...,m \quad \text{and}$$
$$f_i(\mathbf{x}) < f_i(\mathbf{x}^*) \quad \text{for at least one i} = 1,...,m. \tag{9}$$

Multi-objective optimization can also be performed by adopting a single objective optimization algorithm using the method in which one criterion is set as a constraint and the other is minimized. When the constrained value is varied, different optimal solutions are found. A multi-objective optimization algorithm has the advantage that it produces all the Pareto optimum solutions at the same time, making the procedure thus faster than if constrains were changed individually in a single-objective method.

Fig. 5 shows Pareto optimal solutions in a criteria space in bold line. The ideal point is obtained by minimizing all the criteria individually. The nadir point consists of all the maximum objective function values of the Pareto optimal set. Ideal and Nadir points may be used to normalize the criteria so that the order of magnitude of objective values is about the same.
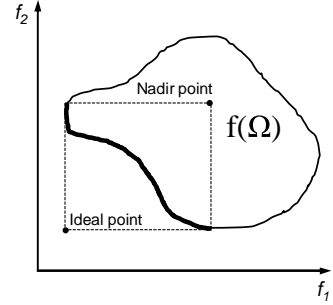

Fig. 5 Pareto optimal solutions in a criterion space (bold line). Image of feasible set Ω in a criterion space [18].

A constrained optimization problem can be converted to an unconstrained optimization problem using an exterior penalty function. In this method, evaluation of the object function $f_i(\mathbf{x})$ is replaced by $F_i(\mathbf{x})$:.

$$F_i(\mathbf{x}) = \begin{cases} f_i(\mathbf{x}) & \mathbf{x} \in \Omega \\ f_{max} + \sum_{i=1}^{n_{ie}} \max\left[0, g_i(\mathbf{x})\right] & \text{otherwise} \end{cases} \tag{10}$$

The evaluation differs from $f_i(\mathbf{x})$ in those solutions that are not located within the feasible area. For those solutions, a large penalty constant f_{max} is added to the sum of inequality constraints, which are greater than zero. The value of penalty constant f_{max} is set as the largest upper bound of design variables. [19]

Various multi-objective optimization algorithms can be found in the literature. We used here a modified version of multi-objective particle swarm optimization (MOPSO) algorithm.

3.2 Particle Swarm Optimization

Particle swarm optimization (PSO) algorithms are based on the social behavior of many species in nature such as schooling of fish and flocking of birds. The first paper on the PSO algorithm was published by Kennedy and Eberhart [20]. Later,

4

Shi and Eberhart [21] introduced a modified version of this algorithm with an inertia component, which improved its performance. These early PSO versions were developed for single-objective optimization problems. The best known multi-objective optimization version of the PSO algorithm (MOPSO) was introduced by Coello Coello et. al [22].

In the MOPSO algorithm, a swarm consists of N particles in the design space. Particle locations are updated at different time steps k and the values of design vectors represent these locations. The algorithm is initialized by scattering the particles randomly inside the design space and by setting the velocities of the particles to zero.

$$\mathbf{x}_{i,k=0} = \mathbf{x}_l + \mathbf{r}(\mathbf{x}_u - \mathbf{x}_l), \quad i=1,...,N$$
$$\mathbf{V}_{i,k=0} = 0, \quad i=1,...,N. \tag{11}$$

In the above equation, $\mathbf{r}$ is a vector of uniform random numbers in the range of [0, 1]. The design space boundary values are within the limits of $[\mathbf{x}_l, \mathbf{x}_u]$.

After initialization, new locations are calculated for the next time step k+1 as follows:

$$\mathbf{x}_{i,k+1} = \mathbf{x}_{i,k} + \mathbf{V}_{i,k+1}$$
$$\mathbf{V}_{i,k+1} = c_1(\text{REP}[h] - \mathbf{x}_{i,k}) + c_2(\text{PBESTS}[i] - \mathbf{x}_{i,k}) + c_3\mathbf{V}_{i,k}, \tag{12}$$

where REP is the repository for all Pareto optimal solutions found by the swarm, and PBESTS is the current personal Pareto optimal solution found by a swarm member i. Variables c_1 and c_2 are uniform random numbers in the range of [0, 2], and c_3 is a function of time step $c_3 = f(k)$. The initial value of variable c_3 is usually set as $c_{3,0} = 1.4$.

We used a modified version of the MOPSO. In this modified version the target individual h, from the repository (REP[h]), for the individual i is determined as the second nearest Pareto optimal solution in the design space measured by the Euclidian norm [23]

$$d_{i,h} = \sqrt{\sum_{j=1}^{N} \left[\frac{\text{REP}[h]_j - x_{i,j}}{x_{u,j} - x_{l,j}} \right]^2}. \tag{13}$$

Moving inside the design space, particles may collide with the space boundaries. If a particle crosses the boundary limit of any component, the value of the crossed component is set as a boundary value, and the velocity vector is set equal to zero. Usually, velocity also has its maximum limit. If the limit is exceeded, the length of the velocity vector is set to the maximum value $|\mathbf{V}| = V_{max}$.

4 Optimization of heat sink

The maximum allowed temperature of the heat sink (limited by component failure), the mass of the heat sink (material costs), and pressure loss or fan power (operating costs) are important criteria in optimizing industrial fin arrays. In our study, the maximum temperature and the total mass of the heat sink were minimized while the fan power was fixed.

The multi-objective industrial fin array optimization problem was formulated in a set of equations (14) (see also Figs. 1 and 6). Fig. 6 shows a dotted line area where the components are located. It can move freely during optimization. Inside this area, the relative locations of components are fixed.

find $\mathbf{x} = (L, W, b, N, t_b, t_t, l, X, Y)^T$

to minimize $\mathbf{f} = (T_{max}(\mathbf{x}), m(\mathbf{x}))^T$

subject to

$$\Omega = \{\mathbf{x} \in \mathfrak{R}^9 \mid \mathbf{x}_l \le \mathbf{x} \le \mathbf{x}_u; g_i(\mathbf{x}) \le 0, i=1,2,...,7\}$$

$$\mathbf{x}_l = (L_{min}, W_{min}, b_{min}, N_{min}, t_{b,min}, t_{t,min}, l_{min}, 0, 0)^T$$

$$\mathbf{x}_u = \begin{pmatrix} L_{max}, W_{max}, b_{max}, N_{max}, t_{b,max}, t_{t,max}, \\ l_{max}, L_{max} - L_c, W_{max} - W_c \end{pmatrix}^T$$

$$g_1 = LWb\rho_b + NLl\rho_f \frac{t_b + t_t}{2} - m_{max} \le 0 \tag{14}$$

$$g_2 = -\left(LWb\rho_b + NLl\rho_f \frac{t_b + t_t}{2} - m_{min} \right) \le 0$$

$$g_3 = b + l \le 0$$

$$g_4 = d_{min} - \frac{W - Nt_b}{N-1} \le 0$$

$$g_5 = d_{min} - \frac{W - Nt_t}{N-1} \le 0$$

$$g_6 = X + L_c - L \le 0$$

$$g_7 = Y + W_c - W \le 0$$

where L, W, and b are the length, width, and thickness of the base plate, respectively, N is the number of fins, t_b is the fin thickness at the base plate and t_t at the fin tip. The fin height is l. The locations of components in the x- and y-directions are X and Y, respectively. The mass is calculated as

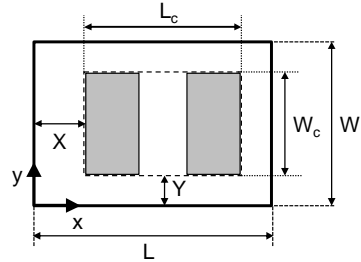$$m = LWb\rho_b + NLl\rho_f \frac{t_b + t_t}{2}. \tag{15}$$

Fig. 6 Coordinates X and Y of a component cluster at base plate.

4.1 Results

Two fin arrays (Figs. 7 and 10) were optimized. The problem in Fig. 7 was practically two-dimensional and the other in Fig. 10 three-dimensional. Optimization was performed with two different fin shapes: rectangular and triangular. The fin thickness of the former was the same at tip and base, i.e., equal to t_b. The thickness of the latter varied linearly from tip to base, where it is t_b (see Fig. 9).

The maximum temperature and mass of the heat sink were the criteria for optimization. The fan characteristic curve was approximated as

$$\Delta p = a_0 Q + C, \tag{16}$$

where a_0 and C are constants. In following cases, values for constants were selected as a_0 = -1000 Pas/m³ and C = 400 Pa to ensure turbulent flow in channels. The heat flux from components to the base plate was assumed to be uniform. The heat sink material was aluminum.

4.2 Case 1

We started optimization with the fin array in Fig. 7, in which one component of size 104×132 mm dissipated the total heat flux Φ = 1200 W. The goal was to design a new array with a smaller mass but with the same maximum temperature, fixed by the component (details of the original configuration in Table 1).

T_{max} = 71.8 °C
Δp = 274 Pa
Φ = 1200 W
Heat generation
132 mm
122 mm
N = 30
150 mm
2 mm
air T_∞ = 27 °C
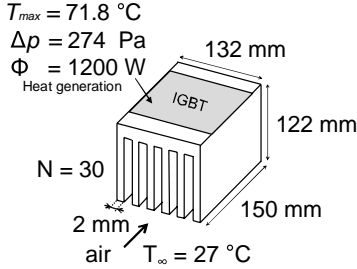
Fig. 7 Reference heat sink 1: m = 3.31 kg

Multi-objective optimization shows that the current design is not good. If the maximum temperature is held constant for rectangular fins, a smaller mass with the same performance can be achieved by choosing a new design based on optimization.

T_{max} = 71.8 °C
Δp = 324 Pa
Φ = 1200 W
Heat generation
135 mm
55 mm
N = 59
115 mm
0.77 mm
air T_∞ = 27 °C
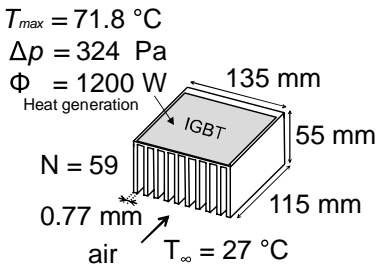
Fig. 8 Optimized array with rectangular fins: m = 0.78 kg

The new geometry is shown in Fig. 8, and the corresponding dimensions are given in Table 1. The optimized array is smaller in weight and volume than the reference case. It has also more fins, which besides thinner are also smaller in length and height. Optimization has produced a very thin base plate, which means that the fins are located directly under the component. In practical industrial designs, the base plate must be at least 1 mm thick, which increases the total mass by less than 10 % in this case.

Optimization was also performed for triangular fins (result shown in Fig. 9. The result is similar to that on rectangular fins, namely, that a single component with a constant heat flux covers almost the whole base plate.
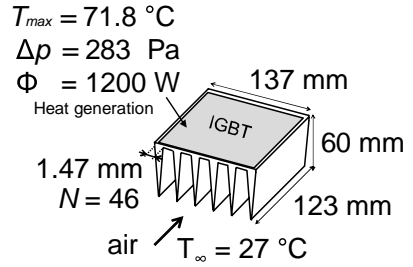
T_{max} = 71.8 °C
Δp = 283 Pa
Φ = 1200 W
Heat generation
137 mm
60 mm
1.47 mm
N = 46
123 mm
air T_∞ = 27 °C

Fig. 9 Optimized array with triangular fins: m = 0.68 kg

Table 1. Comparison of original array dimensions with optimized values for case 1.

	Original design		Optimized design	
			Rectangular	Triangular
T_{max} (°C)	71.8		71.8	71.8
m (kg)	3.31		0.78	0.68
L (mm)	150		115.0	123.4
W (mm)	132		134.7	137.1
b (mm)	12		0.01	0.025
N (mm)	30		59	46
t_b (mm)	2		0.77	1.47
t_t (mm)	2		0.77	0
l (mm)	110		55.0	60.1
X (mm)	23		0	0.6
Y (mm)	0		1.7	1.3

4.3 Case 2

In the second case, two 100×100-mm components were placed 50 mm apart on the base plate. The first component in the flow direction dissipated Φ_1 = 550 W and the second Φ_2 = 450 W, yielding a total heat release of 1000 W. The components were located symmetrically around the center line (Fig. 10).

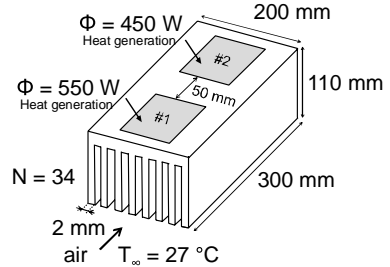Φ = 450 W
Heat generation
200 mm
#2
110 mm
Φ = 550 W
Heat generation
50 mm
#1
N = 34
300 mm
2 mm
air T_∞ = 27 °C

Fig. 10 Reference heat sink 2: m = 7.13 kg

Optimization was carried out for rectangular and triangular fins. The components were kept a constant 50 mm apart. Fig. 11 shows the optimal geometry for rectangular fins when the maximum temperature of the heat sink is held constant at T_{max} = 53.8 °C, as in reference case 2.
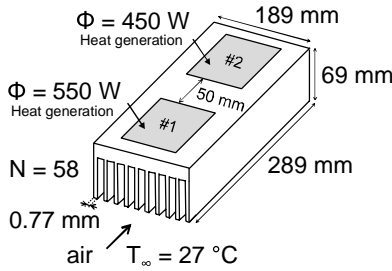
Fig. 11 Optimized array with rectangular fins: m = 3.85 kg

In its main dimensions, the above optimal design differs little from the original one though its mass is greatly reduced, 3.85 kg as opposed to 7.13 kg. In width as in length, the heat sink is somewhat narrower that the original, and its fins are shorter. The essential point is that its fins have now almost doubled, from 34 to 58.
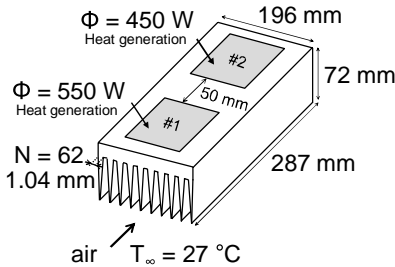

Fig. 12 Optimized array with triangular fins: m = 3.35 kg

The array with triangular fins was similar to that with rectangular fins, the former being somewhat smaller in mass than the latter. The small difference (only 13 % less) in mass is surprising because with single fins, the difference in the heat transfer rate between the same-mass rectangular and triangular fins is significant [2] (dimensions of the cases in Figs. 11 and 12 are given in Table 2).
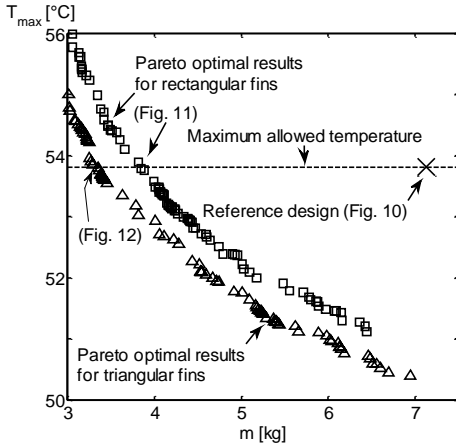

Fig. 13 Optimization results for case 2

The multi-objective optimization results for case 2 are shown in Fig. 13 with the maximum temperature and array mass simultaneously minimized. The optimum design values of the fin arrays in Figs. 11 and 12 lie at the intersections of the dotted line and the Pareto optimal solutions. The geometries in Figs. 11 and 12 may be obtained also by using a single-objective optimization method if the temperature is set at constraint, whose value is the same as that shown in Fig. 13 in dotted line. On the other hand, the temperature can also be limited to values other than 53.8 °C. The mass of the corresponding optimized array can be found in Fig. 13, but, of course, the geometry differs from those in Figs. 11 and 12.

Table 2. Comparison of original array dimensions with optimized values for case 2.

	Original design	Optimized design	
		Rectangular	Triangular
T_{max} (°C)	53.8	**53.8**	**53.8**
m (kg)	7.13	**3.85**	**3.35**
L (mm)	300	288.8	286.5
W (mm)	200	189.1	195.9
b (mm)	10	12.8	12.4
N (mm)	34	58	62
t_b (mm)	2	0.77	1.04
t_t (mm)	2	0.77	0
l (mm)	100	56.4	59.4
X (mm)	20	14.4	12.7
Y (mm)	50	42.4	53.9

5 Conclusions

Cooling equipment in electronics should fulfill many conflicting requirements such as high heat transfer rate, small mass, volume, and pressure drop. In addition, the temperature of the components sets limits due to failure if it exceeds a given value. The present paper introduced a procedure to combine analytical results of convection and numerical solution of conduction and applied it to optimization of a fin array. Only turbulent flow in channels was considered because especially in minimizing volume or mass, the flow must be turbulent.

The method is considered suitable for industrial optimization purposes, in which simple boundary conditions such as isothermal base plate or constant heat flux on the base plate are not accurate enough. Our method is much more practical in optimizing heat sinks than use of commercial numerical simulation codes with an optimization algorithm. Simultaneous numerical solution of turbulent flow and heat transfer in channels and fins would take considerable time, because practical optimization calls for hundreds of cases to be calculated. We validated our method by comparing the results with ones obtained purely numerically in a simple two-dimensional case and by using experimental data.

Heat sink maximum temperature and mass were chosen as criteria in optimization. Because criteria are conflicting, multi-objective optimization was performed with an algorithm modified from the original MOPSO algorithm for multi-objective optimization purposes.

The results showed that our approach was well suited even for multi-objective optimization, making it easy to find geometries best fulfilling different requirements. Furthermore, triangular fins reduced mass somewhat better than rectangular fins, as evidenced by the single fin results.

Acknowledgments

References

[1] Karvinen R., Lampio K., Combined numerical and analytical method for fin array heat transfer, Proceedings of CHT-12, International Symposium on Advances in Computational Heat Transfer 2012, Bath, England, July 1-6 2012.

[2] Karvinen R., Karvinen T., Optimum Geometry of Plate Fins[J], Journal of Heat Transfer, 2012, 134:081801:1-7.

[3] Lindstedt M., Karvinen R., Optimization of isothermal plate fin array with laminar convection[J], Journal of Enhanced Heat Transfer, 2012, 19(6):535-547.

[4] Bejan A., Sciubba E., The optimal spacing of parallel plates cooled by forced convection[J], International Journal of Heat and Mass Transfer, 1992, 35(12):3259-3264.

[5] Bejan A., Morega M., The optimal spacing of a stack of plates cooled by turbulent forced convection[J], International Journal of Heat and Mass Transfer, 1994, 37(6):1045-1048.

[6] Mereu S., Sciubba E., Bejan A., The optimal cooling of a stack of heat generating boards with pressure drop, flowrate or pumping power[J], International Journal of Heat and Mass Transfer, 1993, 36(15):3677-3686.

[7] Kim D-K., Kim S., Closed-form correlations for thermal optimization of microchannels[J], International Journal of Heat and Mass Transfer, 2007, 50:5318-5322.

[8] Liu D., Garimella S., Analysis and optimization of the thermal performance of microchannel heat sinks[J], International Journal for Numerical Methods in Heat & Fluid Flow, 2005, 15(1):7-26.

[9] Lindstedt M., Karvinen R., Optimization of Plate Fin Arrays with Laminar and Turbulent Forced Convection[J], Journal of Physics: Conference Series, 2012, 395:012059.

[10] Teertstra P., Yovanovich M. M., Culham J. R., Analytical forced convection modeling of plate fin heat sinks[J], Journal of Electronics Manufacturing, 2000, 10(4):253-261.

[11] Lehtinen A., Analytical Treatment of Heat Sinks Cooled by Forced Convection,. PhD. Thesis, Tampere University of Technology, TUT Publication 579, Tampere, 2005.

[12] Ryu J. H., Choi D. H., Kim S. J., Numerical optimization of the thermal performance of a microchannel heat sink[J], International Journal of Heat and Mass Transfer, 2002, 45:2823-2827.

[13] Wang Z-H., Wang X-D., Yan W-M., Duan Y-Y, Lee D-J, Xu J-L., Multi-parameters optimization for microchannel heat sink using inverse problem method[J], International Journal of Heat and Mass Transfer, 2011, 54:2811-2819.

[14] Li J., Peterson G. P., 3-Dimensional numerical optimization of silicon-based high performance parallel microchannel heat sink with liquid flow[J], International Journal of Heat and Mass Transfer, 2007, 50:2895-2904.

[15] Hewitt G. F., Heat Exchanger Design Handbook, Begell House, 1998.

[16] White F., Viscous Fluid Flow, McGraw-Hill, 1991.

[17] Webb R., Entrance and Exit Losses for Developing Flow in Parallel Channels[J], Heat transfer Engineering, 2006, 27(10):30-35.

[18] Miettinen K., Nonlinear multiobjective optimization, Kluwer academic Publishers. Boston, 1999.

[19] Deb Kalyanmoy, Multi-Objective Optimization using Evolutionary Algorithms, John Wiley & Sons, 2001.

[20] Kennedy J., Eberhart R C., Particle Swarm Optimization, Proceedings of IEEE International Conference on Neural Networks, Piscataway, NJ, USA, 1995.

[21] Shi Y., Eberhart R., A Modified Particle Swarm Optimizer, Evolutionary Computation Proceedings, IEEE World Congress on Computational Intelligence 1998.

[22] Coello Coello C., Pulido G., Lechuga M., Handling Multiple Objectives With Particle Swarm Optimization[J], IEEE Transactions on evolutionary computation, 2004, 8(3).

[23] Lindstedt M., Huhtanen J-P., Karvinen R., Improvements of refiner performance using flow modeling and optimization, Proceedings of international Mechanical Pulping Conference 2011, Xian, China, June 26-29, 2011, pp. 129-132.

Publication III

Matti Lindstedt, Kaj Lampio, Reijo Karvinen

Optimal shapes of straight fins and finned heat sinks

ASME Journal of Heat Transfer, Volume 136, Issue 6, 2015, Pages 061006-1 – 061006-8

Matti Lindstedt
Tampere University of Technology,
P.O. Box 589,
Tampere FI-33101, Finland
e-mail: matti.lindstedt@tut.fi

Kaj Lampio
Tampere University of Technology,
P.O. Box 589,
Tampere FI-33101, Finland
e-mail: kaj.lampio@tut.fi

Reijo Karvinen
Professor
Tampere University of Technology,
P.O. Box 589,
Tampere FI-33101, Finland
e-mail: reijo.karvinen@tut.fi

Optimal Shapes of Straight Fins and Finned Heat Sinks

Finned heat sinks are used to cool power electronics components. We present optimization results for single rectangular, triangular, and trapezoidal fins. After that, we minimize the mass of an existing heat sink consisting of a base plate and a fin array by optimizing the geometrical variables and component locations on the base plate. An analytical solution is used with rectangular fins and a numerical model with trapezoidal fins. Whereas the triangle is the best shape for single fins, in a heat sink flow velocity coupled with geometry favors trapezoids over triangles and rectangles. [DOI: 10.1115/1.4029854]

Keywords: heat sink, trapezoidal fin, forced convection, analytical solution, optimization, component placement

1 Introduction

Plate fin heat sinks cooled with forced air flow are commonly used to thermally manage electronics components in many applications [1]. Though air-cooling is typical in industrial inverters, there is an increasing trend to adopt liquid or two-phase cooling [2]. Reduction of available space and limitations of mass and consumed fan power continuously call for more efficient cooling systems. In this respect, there is no difference between air and liquid cooling.

The design of finned heat sinks often relies on fin theory, which assumes one-dimensional heat conduction, a constant heat transfer coefficient, and a uniform base temperature T_B [3]. This approach is correct for the fin in Fig. 1(*a*), when the mean heat transfer coefficient of the flow over an isothermal surface is used [4]. Consequently, simple analytical expressions have been found for optimal fin geometries [5].

Many recent numerical optimization studies on heat sinks focus on the whole base plate receiving a uniform heat flux from the components [6–9]. On the other hand, in the analytical model of Muzychka et al. [10], three-dimensional heat conduction in the base plate was solved with discrete heat sources at the bottom, but on the fin side, thermal resistance was modeled with a uniform effective heat transfer coefficient. This method was applied in the study of Türkakar and Okutucu-Özyurt [11]. A channel side heat transfer coefficient can be obtained, e.g., from the model of Teertstra et al. [12].

Heat sinks have also been studied using methods that differ from traditional ones. Entropy methods, developed by Bejan [13], have been suggested to replace the traditional criteria in optimization, and some related studies have been published [14]. Although minimum entropy design may be interesting from a theoretical point of view, it does not guarantee that the underlying important quantities, e.g., thermal resistance and mass, are optimal.

Lehtinen [15] derived an analytical solution for a plate fin heat sink with fluid heating in the flow direction, conjugate heat transfer in fins, and the effect of component locations on the base plate temperature taken into account. The model gives the temperature field in the base plate and fins in 3D and 2D Fourier series expansion. For a laminar, thermally developing (Graetz) flow, the solution is exact, and for a turbulent flow, a uniform heat transfer coefficient in channels can be used in practical applications.

In the literature, the results of optimal fin geometry are often presented in a difficult manner, and in many cases, an arbitrary heat transfer coefficient is used. The underlying optimal dimensions of the fin may be hard to acquire, even if all the appropriate initial values are given. Results on heat sinks are inevitably less general because of a larger number of constraints.

In this paper, we give simple explicit expressions for the optimal dimensions of rectangular, triangular, and trapezoidal fins, when the fin is cooled by forced convection. After that, we present a case study in which the mass of a plate fin heat sink is minimized while the fan power is fixed. Every geometrical design variable as well as component locations on the base plate are used as design variables. We show that the effect of fin shapes, i.e., rectangular, triangular, and trapezoidal, is different from that of single fins because of the constraint on fan power.

2 Optimization of Heat Transfer

The purpose of a heat sink is to limit the temperature of heat generating components. The optimization criteria could then be heat transfer rates, temperature limits of components, mass, volume, and pressure drop, and the power of the fan used for forced cooling. Other aspects such as noise and fouling may also count. The criteria are conflicting in that, e.g., lowering the fan power increases the maximum temperature of the components.

In practice, there is only one objective function that is minimized or maximized, whereas the other criteria are constrained to remain at, below, or above some fixed values. The standard form of this constrained optimization problem is

$$
\begin{aligned}
\text{find} \quad & \mathbf{x} \\
\text{to minimize} \quad & f(\mathbf{x}) \\
\text{subject to} \quad & h_i(\mathbf{x}) = 0, \quad i = 1, 2, \ldots, m \\
& g_j(\mathbf{x}) \leq 0, \quad j = 1, 2, \ldots, n
\end{aligned}
\tag{2.1}
$$

where $\mathbf{x}$ is the design variable vector, $f(\mathbf{x})$ is the objective function, and $h_i(\mathbf{x})$ and $g_j(\mathbf{x})$ are equality and inequality constraints. In fin design, the design variable vector contains, e.g., the fin dimensions. To be a solution of problem (2.1), the design $\mathbf{x}^*$ must satisfy the Karush–Kuhn–Tucker (KKT) conditions [16, p. 321]

$$\nabla f(\mathbf{x}^*) + \sum_{i=1}^{m} \lambda_i \nabla h_i(\mathbf{x}^*) + \sum_{j=1}^{n} \mu_j \nabla g_j(\mathbf{x}^*) = 0$$
$$h_i(\mathbf{x}^*) = 0, \quad i = 1, 2, \ldots, m$$
$$g_j(\mathbf{x}^*) \leq 0, \quad j = 1, 2, \ldots, n \qquad (2.2)$$
$$\mu_j g_j(\mathbf{x}^*) = 0, \quad j = 1, 2, \ldots, n$$
$$\mu_j \geq 0, \quad j = 1, 2, \ldots, n$$

where λ_i and μ_j are unknown KKT multipliers. Many optimization methods seek directly to solve the set of Eq. (2.2).

Gradient-based optimization methods usually converge on a local minimum that is nearest to the initial guess. In our case, this was sufficient, and methods suitable for global optimization, such as particle swarm optimization and genetic algorithm, were not needed.

Sequential quadratic programming (SQP) is a gradient-based optimization method suitable for solving problem (2.1). The idea behind SQP is to construct a quadratic model for the objective function $f(\mathbf{x})$ using a Hessian matrix, i.e., a matrix of second derivatives with respect to each variable. The quadratic model
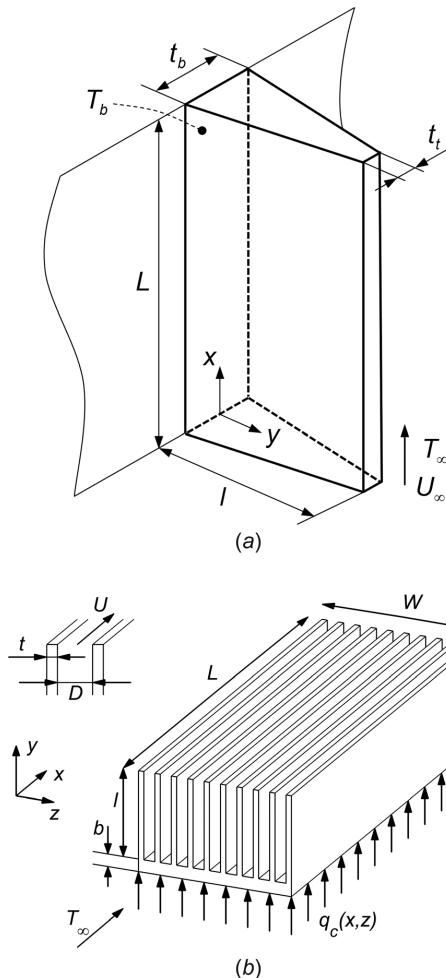

Fig. 1 Schematics of a single fin (*a*) and a plate fin heat sink (*b*)

Table 1 Constants for Eq. (1) [18]

Flow type	C	m	n
Laminar	0.332	1/2	1/3
Turbulent	0.0287	4/5	3/5

function is minimized subject to linearized constraints. The Hessian matrix and the linearization of the constraints are updated during every iteration round. Nodecal and Wright [16] discuss many different ways to implement the algorithm. In our study, we used MATLAB's *fmincon*-function [17], which includes an efficient implementation of the SQP-algorithm.

3 Optimal Shape of Straight Fins

The fin in Fig. 1(*a*) is a basic element of a larger system such as the heat sink in Fig. 1(*b*). As observed, when such a single fin is placed in a free stream, the total heat flux can be calculated very accurately by using the mean heat transfer coefficient of an isothermal surface in fin theory [4]. When the mean heat transfer coefficient is expressed with the mean Nusselt number [18]

$$\mathrm{Nu}_{m,T} = \frac{C}{m} \left(\frac{U_\infty L}{\nu} \right)^m \mathrm{Pr}^n \qquad (3.1)$$

the fin parameter $X_T = \sqrt{2hl^2/k_s t}$ becomes

$$X_T = \frac{l}{L} \sqrt{2 \frac{C}{m} \left(\frac{U_\infty L}{\nu} \right)^m \mathrm{Pr}^n \frac{k_f L}{k_s t_b}} \qquad (3.2)$$

The constants in Eqs. (3.1) and (3.2) are given in Table 1 for laminar and turbulent boundary layers.

Table 2 shows the thermal resistance R for different fin shapes in the above notation when the fin base is isothermal and the fin tip and edges are insulated.

$$R = \frac{T_b - T_\infty}{\Phi} \qquad (3.3)$$

The functions I_0 and I_1 are modified Bessel functions of the first kind of order 0 and 1, and K_0 and K_1 are modified Bessel functions of the second kind of order 0 and 1. The solutions for rectangular ($t_t = t_b$) and triangular ($t_t = 0$) fins are, in fact, limiting cases of the solution for a trapezoidal fin. These models also require that the thermal conductivity of the fin material be high and the heat transfer coefficient low so that the temperature gradients across the fin thickness can be ignored. These assumptions are justified for air cooled aluminum fins.

Table 2 Thermal resistance of straight fins [3]. X_T is given in Eq. (3.2).

Rectangular	$R = \dfrac{l}{L t_b k_s X_T \tanh X_T}$
Triangular	$R = \dfrac{l}{L t_b k_s} \dfrac{I_0(2X_T)}{X_T I_1(2X_T)}$
Trapezoidal	$R = \dfrac{1}{L k_s \mu_b \tan \kappa} \dfrac{I_0(\mu_b) K_1(\mu_a) + I_1(\mu_a) K_0(\mu_b)}{K_1(\mu_a) I_1(\mu_b) - I_1(\mu_a) K_1(\mu_b)}$
	$\kappa = \mathrm{atan} \dfrac{t_b - t_t}{2l}$
	$\mu_a = 2X_T \sqrt{\dfrac{t_b}{2l^2 \sin \kappa}} \sqrt{\dfrac{t_t(1 - \tan \kappa)}{2 \tan \kappa}}$
	$\mu_b = 2X_T \sqrt{\dfrac{t_b}{2l^2 \sin \kappa}} \sqrt{l + \dfrac{t_t(1 - \tan \kappa)}{2 \tan \kappa}}$

Table 3 Optimal fin geometry and R with fixed V and L for laminar ($m = 1/2$) and turbulent ($m = 4/5$) flow

Rectangular	$t_b = 0.998 L^{-1} \left(\dfrac{C}{m} V^2 \left(\dfrac{U_\infty L}{\nu} \right)^m \mathrm{Pr}^n \dfrac{k_f}{k_s} \right)^{1/3}$
	$l = V/(L t_b)$
	$R = 0.796 (k_s V)^{-1/3} \left(\dfrac{C}{m} \left(\dfrac{U_\infty L}{\nu} \right)^m \mathrm{Pr}^n k_f \right)^{-2/3}$
Triangular	$t_b = 1.671 L^{-1} \left(\dfrac{C}{m} V^2 \left(\dfrac{U_\infty L}{\nu} \right)^m \mathrm{Pr}^n \dfrac{k_f}{k_s} \right)^{1/3}$
	$l = 2V/(L t_b)$
	$R = 0.704 (k_s V)^{-1/3} \left(\dfrac{C}{m} \left(\dfrac{U_\infty L}{\nu} \right)^m \mathrm{Pr}^n k_f \right)^{-2/3}$
Trapezoidal	Optimal trapezoidal fins take triangular shape

3.1 Optimal Fin Geometry. Studies of fin optimization usually focus on minimizing thermal resistance with a fixed volume [3,5,19–21], which gives the maximum heat transfer rate when the base temperature is fixed. Equivalent results are obtained also when volume is minimized and thermal resistance is fixed. In practice, fin dimensions are limited due to spatial restrictions and manufacturing techniques, which lead to the following optimization problem:

$$
\begin{aligned}
\text{find} \quad & \mathbf{x} = \{ L, t_b, t_t, l \} \\
\text{to minimize} \quad & R(\mathbf{x}) \\
\text{subject to} \quad & V = V_0 \\
& L_{\min} \le L \le L_{\max} \\
& t_{b,\min} \le t_b \le t_{b,\max} \\
& t_{t,\min} \le t_t \le t_{t,\max}
\end{aligned}
\tag{3.4}
$$

The fixed volume constraint can be used to eliminate the fin height l; thus, l is not listed as a design variable. The limits for thickness at the tip t_t are used only with trapezoidal fins.

Solutions of problem (3.4) for rectangular and triangular fins are often found either at the maximum admissible length $L_{\max}$ or at the minimum admissible thickness $t_{b,\min}$. Consequently, generally valid results have been obtained when thermal resistance is minimized with volume and when either L or t_b is fixed. The method to find optimal geometries for a rectangular plate fin is given in Ref. [21] and applied to other fin shapes in Ref. [5]. The case where l is fixed has no solution.

Table 4 Optimal fin geometry and R with fixed V and t_b for laminar ($m = 1/2$) and turbulent ($m = 4/5$) flow

| Rectangular	$L = \xi \left(V^2 \dfrac{C}{m} \left(\dfrac{U_\infty}{\nu} \right)^m \mathrm{Pr}^n \dfrac{k_f}{k_s} t_b^{-3} \right)^{\frac{1}{3-m}}$,
	$\xi = \begin{cases} 1.411, & \text{laminar} \\ 2.323, & \text{turbulent} \end{cases}$
	$l = V/(L t_b)$
	$R = \xi \dfrac{1}{k_s t_b} \left(\dfrac{V}{t_b} \right)^{\frac{m+1}{m-3}} \left(\dfrac{C}{m} \left(\dfrac{U_\infty}{\nu} \right)^m \mathrm{Pr}^n \dfrac{k_f}{k_s t_b} \right)^{\frac{2}{m-3}}$,
	$\xi = \begin{cases} 0.7526, & \text{laminar} \\ 0.6523, & \text{turbulent} \end{cases}$
Triangular	$L = \xi \left(V^2 \dfrac{C}{m} \left(\dfrac{U_\infty}{\nu} \right)^m \mathrm{Pr}^n \dfrac{k_f}{k_s} t_b^{-3} \right)^{\frac{1}{3-m}}$,
	$\xi = \begin{cases} 2.793, & \text{laminar} \\ 5.176, & \text{turbulent} \end{cases}$
	$l = 2V/(L t_b)$
	$R = \xi \dfrac{1}{k_s t_b} \left(\dfrac{V}{t_b} \right)^{\frac{m+1}{m-3}} \left(\dfrac{C}{m} \left(\dfrac{U_\infty}{\nu} \right)^m \mathrm{Pr}^n \dfrac{k_f}{k_s t_b} \right)^{\frac{2}{m-3}}$,
	$\xi = \begin{cases} 0.5346, & \text{laminar} \\ 0.3834, & \text{turbulent} \end{cases}$
Trapezoidal	Optimal trapezoidal fins take triangular shape
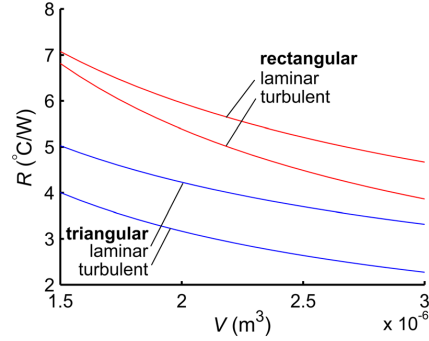
Fig. 2 Minimum thermal resistance as a function of volume for rectangular and triangular fins with an isothermal base. $U_\infty = 10\,\mathrm{m/s}$, $t_b = 1\,\mathrm{mm}$, and $T_b - T_\infty = 60\,^\circ\mathrm{C}$.

The optimal fin geometry derived for different fin shapes in Ref. [5] was presented using nondimensional variables, which might be difficult to use. We present these results in a simplified form in Tables 3 and 4. Table 3 gives explicit expressions for t_b and l and also for the minimum thermal resistance R for a case in which the fin volume V and fin length L are fixed. The corresponding results on a case in which t_b is fixed are given in Table 4. The results are different for laminar and turbulent flows, because the exponent m in Eq. (3.1) changes with the flow type.

The results in Tables 3 and 4 are simpler to use than any previous results on fin optimization; no calculation of heat transfer coefficients or Bessel functions is necessary, because detailed convection and optimization criteria are already included in the given expressions. The same results are valid also when thermal resistance is fixed and volume is minimized. In this case, the minimum volume can be solved from the expression for thermal resistance.

3.2 Comparison of Fin Shapes and Flow Types. To illustrate the differences between different fin shapes and flow types, we present a simple example where aluminum ($k_s = 170\,\mathrm{W/mK}$) fins were cooled with air flow ($U_\infty = 10\,\mathrm{m/s}$). The fin thickness at base was a fixed $t_b = 1\,\mathrm{mm}$; thus, the results in Table 4 were used. The base temperature was $T_b = 80\,^\circ\mathrm{C}$ and the flow temperature $T_\infty = 20\,^\circ\mathrm{C}$. The air properties were taken at $T_{\mathrm{ref}} = 67\,^\circ\mathrm{C}$.

The optimal thermal resistances from Table 4 are shown in Fig. 2 as a function of the available volume V. For instance, when the fin volume is a fixed $V = 2 \cdot 10^{-6}\,\mathrm{m}^3$, and when the boundary layer is laminar, the maximum heat transfer rate of an optimally
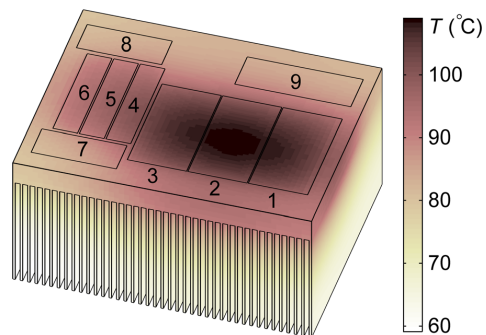

Fig. 3 Original heat sink, $M = 6.65\,\mathrm{kg}$

designed triangular fin is approximately 40% more than that of a rectangular fin. If the boundary layer is turbulent, heat transfer is almost twice as large as in a rectangular fin of the same volume. A turbulent boundary layer can be created, e.g., with a small roughness at the leading edge.

Results for trapezoidal fins are not given in Tables 3 and 4 or in Fig. 2, because when the fin thickness at the tip t_t is allowed to vary freely between 0 and t_b, optimal trapezoidal fins assume a triangular shape ($t_t = 0$) regardless of whether the fin length L or thickness t_b is fixed. This is consistent with a previous finding that triangular fins are better than parabolic fins, which again are better than rectangular fins [5]. In other words, making the fin surface more concave is the best compromise between mass and thermal resistance for single straight fins.

4 Optimal Geometry of Finned Heat Sinks

In Sec. 3, we presented some theoretical results on optimal fin geometry. A major approximation in these results was that we assumed a boundary layer flow over the fin surface. To judge the value of these results for dense fin arrays, we present a case study in which the mass of an existing industrial heat sink was minimized. Simple optimum results such as those with single fins above are difficult to obtain with heat sinks due to a larger number of variables and constraints. Such design is constrained not only by volume or mass, but also by the available fan power.

An optimal fin shape in a heat sink depends on the initial values of the problem, the locations and power of the heat sources, and other constraints. We could combine the manufacturing, transportation, and operational costs into a single cost function and find a fin geometry to minimize the life time costs. However, many of these costs are unknown at the time of manufacturing. To simplify, we minimized the material costs (mass), while the operational cost (fan power) remained fixed.

In Sec. 4.1, we present the original heat sink design and discuss the selection of design variables and constraints for optimization. In Sec. 4.2, we examine rectangular fins and use an analytical solution for a plate fin heat sink, which is presented in Appendix A. A numerical finite volume model is used in Sec. 4.3 to study how much mass can be reduced by using trapezoidal or triangular fins instead of rectangular ones.

4.1 Case Study.
Figure 3 shows the geometry and temperature field of the original heat sink together with the locations of nine heat producing components. The temperature field was calculated using the analytical solution in Appendix A with component sizes and heat powers given in Table 5. The original design geometry is given in detail in Table 6.

The inlet air temperature was $T_\infty = 40\,^\circ\text{C}$ and fan power $P_0 = 6\,\text{W}$, which was estimated based on the existing system using the pressure drop equations in Appendix B. The mass of the original heat sink was $M_0 = 6.65\,\text{kg}$, and the maximum base temperature near the center of component 2 was $T_{\text{max},0} = 109.1\,^\circ\text{C}$. The material properties of air and aluminum were taken at $T_{\text{ref}} = 67\,^\circ\text{C}$.

4.1.1 Objective Function. The objective function in optimization is the heat sink mass

$$M = \rho_s L\left(Nl\frac{(t_b + t_t)}{2} + (N-1)(D + t_b)b\right) \qquad (4.1)$$

where $\rho_s = 2700\,\text{kg/m}^3$ is the density of aluminum.

4.1.2 Design Variables. Treating the location and orientation of each component as a separate design variable would lead to a difficult optimization problem with many continuous and discrete variables and many constraints. To simplify optimization, the components were first located in a new arrangement shown in Fig. 4 and then fixed relative to each other into a component

Table 5 Component properties

Component	Size (mm^2)	Heat power (W)
1–3	94×48	450
4–6	93×20	150
7–8	29×69	15
9	34×94	0

cluster. The distance between components 1–3 and 4–6 in the flow direction was kept as in the original design.

Consequently, the design variable vector $\mathbf{x} = \{N, U, D, L, b, t_b, l, d_{LE}\}$ contains the number of fins, flow velocity, geometrical variables, and the distance d_{LE} of the component cluster from the leading edge. In Sec. 4.2, the fins have a uniform thickness ($t_t = t_b$), but in Sec. 4.3, they are triangular ($t_t = 0$) or trapezoidal with the fin thickness at the tip t_t as an additional design variable.

4.1.3 Constraints. The design was primarily constrained by space availability and manufacturing techniques. The fin thickness had to be more than $t_b \geq 1.5\,\text{mm}$ and the base plate thicker than $b \geq 6\,\text{mm}$. The width was a fixed $W_0 = N(D + t_b) - D = 242\,\text{mm}$. The components had to lie a minimum of 4 mm from the edges of the base plate. Further, the optimization algorithm in Sec. 2 requires that each design variable has a lower and upper limit. The variable limits were selected so that the original heat sink could be modified within realistic limits.

The maximum temperature of the components was limited to below the maximum temperature in the original design: $T_{\text{max},0} = 109.1\,^\circ\text{C}$. The fan power was fixed to $P_0 = 6\,\text{W}$, even when the geometry of the heat sink was altered. Fan power was calculated using the equations in Appendix B. This constraint allows the flow velocity to change when the geometry is changed unlike with single fin mentioned earlier. To reduce the error associated with using the Nusselt number correlation Eq. (A8) at low Reynolds numbers, the Reynolds number was kept constant and equal to $\text{Re}_0 = 3300$. With certain initial values, the Reynolds number can become too low without this constraint.

4.1.4 Problem Statement. Based on the above discussion about the objective function, design variables, and constraints, we have the following optimization problem:

$$\begin{aligned}
\text{find} \quad & \mathbf{x} = \{N, U, D, L, b, t_b, l, d_{LE}\} \\
\text{to minimize} \quad & M \\
\text{such that} \quad & T_{\text{max}} \leq 109.1\,^\circ\text{C} \\
& P = 6\,\text{W} \\
& \text{Re} = 3300 \\
& W = 242\,\text{mm} \\
& d_{LE} + 156\,\text{mm} \leq L \qquad (4.2)\\
& 156\,\text{mm} \leq L \leq 220\,\text{mm} \\
& 1.5\,\text{mm} \leq t_b \leq 3\,\text{mm} \\
& 0.3\,\text{mm} \leq t_t \leq 3\,\text{mm} \\
& 6\,\text{mm} \leq b \leq 26\,\text{mm} \\
& 4\,\text{mm} \leq d_{LE} \leq 45\,\text{mm} \\
& N \in [38, 39, \ldots, 55]
\end{aligned}$$

Problem (4.2) is solved separately for each value of N to avoid discrete variables in optimization.

With rectangular fins, the equality constraints for width, fan power, and Reynolds number were treated by elimination as follows. First, the channel width D was calculated from $N(D + t_b) - D = 242\,\text{mm}$. Then, the flow velocity U was calculated from $2DU/\nu = 3300$. Last, the fin height l was calculated from Eq. (B2). With these simplifications, only four design variables, namely, L, b, t_b, and d_{LE} remained for numerical optimization.

With trapezoidal and triangular fins, the finite volume method was adopted because an analytical solution, as that in

Case	N	U(m/s)	D(mm)	L(mm)	b(mm)	t_b(mm)	l(mm)	d_{LE}(mm)	t_t(mm)
Original	41	8.0	4.0	190	20	2.00	99	—	2.00
Optimized rectangular	48	8.8	3.6	176.4	8.8	1.50	69.7	19.4	1.50
Optimized trapezoidal	53	8.7	2.9–4.3	174.5	8.8	1.71	68.3	15.0	0.33

Appendix A, was not available. The fin thickness at the tip t_t was an additional design variable, and the channel width D at the base was calculated as with rectangular fins. The constraints for the Reynolds number and fan power could not be used to further eliminate variables, because the channel width was not constant in the y-direction. The calculation method is explained in Sec. 4.3.

4.2 Results With Rectangular Fins. With rectangular fins, we used Lehtinen's analytical solution [15] presented in Appendix A. It comprises a set of equations to calculate temperature at any prescribed location in the fins and base plate. Finding the location and value of the maximum base temperature required an optimization routine of its own. This subroutine was performed by starting the search from the midpoint of component 1, which was the hottest component in the new component arrangement in Fig. 4. Thus, maximization of a function with two variables (x- and z-positions) was required.

Figure 4 and Table 6 show the details of the optimized heat sink. In spite of strict design constraints, optimization reduced the heat sink mass considerably over the original design, from 6.65 kg to 3.41 kg. Most of the saving came from thinner fins and base plate and from shorter length in the flow direction. The key factor here was that the components which generated most heat were located farther apart. This resulted in a more uniform temperature distribution in the base plate—which, however, can also be a disadvantage. In the original design, high temperature affected only components 1–3, but in the optimized heat sink also components 4–6 were subjected to high temperature. However, the maximum temperatures of each component could be kept below those of the original design by accepting less reduction in mass.

The lower limit for fin thickness was the only active variable limit in the optimal design. Lowering this limit would further decrease the mass. Depending on the variable limits and other initial values, more than one limit can be active. Moreover, the component placement has a considerable effect on how small a mass can give the required thermal resistance. These issues prevent us from finding simple general rules for the optimal design of heat sinks.

4.3 Results With Triangular and Trapezoidal Fins. The heat sink in Fig. 4 could be further improved by using triangular
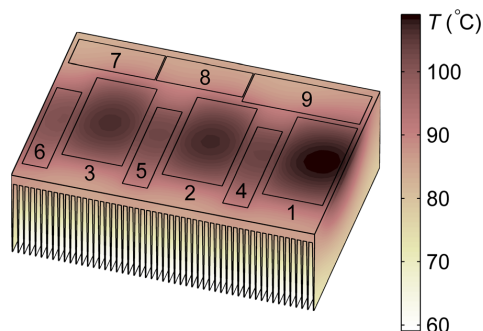

Fig. 5 Optimized heat sink with trapezoidal fins using the finite volume method M = 2.75 kg

or trapezoidal fins. No analytical solution applied then, but the temperature field in the base plate and fins was calculated using the finite volume method. In the model, the fins and the channels between the fins were divided into rectangular control volumes in x- and y-directions, but only one volume was used in z-direction for the fins and channels. The base plate in turn was divided into several control volumes in all three directions.

Because the fin thickness decreased towards the tip, the mean flow velocity was lower near the base and higher near the tip. Each control volume with the same y-coordinate had the same flow velocity. Flow velocities were calculated from the pressure loss equation (B1) from the condition that pressure loss over the channel was equal independent of the y-coordinate. The total flow rate had to satisfy the constraint for fixed fan power in Eq. (B2). The Reynolds number was calculated based on the mean flow velocity.

Heat transfer coefficients at fin surfaces were obtained from Eq. (A8) and given as boundary conditions for control volumes in the fins. Heat flux from the components was used as a boundary condition at the base plate, and all the other boundaries were
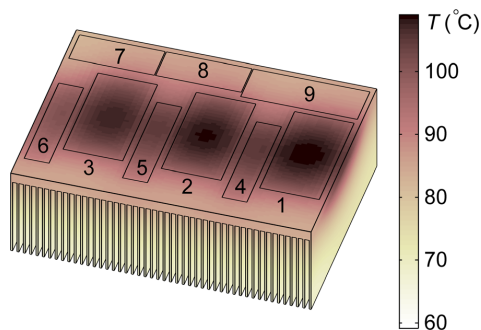

Fig. 4 Optimized heat sink with rectangular fins using the analytical solution in Appendix A, M = 3.41 kg
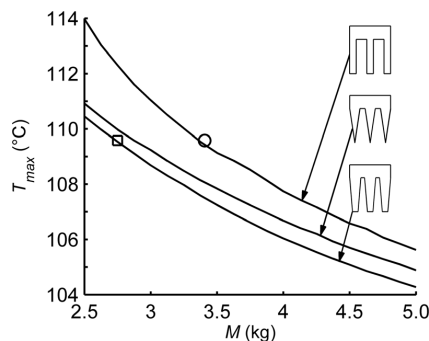

Fig. 6 Mass and maximum temperature of optimized heat sinks with rectangular, triangular, and trapezoidal fins. The performance of heat sinks in Figs. 4 and 5 is marked with a circle and a square.

considered thermally insulated. Temperature fields of the heat sink and fluid were solved iteratively. At first, air was at ambient temperature, and the temperature field in the solid was calculated. Then, the air temperature field was calculated, whereas the solid part temperature distribution remained fixed. Solid and air temperatures were calculated repeatedly until the change in the maximum temperature in subsequent iteration rounds was under $10^{-6}\,^{\circ}$C.

In case of the original heat sink in Fig. 3, the finite volume method gave a maximum temperature of 109.6 °C, which was slightly higher than the 109.1 °C obtained with the analytical method. Yet the difference was small, and $T_{\mathrm{max,0}} = 109.6\,^{\circ}$C was used as the temperature limit in finite volume calculations. Optimization was performed using trapezoidal fins with the heat sink in Fig. 4 as the initial guess. The resulting geometry is shown in Fig. 5, and the details of the geometry are given in Table 6. By changing the fin shape, the heat sink mass could still be reduced from 3.41 kg to 2.75 kg. The saving came from the reduced volume of fins.

In optimization, the fin shapes were limited by the lower and upper limits for t_{b} and t_{t}. Because the optimal fin thickness at tip $t_{\mathrm{t}} = 0.33$ mm is higher than the lower limit of 0.3 mm in problem (4.2), the same optimal design would be also obtained without this constraint. When the fin shape is allowed to change freely, optimization does not yield triangular or rectangular fins. The best result is obtained with a trapezoidal shape.

The optimization problem (4.2) was solved with many different fixed values of maximum temperature (results shown in Fig. 6). Figure 6 shows directly how much mass can be reduced by changing the shape of the fins while keeping the same maximum temperature. As an example, the optimized heat sink with rectangular fins from Sec. 4.2 is shown as a circle in Fig. 6. When the maximum temperature was kept constant and trapezoidal fins were used, optimization gave the heat sink shown in Fig. 5. The corresponding point is marked with a square in Fig. 6.

When all geometrical variables were included in optimization, minimum mass was obtained by using trapezoidal fins. Furthermore, triangular fins are problematic to manufacture. These results can be explained as follows: with triangular fins, too much flow passes near the fin tip, where temperature is low. On the other hand, with rectangular fins, the mean flow velocity does not vary in the y-direction, but too much mass is used near the tip region. The trapezoidal fin is the best practical compromise between thermal resistance, mass, and fan power.

5   Conclusions

We have presented optimization results for a single fin and heat sinks. Using analytical expressions for convection heat transfer, we derived simple equations in Tables 3 and 4, which explicitly give an optimal geometry for rectangular, triangular, and trapezoidal fins of fixed volume. Because of coupling convection and conduction, the most concave form, i.e., triangular, is the best.

The thermal performance of heat sinks depends on fin and base plate geometry and the locations and power of the heat sources on the base plate. With rectangular fins, an analytical solution gives 2D and 3D temperature fields in fins and base plate with fluid heating between fins taken into account. A finite volume solution was used with triangular and trapezoidal fins.

The mass of an existing heat sink was minimized by keeping maximum base temperature and fan power fixed. Heat generating components were rearranged on the base plate, and all geometrical variables were optimized, which resulted in a considerable reduction in mass. With a single fin, where ambient flow velocity was constant over the fin surface, triangular fin gave the smallest mass. On the other hand, with heat sinks, trapezoidal fins worked better than rectangular or triangular. Flow velocity was linked with fin geometries, because of the constraint on fan power. Consequently, with triangular fins, too much flow passes near the tip where the fins are thin and at low temperature. With rectangular fins, flow

velocity is the same near the base and tip, but too much mass is located at the tip area. Trapezoidal fins are the best practical compromise for thermal resistance, fan power, and mass in heat sinks. This result shows that optimized shapes of single fins cannot be used to optimize fin arrays in heat sinks. In the future, we will present corresponding optimization results for single fins and finned heat sinks cooled with natural convection.

Nomenclature

b = base plate thickness m
C = constant given in Table 1
c_{p} = fluid specific heat at constant pressure, J/kgK
D = channel width, m
d_{LE} = distance of components 4–6 from leading edge, m
D_{h} = hydraulic diameter, 2D, m
$f(\mathbf{x})$ = objective function
$g_j(\mathbf{x})$ = inequality constraint
h = mean heat transfer coefficient
$h_i(\mathbf{x})$ = equality constraint
k_{f} = fluid thermal conductivity, W/mK
k_{s} = solid thermal conductivity, W/mK
l = fin height in y-direction, m
L = fin (heat sink) length in x-direction, m
M = heat sink mass, kg
m, n = constants given in Table 1
N = number of fins
N_i = largest Fourier mode
$\mathrm{Nu}_{\mathrm{m,T}}$ = mean Nusselt number of isothermal surface
P = fan power, Eq. (B2), W
Pr = Prandtl number, $\nu \rho c_p / k_f$
$q_{\mathrm{c}}(x,z)$ = heat flux distribution at base plate, W/m^2
R = thermal resistance, in Eq. (3.3) and Table 2, K/W
Re = Reynolds number, UD_h/ν
t_{b} = fin thickness at base, m
t_{t} = fin thickness at tip, m
T_{b} = uniform temperature at fin base, K
T_∞ = ambient temperature, K
U = mean flow velocity in channel, m/s
U_∞ = ambient flow velocity, m/s
V = fin volume, m^3
W = heat sink width in z-direction, m
$\mathbf{x}$ = design variable vector
x = coordinate in flow direction, m
$\mathbf{x}^*$ = optimal design variable vector
X_T = fin parameter in Eq. (3.2)
y = coordinate normal to base plate, m
z = coordinate normal to fin surface, m

Greek Symbols

γ_{ij} = see Eq. (A10)
Δp = pressure drop, Eq. (B1), Pa
θ = temperature excess, $T - T_\infty$, K
θ_{b} = temperature excess in base plate, K
θ_{f} = temperature excess in fins, K
ν = kinematic viscosity of fluid, m^2/s
ρ = density of fluid, kg/m^3
Φ = total heat transfer rate, W

Subscript

0 = original design

Appendix A: Analytical Solution for Heat Sink

The analytical solution for a plate fin heat sink presented here was derived by Lehtinen [15].

The temperature field in the fins and base plate of the heat sink in Fig. 1(b) is governed by the following equations:

$$\frac{\partial^2 \theta_b}{\partial x^2} + \frac{\partial^2 \theta_b}{\partial y^2} + \frac{\partial^2 \theta_b}{\partial z^2} = 0 \tag{A1}$$

$$\frac{\partial^2 \theta_f}{\partial x^2} + \frac{\partial^2 \theta_f}{\partial y^2} = 0 \tag{A2}$$

Lehtinen wrote the temperature field in the base plate and fins in a truncated 3D and 2D Fourier series

$$\theta_b(x,y,z) = \sum_{i=0}^{N_i} \theta_{b,ij}(y) \cos\left(\frac{i\pi x}{L}\right) \cos\left(\frac{j\pi z}{W}\right) \tag{A3}$$

$$\theta_f(x,y) = \sum_{i=0}^{N_i} \theta_{f,i}(y) \cos\left(\frac{i\pi x}{L}\right) \tag{A4}$$

where $\theta_{b,ij}(y)$ and $\theta_{f,i}(y)$ are yet unknown Fourier coefficients.

The heat sink surface, except for fin surfaces and the area under the components, is insulated. At the junction of fins and base, temperatures and heat flows are continuous.

$$\theta_b\big|_{y=0^-} = \theta_f\big|_{y=0^+} \tag{A5}$$

$$k_b \frac{\partial \theta_b}{\partial y}\bigg|_{y=0^-} = \frac{t}{t+D} k_s \frac{\partial \theta_f}{\partial y}\bigg|_{y=0^+} \tag{A6}$$

where $y = 0^-$ and $y = 0^+$ refer to locations directly below and above the junction. In Eq. (A6), k_b is the thermal conductivity of the base material, which can differ from that of fins.

Fluid heating in fin channels is taken exactly into account by the equation

$$q(x,y) = \frac{\mathrm{Nu}_{m,T} k_f}{2D}\left(\theta_f(x,y) - \frac{4L^* \mathrm{Nu}_{m,T}}{L} \int_0^x \right.$$
$$\left. \times \exp\left[\frac{4L^* \mathrm{Nu}_{m,T}}{L}\left(\frac{\xi - x}{L}\right)\right] \theta_f(\xi,y)\mathrm{d}\xi\right) \tag{A7}$$

where $L^* = L/(2DRePr)$ and $\mathrm{Nu}_{m,T}$ is the mean Nusselt number [22].

$$\mathrm{Nu}_{m,T} = \frac{(f/2)(\mathrm{Re} - 1000)\mathrm{Pr}}{1 + 12.7\sqrt{f/2}\left(\mathrm{Pr}^{2/3} - 1\right)}\left[1 + \left(\frac{D_h}{L}\right)^{2/3}\right] \tag{A8}$$

The assumption that the heat transfer coefficient is uniform over the fin surfaces is the largest approximation in the solution.

Equations (A1)–(A8) constitute a linear system of differential equations, from which the Fourier coefficients $\theta_{b,ij}$ and $\theta_{f,i}$ can be solved. Lehtinen [15] started with a general solution for the base plate

$$\theta_b(x,y,z) = A_{00} + B_{00}y$$
$$+ \sum_{\substack{i=0 \\ i+j \neq 0}}^{N_i} \sum_{j=0}^{N_i} \left[A_{ij} \cosh(\gamma_{ij}y) \right.$$
$$\left. + \frac{B_{ij}}{\gamma_{ij}} \sinh(\gamma_{ij}y)\right] \cos\left(\frac{i\pi x}{L}\right) \cos\left(\frac{j\pi z}{W}\right) \tag{A9}$$

where

$$\gamma_{ij} = \sqrt{\left(\frac{i\pi x}{L}\right)^2 + \left(\frac{j\pi z}{W}\right)^2} \tag{A10}$$

Equation (A9) was also derived earlier by Muzychka et al. [10]. Accurate results are obtained with $N_i = 50$. Lehtinen obtained matrices **A** and **B** from the boundary conditions at the base plate and from Eqs. (A5) and (A6), which connect the fins with the base plate. The j:th columns of these matrices are

$$\boldsymbol{a}_j = \mathbf{E}_j^{-1} \frac{\boldsymbol{q}_j}{k_b} \tag{A11}$$

$$\boldsymbol{b}_j = -\frac{k_s t}{k_b^2 l(D+t)} \mathbf{R} \mathbf{E}_j^{-1} \boldsymbol{q}_j \tag{A12}$$

In Eqs. (A2) and (A3), $\boldsymbol{q}_j$ is the j:th column of the coefficient matrix for the base heat flux

$$Q_{ij} = \frac{\int_0^L \int_0^L q_c(x,z) \cos\left(\frac{i\pi x}{L}\right) \cos\left(\frac{j\pi z}{W}\right) \mathrm{d}z \mathrm{d}x}{\int_0^L \int_0^L \cos^2\left(\frac{i\pi x}{L}\right) \cos^2\left(\frac{j\pi z}{W}\right) \mathrm{d}z \mathrm{d}x} \tag{A13}$$

where $q_c(x,z)$ is the distribution of the component heat flux at the bottom of the base plate.

Matrix **R** in Eq. (A12) is obtained from the solution of a fin with an arbitrary temperature at the base together with the convection model in Eq. (A7)

$$\mathbf{R} = \mathbf{M}l \tanh(\mathbf{M}l) \tag{A14}$$

which reduces into the familiar one-dimensional fin solution when $N_i = 0$. The diagonal and off-diagonal elements of matrix $\mathbf{M}^2$ are

$$M_{ii}^2 = \left(\frac{i\pi}{L}\right)^2 + \frac{\mathrm{Nu}_{m,T} k_f}{k_s 2Dt}\left[\frac{(i\pi)^2}{N_{tu}^2 + (i\pi)^2}\right.$$
$$\left. + \left(\frac{2N_{tu}^3}{1+\delta(i)}\right)\left(\frac{1 - (-1)^i \exp(-N_{tu})}{\left(N_{tu}^2 + (i\pi)^2\right)^2}\right)\right] \tag{A15a}$$

$$M_{iI}^2 = \frac{\mathrm{Nu}_{m,T} k_f}{k_s 2Dt}\left(\frac{2N_{tu}}{1+\delta(i)}\right)\left[\frac{N_{tu}^2\left(1 - (-1)^i \exp(-N_{tu})\right)}{\left(N_{tu}^2 + (i\pi)^2\right)\left(N_{tu}^2 + (I\pi)^2\right)}\right.$$
$$\left. + \left(\frac{I^2\left(1 - (-1)^{i+I}\right)}{(i^2 - I^2)N_{tu}^2 + (i\pi)^2}\right)\right] \tag{A15b}$$

Matrix $\mathbf{M}^2$ has the eigenvalue decomposition $\mathbf{M}^2 = \mathbf{V}\Lambda^2\mathbf{V}^{-1}$, and thus $\mathbf{M} = \mathbf{V}\Lambda\mathbf{V}^{-1}$, where $\Lambda = \sqrt{\Lambda^2}$ is obtained by elementwise operation. The Delta-function is $\delta(x) = 1$, when $x = 0$ and $\delta(x) = 0$, when $x \neq 0$.

The diagonal and off-diagonal elements of matrices $\mathbf{E}_j, j = 1..N_i$ needed in Eqs. (A10) and (A11) are

$$E_{j,ii} = \gamma_{ij} \sinh(\gamma_{ij}b) + \cosh(\gamma_{ij}b)\frac{k_s t}{k_b l(D+t)} R_{ii} \tag{A16a}$$

$$E_{j,iI} = \cosh(\gamma_{ij}b)\frac{k_s t}{k_b l(D+t)} R_{iI} \tag{A16b}$$

Appendix B: Calculation of Pressure Drop

Pressure drop in a flow over a channel can be calculated as

$$\Delta p = \frac{1}{2}\rho U^2\left(K_{in} + 4f\frac{L}{D_h} + K_{out}\right) \tag{B1}$$

Fan power depends also on flow rate

$$P = (N-1)lDU\Delta p \tag{B2}$$

The friction factor for a turbulent flow between parallel plates can be obtained from the Blasius correlation, when the effective Reynolds number of Jones [23] is used.

$$f = 0.0791 \left(\frac{2}{3} \mathrm{Re} \right)^{-1/4} \tag{B3}$$

The inlet loss coefficient K_{in} has been curve fitted from Fig. 5 by Kays [24],

$$K_{in} = 0.4 \left(1 - \sigma^{2.1} \right) \tag{B4}$$

where the contraction ratio is

$$\sigma = \frac{D}{D + t} \tag{B5}$$

The outlet loss coefficient K_{out} can be derived from one-dimensional momentum equation [24]

$$K_{out} = 1 - 2\beta\sigma + \sigma^2 \tag{B6}$$

where $\beta = 1$ is the momentum correction factor. For a turbulent flow, the value is near unity. If β were modeled, it would have to be taken into account in the apparent friction factor as well. When $\beta = 1$ and fully developed turbulent friction factor are used, most of the error is canceled out.

References

[1] Sunden, B., and Heggs, P. J., 1999, *Recent Advances in Analysis of Heat Transfer for Fin Type Surfaces*, Wiley, New York.

[2] Wang, P., McCluskey, P., and Bar-Cohen, A., 2013, "Two-Phase Liquid Cooling for Thermal Management of IGBT Power Electronic Module," ASME J. Electron. Packag., **135**(2), p. 021001.

[3] Kraus, A. D., Aziz, A., and Welty, J., 2001, *Extended Surface Heat Transfer*, Wiley, New York.

[4] Karvinen, R., 1983, "Efficiency of Straight Fins Cooled by Natural or Forced Convection," Int. J. Heat Mass Transfer, **26**(4), pp. 635–638.

[5] Karvinen, R., and Karvinen, T., 2012, "Optimum Geometry of Plate Fins," ASME J. Heat Transfer, **134**(8), p. 081801.

[6] Ryu, J. H., Choi, D. H., and Kim, S. J., 2002, "Numerical Optimization of the Thermal Performance of a Microchannel Heat Sink," Int. J. Heat Mass Transfer, **45**(13), pp. 2823–2827.

[7] Li, J., and Peterson, G. P., 2007, "3-Dimensional Numerical Optimization of Silicon-Based High Performance Parallel Microchannel Heat Sink With Liquid Flow," Int. J. Heat Mass Transfer, **50**(15–16), pp. 2895–2904.

[8] Husain, A., and Kim, K.-Y., 2009, "Thermal Optimization of a Microchannel Heat Sink With Trapezoidal Cross Section," ASME J. Electron. Packag., **131**(2), p. 021005.

[9] Wang, Z.-H., Wang, X.-D., Yan, W.-M., Duan, Y.-Y., Lee, D. J., and Xu, J.-L., 2011, "Multi-Parameters Optimization for Microchannel Heat Sink Using Inverse Problem Method," Int. J. Heat Mass Transfer, **54**(13–14), pp. 2811–2819.

[10] Muzychka, Y. S., Culham, J. R., and Yovanovich, M. M., 2003, "Thermal Spreading Resistance of Eccentric Heat Sources on Rectangular Flux Channels," ASME J. Electron. Packag., **125**(2), pp. 178–185.

[11] Türkakar, G., and Okutucu-Özyurt, T., 2012, "Dimensional Optimization of Microchannel Heat Sinks With Multiple Heat Sources," Int. J. Therm. Sci., **62**, pp. 85–92.

[12] Teertstra, P., Yovanovich, M. M., and Culham, J. R., 2000, "Analytical Forced Convection Modeling of Plate Fin Heat Sinks," J. Electron. Manuf., **10**(4), pp. 253–261.

[13] Bejan, A., 1996, *Entropy Generation Minimization*, CRC Press, Boca Raton, FL.

[14] Iyengar, M., and Bar-Cohen, A., 2003, "Least-Energy Optimization of Forced Convection Plate-Fin Heat Sinks," IEEE Trans. Compon. Packag. Technol., **26**(1), pp. 62–70.

[15] Lehtinen, A., 2005, "Analytical Treatment of Heat Sinks Cooled by Forced Convection," Doctoral thesis, Tampere University of Technology, Tampere, Finland.

[16] Kays, W., Crawford, M., and Weigand, B., 2005, *Convective Heat and Mass Transfer*, McGraw-Hill, New York.

[17] Nodecal, J., and Wright, S. J., 2006, *Numerical Optimization*, Springer, New York.

[18] MATLAB and Optimization Toolbox R2012b, The MathWorks, Inc., Natick, MA.

[19] Lindstedt, M., 2013, "Modeling and Optimization of Plate Fins and Plate Fin Heat Sinks," Doctoral thesis, Tampere University of Technology, Tampere, Finland.

[20] Razelos, P., 2003, "A Critical Review of Extended Surface Heat Transfer," Heat Transfer Eng., **24**(6), pp. 11–28.

[21] Karvinen, R., and Karvinen, T., 2010, "Optimum Geometry of Fixed Volume Plate Fin for Maximizing Heat Transfer," Int. J. Heat Mass Transfer, **53**(23–24), pp. 5380–5385.

[22] Gnielinski, V., 1975, "Neue Gleichungen für den Wärme- und den Stoffübergang in Turbulent Durchströmten Rohren und Kanälen," Forsch. Ingenieurwes., **41**(1), pp. 8–16.

[23] Jones, O. C., 1976, "Improvement in the Calculation of Turbulent Friction in Rectangular Ducts," ASME J. Fluids Eng., **98**(2), pp. 173–181.

[24] Kays, W. M., 1950, "Loss Coefficient for Abrupt Changes in Flow Cross Section With Low Reynolds Number Flow in Single and Multiple Tube Systems," Trans. ASME, **72**, pp. 1067–1074.

Publication IV

Kaj Lampio, Reijo Karvinen

A new method to optimize natural convection heat sinks

CrossMark

A new method to optimize natural convection heat sinks

K. Lampio[1] (ORCID) · R. Karvinen[1]

Abstract The performance of a heat sink cooled by natural convection is strongly affected by its geometry, because buoyancy creates flow. Our model utilizes analytical results of forced flow and convection, and only conduction in a solid, i.e., the base plate and fins, is solved numerically. Sufficient accuracy for calculating maximum temperatures in practical applications is proved by comparing the results of our model with some simple analytical and computational fluid dynamics (CFD) solutions. An essential advantage of our model is that it cuts down on calculation CPU time by many orders of magnitude compared with CFD. The shorter calculation time makes our model well suited for multi-objective optimization, which is the best choice for improving heat sink geometry, because many geometrical parameters with opposite effects influence the thermal behavior. In multi-objective optimization, optimal locations of components and optimal dimensions of the fin array can be found by simultaneously minimizing the heat sink maximum temperature, size, and mass. This paper presents the principles of the particle swarm optimization (PSO) algorithm and applies it as a basis for optimizing existing heat sinks.

List of symbols

b Base plate thickness (m)
C_1 Constant in (14)

✉ K. Lampio
    kaj.lampio@tut.fi

    R. Karvinen
    reijo.karvinen@tut.fi

[1]   Tampere University of Technology, P.O. Box 541,
    FI-33101 Tampere, Finland

C_2 Constant in (14)
c_p Specific heat (J/kgK)
d Channel width (m)
d_h Hydraulic diameter = $2d$ (m)
$d_{i,h}$ Distance between swarm member i and target h in optimization
El   Elenbaas number = $g\beta\Delta T d^4 \mathrm{Pr}/(\nu^2 L)$
f Mean friction factor
$f_i(\boldsymbol{x})$ Objective function i in optimization
$F_i(\boldsymbol{x})$ Modified objective function i in optimization
g Acceleration of gravity = 9.81 (m/s^2)
$g_i(\boldsymbol{x})$ Constraint i in optimization
G_n Constant in (10) and (14)
h Heat transfer coefficient (W/m^{2}K)
k Thermal conductivity of fluid (W/mK)
k_s Thermal conductivity of solid (W/mK)
L Heat sink length (m)
l Fin height (m)
L_c Component length in Fig. 1 (m)
L_d Distance between components in Fig. 1 (m)
m Mass (kg)
N Number of fins
n_{ie} Number of inequality constraints g_i in optimization
N_p Number of particles in optimization
Nu   Mean Nusselt number = hd_h/k
Nu$_x$ Local Nusselt number
Pr   Prandtl number = $\nu \rho c_p/k$
q Heat flux (W/m^2)
Re   Reynolds number = Vd_h/ν
REP   Repository of Pareto optimal solutions in optimization
$\boldsymbol{r}_i$ Vector of random numbers in optimization
t Fin thickness (m)
T Local temperature (K)
T_0 Wall temperature at x = 0 in (13) (K)
T_{avg} Average temperature in (6) (K)

Springer

T_∞	Ambient temperature (K)
T_L	Wall temperature at x = L in (13) (K)
T_m	Mean temperature (K)
T_w	Wall temperature (K)
u	Velocity component in x-direction (m/s)
V	Mean velocity (m/s)
W	Heat sink width (m)
W_c	Component width in Fig. 1 (m)
$V_{i,k}$	Velocity component vector of swarm member i in optimization
x	x-coordinate (m)
x^*	Dimensionless coordinate = $x/(RePrd_h)$
x^+	Dimensionless coordinate = $x/(Red_h)$
X_C	Location vector of components in x-direction (m)
$x_{i,k}$	Design variable vector of swarm member i in optimization
x_l	Design variable vector lower bound in optimization
x_u	Design variable vector upper bound in optimization
y	y-coordinate (m)
Y_C	Location vector of components in y-direction (m)
z	z-coordinate (m)

Greek symbols

β	Volumetric expansion coefficient, for gas = $1/T_\infty$ (1/K)
ΔT	Temperature difference = T_w- T_∞ (K)
θ	Dimensionless temperature = $(T_w- T)/(T_w- T_\infty)$
λ_n	Eigenvalue in (10) and (14)
ν	Kinematic viscosity (m²/s)
ξ	Dummy coordinate variable in (10)
ρ	Fluid density (kg/m³)
ρ_{avg}	Average fluid density in channel (kg/m³)

ρ_∞	Ambient fluid density (kg/m³)
τ_w	Mean wall shear stress (N/m²)
ϕ_c	Heat dissipation of component in Fig. 1 (W)
ϕ_{ic}	Heat transfer rate from isothermal channel (W)
ϕ'_{CFD}	Heat transfer rate per unit length with CFD in Table 4 (W/m)
ϕ'_p	Heat transfer rate per unit length with new model in Table 4 (W/m)
ϕ'_{sp}	Heat transfer rate per unit length with superposition principle in Table 4 (W/m)

1 Introduction

A typical cooling heat sink contains many discrete surface- or flush-mounted components. An example heat sink containing two components with heat dissipation is shown in Fig. 1. It is composed of rectangular plate fins and a base plate. The main design criterion is to keep component temperatures below safe values to prevent overheating. If the fins are far apart, a single fin heat transfer analysis is adequate, but this approach is limited in practical applications, which often require calculation of flow and heat transfer in the channels between the fins.

There is abundant literature on the heat transfer of finned surfaces [1]. Single fin optimization results do not generally correspond to optimal fin shapes in fin arrays. However, such results can be used as an initial guess to optimize the geometry of an array. Analysis of the optimum shape of a single plate fin has been studied in [2]. Results of optimum fins with other cross-sections such as rectangular also appear in the literature [3]. Easy-to-use analytical formulae for heat transfer in forced

Fig. 1 A natural convection heat sink

Dimension	Value [mm]
L	200
l	120
W	100
b	10
t	1
d	10
L_c	32
W_c	30
L_d	24
N	10

$\phi_c = 32.3\ W$
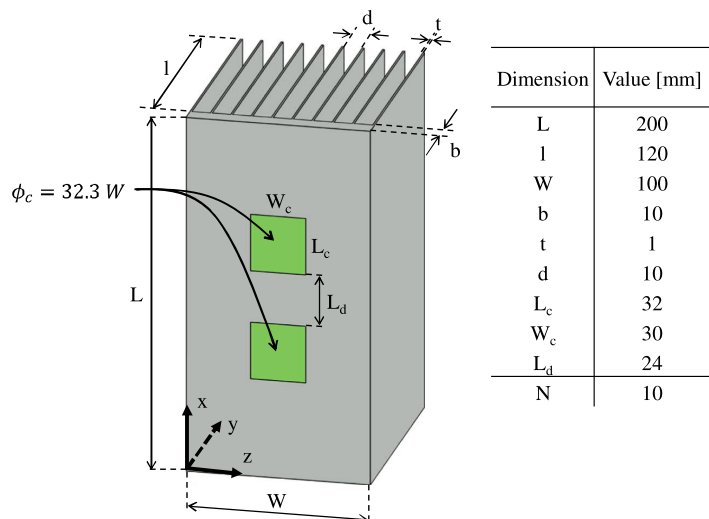
and natural convection when the fin base has constant heat flux are given in [4].

Designing a fin array is more challenging case than designing a single fin, because the former contains more variables. An optimization problem arises when we try to find a suitable combination of location of heat generating components, number and geometry of fins, outer volume of array, and amount of manufacturing material. Because the method proposed in this paper for natural convection is based on the results of forced convection, let us first quickly review forced convection.

Optimal results for channel width in isothermal arrays with forced flow have been studied, e.g., in [5], but if we seek to minimize mass or size, we must resort to non-isothermal analysis. The first analytical study of an isothermal base plate with a non-isothermal fin array for forced convection was presented in [6], where non-isothermal effect was examined by using the fin efficiency concept. Because temperature distributions in a solid and a fluid are solved simultaneously, this is a typical conjugated heat transfer problem. If we consider multi-objective optimization problems with many discrete heat dissipating components, such problems can always be solved numerically [7].

Natural convection is used to cool electronics, especially when reliability or low noise level is required. One such application is the mobile phone base station, where forced convection should be replaced with natural convection to avoid possible fan failure. If cooling is based on natural convection, the problem is even more challenging than with forced convection. Because natural convection heat sinks have a limited cooling rate, their design must be optimized to maintain their maximum temperatures and the heat sink outer dimensions within specified limits. Natural convection heat sinks were first studied in the 1940s by Elenbaas [8], who developed a model based on asymptotic solutions of developing and fully developed flow. Elenbaas also discovered that combined forced convection results of the friction factor and the Reynolds number could be used as part of the Nusselt number correlation in natural convection cooling. Later, these Nusselt number results were correlated into an easy-to-use Nusselt number formula by Bar-Cohen and Rohsenow [9].

Elenbaas's model and the idea of using forced convection friction factor results were reviewed and refined by Aihira [10] and Raithby and Hollands [11], who introduced the Nusselt number for isothermal channels with arbitrary cross sections and used the forced convection fRe product as part of their model. In addition, experimental results exist for the optimum geometry of 3D heat sinks with isothermal base plates [12]. Interesting comparison between optimized pin-fin and plate-fin arrays is also presented in [13], where plate-fin array results are based on the results in [9].

The above studies deal mainly with isothermal fins and base plates, but no solution exists for fin array with heat dissipating components at arbitrary locations on a base plate.

This paper presents a method that can be used to optimize practical industrial applications. The main idea here is that convection heat transfer is solved from analytical equations, and that a numerical solution is used only for conduction. We present practical examples of how multi-objective optimization can help to determine the minimum size and mass of a heat sink for natural convection cooling.

2 Heat transfer from a plate fin array

In Fig. 1, heat conduction in the fins and base plate is governed by the energy equation

$$\frac{\partial^2 T}{\partial x^2} + \frac{\partial^2 T}{\partial y^2} + \frac{\partial^2 T}{\partial z^2} = 0, \qquad (1)$$

which we solve numerically using the finite volume method. We treat fins as two-dimensional, because their temperature gradient is negligible in the direction of their thickness. In the base plate, we consider conduction in all three directions. To solve convection between fins and flow, we need to know the mean velocity and flow temperature in the channel in Fig. 2.

2.1 Mean flow velocity in a channel

In Fig. 2, the flow mean temperature T_m varies in the x- and y-direction, as does also the flow average temperature T_{avg}. In a vertical slice, each part-channel in the y-direction is solved individually for their mean velocity V. We restrict our analysis to laminar flow in a channel, because turbulent flows occur very seldom in natural convection cooling. In fact, the
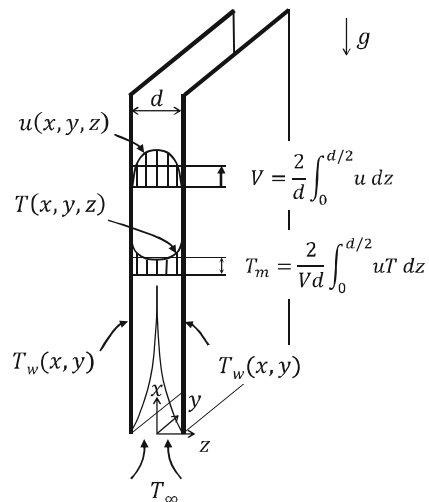

Fig. 2 Schematics of a channel

turbulent case would be easier, because we can use the results of fully developed flows.

If we know the mean flow velocity V, the mean friction factor f is calculated from equation [14]

$$f\mathrm{Re} = 3.44(x^+)^{-0.5} + \frac{\dfrac{0.647}{4x^+} + 24 - 3.44(x^+)^{-0.5}}{1 + 0.000029(x^+)^{-2}}, \qquad (2)$$

where the dimensionless length $x^+ = x/(\mathrm{Re}d_h)$, and the hydraulic diameter of a channel $d_\mathrm{h} = 2d$, which is used in the Reynolds number $\mathrm{Re} = Vd_h/\nu$. Eq. (2) takes into account the increase in the friction factor due the flow developing at the lower part of the channel in Fig. 2. With a large channel aspect ratio d/L, we have a fully developed parabolic velocity profile and $f\mathrm{Re} = 24$.

In natural convection, flow is driven by buoyancy. Here, we calculate the mean velocity V at a fixed y in a vertical channel slice (see Fig. 2) from the force balance between the wall mean shear stress τ_w and buoyancy based on the fluid average temperature T_avg and density ρ_avg in a channel

$$\left(\rho_\infty - \rho_{avg}\right)gd - 2\tau_w = 0, \qquad (3)$$

where the wall shear stress is

$$\tau_w = \frac{1}{2}\rho_{avg}V^2 f. \qquad (4)$$

Using the ideal gas law $\rho = p/RT$ and assuming $p \approx p_\infty$, we get

$$V = \frac{g\beta d_h^{\,2}}{2\upsilon(f\mathrm{Re})}\left(T_{avg} - T_\infty\right), \qquad (5)$$

where the average temperature is

$$T_{avg} = \frac{1}{L}\int_0^L T_m dx, \qquad (6)$$

and where the coefficient of volumetric expansion for gas is $\beta = 1/T_\infty$. Eq. (5) assumes that the fluid density is constant outside the channels (Boussinesq approximation). The fluid mean and average temperatures T_m and T_avg must be known in order to solve the mean velocity from Eq. (5).

2.2 Fluid temperature in a channel

Local heat transfer between the fin surface and channel flow is governed by the equation

$$\rho c_p V d \frac{\partial T_m}{\partial x} = 2h(x,y)(T_w - T_m), \qquad (7)$$

where $h(x,y)$ is the local heat transfer coefficient, assuming that both walls have the same temperature distribution T_w, ρ is fluid density, and c_p is the specific heat of the fluid. The

assumption that both walls share the same temperature is typically adequate with fin arrays in which temperature varies only little between adjacent fins. In our model, the local wall temperature T_w is thus assumed to be the average of the local fin temperatures in a channel.

In every fin point (x,y) the same amount of heat as is transferred by convection to fluid must be conducted through a fin to that point. The fin temperature distribution $T_w(x,y)$ is coupled with the local mean fluid temperature by the equation

$$q(x,y) = h_1(x,y)[T_{m1}(x,y) - T_w(x,y)]$$
$$+ h_2(x,y)[T_{m2}(x,y) - T_w(x,y)], \qquad (8)$$

where $h_1(x,y)$ and $h_2(x,y)$ are heat transfer coefficients in the channels on both sides of the fin, and $T_{m1}(x,y)$ and $T_{m2}(x,y)$ are the corresponding fluid mean temperatures in these channels. The heat flux by conduction in a fin, namely q(x,y), is obtained from Eq. (1) using the control volume method. For heat transfer calculations, it makes no difference if the flow is created by buoyancy in natural convection or by a fan in forced flow. We calculate the local heat transfer coefficient in the channel from the forced convection result of an isothermal wall channel [14]

$$\mathrm{Nu_x} = \frac{h(x,y)d_\mathrm{h}}{k} = 7.541 + 6.874\left(1000x^*\right)^{-0.488}e^{-245x^*}, \quad (9)$$

where $x^* = x^+/\mathrm{Pr}$, Pr is Prandtl number and k is the fluid thermal conductivity.

It is also possible to use a more complicated approach that considers the effect of a varying fin temperature distribution using the superposition principle [15]

$$q(x,y) = \frac{4k}{d_h}\sum_{n=0}^{\infty} G_n\left(\theta_0(0,z)\exp(-2\lambda_n^2 x^*) + \int_0^{x^*}\exp(-2\lambda_n^2(x^*-\xi))\frac{\partial\theta(\xi,z)}{\partial\xi}\,\mathrm{d}\xi\right), \qquad (10)$$

where the eigenvalues λ_n and constants G_n are given in Table 1. The dimensionless temperature $\theta = (T_w - T)/(T_w - T_\infty)$, and ξ is the dummy coordinate variable.

2.3 Solution algorithm

The above equations are solved using a similar approach as in [16]. The solution algorithm for a natural convection array is as follows:

1. Initial guess of the average fluid and wall temperature T_avg and $T_\mathrm{w}(x,y)$.
2. The mean velocity V from (5), f Re from (2).
3. $T_\mathrm{m}(x,y)$ from (7), for which $h(x,y)$ is obtained from (9).
4. A new Tw(x) distribution by solving conduction in fins and base plate using the finite volume method and combining it with heat flux at channel walls with (8).

Table 1 Infinite-series-solution functions for thermal-entry length in a parallel plate channel in Eqs. (10) and (14)

n	λ_n	G_n
0	3.885	1.717
1	13.09	1.139
2	22.32	0.952
>2	$16\sqrt{\frac{1}{3}}n + \frac{20}{3}\sqrt{\frac{1}{3}}$	$2.68\lambda_n^{-1/3}$

5. Updating the average fluid temperature T_{avg} TfromT(x) values using (6).
6. If T_{avg} differs from the previous value, calculation is repeated starting from point 2.

3 Accuracy of the present model

The model was tested by comparing its results with those of a single isothermal 2D channel, a single non-isothermal 2D channel, and a full scale 3D heat sink, as described below.

3.1 Isothermal 2D–channel

The mean Nusselt number of an isothermal vertical channel with natural convection was presented by Bar-Cohen et al. [9]:

$$\text{Nu} = \frac{hd}{k} = \left(\frac{576}{\text{El}^2} + \frac{2.873}{\sqrt{\text{El}}}\right)^{-1/2}, \quad \text{El} = \frac{g\beta(T_w - T_\infty)d^3}{v^2}\Pr\frac{d}{L}, \quad (11)$$

where El is the Elenbaas number, also called the modified Rayleigh number in many papers. The total heat transfer rate from an isothermal channel is

$$\phi_{ic} = 2hLl(T_w - T_\infty). \quad (12)$$

An isothermal 2D channel was calculated using the present model and different combinations of geometry and temperature (Table 2). The results of our model are given in Fig. 3, which also shows the results of reference CFD calculations and the Bar-Cohen Eq. (11). Modelling was performed using the open source CFD software OpenFOAM with a compressible (ideal gas law) flow solver (buoyantPimpleFoam),

Table 2 Dimensions and temperatures of the tested 2D channel

Variable	Value	Unit
L	50; 100; 200; 400	mm
d	5; 7.5; 10; 15	mm
T_w	310; 320; 330	K
T_∞	280; 290; 300	K
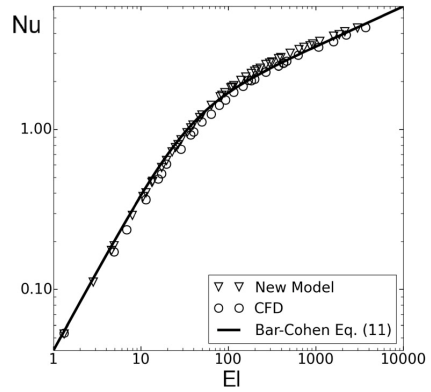
Fig. 3 Comparison of different methods in an isothermal 2D channel

laminar 2D flow, the Sutherland viscosity law, and Pr = 0.7 and c_p = 1006 J/kgK.

Only some combinations from Table 2 are shown in Fig. 3. These results are in good agreement, and the most noticeable detail is that the Nusselt numbers calculated with the present model tend to be slightly higher than CFD results.

3.2 Non-isothermal 2D channel

Our method uses the Nusselt number correlation of a constant wall temperature channel, but practical heat sinks are seldom isothermal. The effect of a non-isothermal wall is tested when the wall temperature changes linearly

$$T_w(x) = T_0 + (T_L - T_0)x, \quad (13)$$

where T_0 is the wall temperature at $x = 0$ and T_L at $x = L$. This simple test gives some idea of the accuracy of our model. Reference solutions are obtained numerically with CFD (OpenFOAM solver buoyantPimpleFoam) and analytically based on the superposition principle from Eq. (10) by substituting temperature distribution in (13) for Eq. (10) [15]. The result is

$$\text{Nu}_x = \frac{C_2 - 8C_2\sum\limits_{n=0}^{\infty}\frac{G_n}{\lambda_n^2}\exp(-2\lambda_n^2 x^*) + 8C_1\sum\limits_{n=0}^{\infty}G_n\exp(-2\lambda_n^2 x^*)}{16C_2\sum\limits_{n=0}^{\infty}\frac{G_n}{\lambda_n^4} - 16C_2\sum\limits_{n=0}^{\infty}\frac{G_n}{\lambda_n^4}\exp(-2\lambda_n^2 x^*) + 16C_1\sum\limits_{n=0}^{\infty}\frac{G_n}{\lambda_n^2}\exp(-2\lambda_n^2 x^*)}, \quad (14)$$

where $C_1 = T_0 - T_\infty$ and $C_2 = \text{RePr}d_h(T_L - T_0)/2L$. Comparison is made between our model, an analytical solution (14), and CFD solutions in 12 different cases (details in Table 3).

Table 4 shows the results of the different methods. Deviation increases when the channel aspect ratio d/L or the wall temperature change increases. An interesting point is that the model predicts heat transfer better for an increasing than decreasing wall temperature case. This is good from the

Table 3 Dimensions and temperature pairs (see Eq. (13)) of a tested non-isothermal 2D channel

Dimension	Value	Unit
L	100	mm
d	5; 10; 20	mm
$[T_0, T_L]$	[300, 320]; [300, 350]; [320, 300]; [350, 300]	K
T_∞	280	K

Fig. 4 Temperature fields of the new model (*left*) and CFD (*right*)

practical point of view, because increasing wall temperature is more relevant in industrial applications with many heat generating components. Our model works also reasonably well when the channel width is 5 or 10 mm, which is a typical range for practical optimum channel width. In fact, with $d = 20$ mm, fins are far from each other, and their heat transfer is the same as from vertical surfaces, and they are not relevant in fin array cooling.

3.3 Full scale 3D heat sink

An aluminium test case ($k_s = 200$ W/mK) is shown in Fig. 1. Full scale 3D heat sink calculations were also done with CFD (OpenFOAM). The solver was chtMultiRegionFoam, which is suitable for conjugated heat transfer. The temperature fields of solid and fluid were modelled as separate regions and coupled at fluid-solid interfaces. The total number of cells in 3D calculation was around 10^6 for the fluid and 5×10^4 for the solid region. A transient approach was used to guarantee a stable solution.

Results of the new model and CFD for the reference 3D fin array in Fig. 1 are shown in Fig. 4. Compared to the CFD result, the new model predicts the maximum temperature, the most interesting variable in terms of thermal management, quite well. Table 5 shows the minimum and maximum temperature excess to ambient temperature.

The main advantage of our model is the reduction of the CPU time. The test case in Fig. 4 was calculated with our model about 3000 times faster than with CFD. We have also tested the calculation time speedup in other 3D cases, and it has always been at least one thousand. The similarity of results and the significantly shorter solution time make the model well suited for industrial optimization.

4 Multi-objective optimization

4.1 Problem formulation

In the multi-objective optimization of a heat sink at least two conflicting objective functions must be minimized simultaneously. Typical objective functions are maximum temperature, material amount, and the outer volume of the heat sink. If maximum temperature and mass are minimized, the multi-objective problem is defined as

$$\begin{aligned} \text{find} \quad & \mathbf{x} = (L, W, b, l, t, N, \mathbf{X_C}, \mathbf{Y_C})^T \\ \text{to minimize} \quad & \mathbf{f} = (T_{max}, m) \\ \text{such that} \quad & g_1 = l + b - l_{max} \le 0 \\ & g_2 = d_{min} - \frac{(W - Nt)}{N - 1} \le 0, \end{aligned} \quad (15)$$

Table 4 Heat transfer of different channels from Table 3; $T_\infty = 280$ K, ϕ'_p solutions of the present model, ϕ'_{CFD} with CFD, and $\phi'_{sp.}$ based on Eq. (14)

L [mm]	d [mm]	T_0 [K]	T_L [K]	ϕ'_{CFD} [W/m]	ϕ'_p [W/m]	difference to CFD [%]	$\phi'_{sp.}$ [W/m]	difference to CFD [%]
100	5	300	320	22.7	23.3	2.7	23.5	3.8
100	5	300	350	46.2	47.6	3.0	48.7	5.4
100	5	320	300	14.6	15.9	9.0	15.5	5.9
100	5	350	300	23.4	27.5	17.7	25.8	10.5
100	10	300	320	42.8	41.9	−2.2	43.5	1.5
100	10	300	350	74.4	68.7	−7.7	74.5	0.2
100	10	320	300	36.6	42.1	14.9	37.9	3.6
100	10	350	300	58.1	71.5	23.2	60.2	3.7
100	20	300	320	42.8	35.0	−18.1	37.4	−12.7
100	20	300	350	73.6	53.4	−27.5	62.4	−15.2
100	20	320	300	36.8	41.1	11.8	33.1	−10.0
100	20	350	300	56.6	71.3	25.9	51.0	−9.8

Table 5 Minimum and maximum temperature difference $\Delta T = T_w - T_\infty$ in Fig. 4

|	CFD	Model	Difference
$\Delta T_{\min}$	23.5	21.4	−8.9%
$\Delta T_{\max}$	41.7	38.9	−6.7%

where **x** is the design variable vector composed of all dimensions of the heat sink from Fig. 1, **f** is the vector of objective functions, N is the number of fins, and X_C and Y_C component locations vectors (dimensions of these vectors are determined by the number of components). In multi-objective optimization, a set of optimal solutions, called Pareto optimal solutions, is obtained instead of a single optimum solution. A solution is Pareto optimal if there exists no other solution, which improves at least one objective without worsening any other. In this case, a solution is Pareto optimal, e.g., if the maximum temperature cannot be lowered without adding any extra mass to the fin array.

The Pareto optimal solutions are shown in Fig. 5 in bold line in an objective space, which also shows the so called Ideal and Nadir points. The Ideal point is obtained by minimizing and the Nadir point by maximizing all the criteria individually from the Pareto optimal set. Ideal and Nadir points are used to normalize the criteria so that the order of magnitude of objective values is about the same in optimization.

We also converted this constrained optimization problem to an unconstrained one by using an exterior penalty function. In this method, evaluation of the object function $f_i(\mathbf{x})$ is replaced by $F_i(\mathbf{x})$:

$$F_i(\mathbf{x}) = \begin{cases} f_i(\mathbf{x}) & \mathbf{x} \in \Omega \\ f_{\max} + \sum_{i=1}^{n_{ie}} \max[0, g_i(\mathbf{x})] & otherwise \end{cases} . \quad (16)$$

The evaluation differs from $f_i(\mathbf{x})$ in those solutions that are not located within the feasible area $f(\Omega)$ (see Fig. 5). For them, a constant $f_{\max}$ is set as same value as the upper bound of the largest objective.
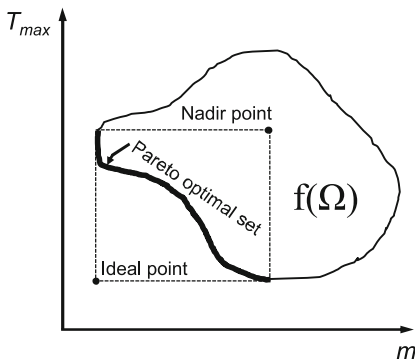
Fig. 5 Feasible area $f(\Omega)$ of all possible solutions in an objective space with the Pareto optimal set, the Nadir point, and the Ideal point

4.2 Different multi-objective optimization methods

Multi-objective optimization may be performed with several different methods. In the weighted sum approach, the objectives are combined into a single objective function with different weights, and depending on the weights, a single Pareto optimal point is determined. The problem here is that not all Pareto optima are accessible unless the problem is convex [17]. In the constraint method, only one objective is minimized, and the other objectives are set as constraints. With this method, one Pareto optimal solution can be determined at a time, and all of them are accessible regardless of the convexity of the problem. A faster method, however, is to use multi-objective optimization algorithms, such as the genetic algorithm (GA) or particle swarm optimization (PSO), to obtain all the Pareto optimal solutions at once. These evolutionary algorithms can usually deal with discrete variables, such as number of fins, with no extra problems.

4.3 Modified PSO algorithm

We chose to use a multi-objective version of a PSO algorithm. PSO algorithms are based on the social behavior of many species in nature such as the schooling of fish and the flocking of birds. The first paper on the PSO algorithm was published by Kennedy and Eberhart [18], who introduced standard PSO (sPSO). Later, Shi and Eberhart [19] introduced a modified version of this algorithm with an inertia component to improve its performance. A significant improvement to these original versions of PSO was introduced in [20], which presented "A locally convergent rotationally invariant PSO" LcRiPSO version of the algorithm. These all are, however, PSO versions for single-objective optimization. The best known multi-objective optimization version of the PSO algorithm (MOPSO) was introduced by Coello Coello [21]. Their MOPSO algorithm is used in this paper with modifications implemented from the LcRiPSO algoritm. A further slight modification is made to a swarm member choosing its target during optimization.

In the MOPSO algorithm, a swarm consists of N_p particles in the design space. Particle locations are updated at different time steps k, and the values of the design vectors represent these locations. The algorithm is initialized by scattering the particles randomly inside the design space and by setting their velocities to random values:

$$\begin{aligned} \mathbf{x}_{i,k=0} &= \mathbf{x}_l + \mathbf{r}_1(\mathbf{x}_u - \mathbf{x}_l) , & i = 1, \ldots, N_p \\ V_{i,k=0} &= \mathbf{r}_2, & i = 1, \ldots, N_p \end{aligned} . \quad (17)$$

In the above equation, $\mathbf{r}_1$ and $\mathbf{r}_2$ are vectors of uniform random numbers in the range of [0, 1]. The design space boundary values are within the limits of $[\mathbf{x}_l, \mathbf{x}_u]$. After the
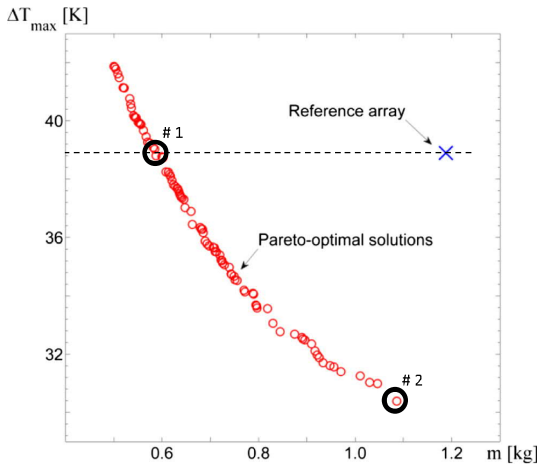
Fig. 6 Pareto-Optimal solutions

Fig. 8 Pareto-Optimal solutions

initialization of the problem, the velocity update rule is somewhat sophisticated, and it is given in detail in [20].

The target for an individual swarm member i is the nearest Pareto optimal solution (calculated for every member h in the repository REP) in the design space measured by the Euclidian norm

$$d_{i,h} = \sqrt{\sum_{j=1}^{N_p} \left[\frac{REP[h]_j - x_{i,j}}{x_{u,j} - x_{l,j}} \right]^2} . \quad (18)$$

Moving inside the design space, particles may collide with the design space boundaries. If a particle crosses the boundary limit of any design variable, the value of the crossed variable

is set as a boundary value, and the corresponding velocity component in the velocity vector is set equal to zero. Usually, velocity also has its maximum limit. If the limit is exceeded, the length of the velocity vector is normalized to its maximum value

$$if |V_i| > V_{max} \rightarrow V_i = \left(\frac{V_{max}}{|V_i|} \right) V_i. \quad (19)$$

4.4 Multi-objective optimization of a fin array

The variables in optimization were the geometrical parameters of a fin array W, L, l, t, b, the number of fins N, and the component locations on the base plate (see Fig. 1). Two different sets of objectives were shown. First, the objectives were the maximum temperature of the heat sink and its material weight. In the second case, the outer volume of the heat sink and its material weight were chosen as objectives.

Fig. 7 Reference and two optimized heat sinks #1 and #2 in Fig. 6. Reference array dimensions are shown in Fig. 1
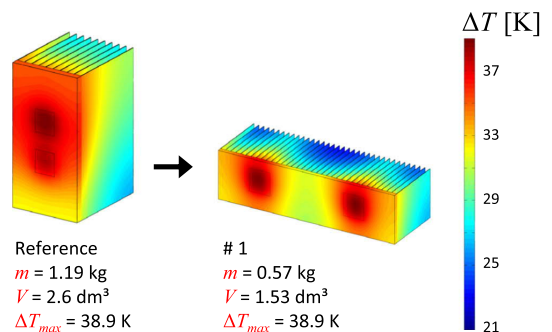
Fig. 9 Reference and optimized array #1 in Fig. 8
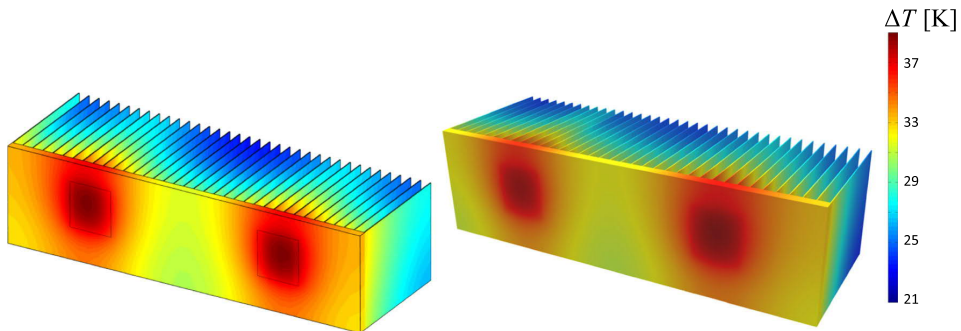
Fig. 10 Temperature field with the new model (*left*) and CFD (*right*)

5 Optimization results

5.1 Minimizing maximum temperature and material weight

Pareto optimal solutions are shown in Fig. 6, and two examples of them (#1 and #2) are presented in detail in Fig. 7. Solution #1 has the same maximum temperature, but its material weight is about 50% lower than in the reference case. Solution #2 has approximately the same material weight, but its maximum temperature is lower. Even though these optima are produced by mathematical optimization, they are impractical, because two small heat generating components are located on a large base plate. Next, we show the results of minimizing material weight and outer volume simultaneously by keeping the constant maximum temperature as a constraint.

5.2 Minimizing outer volume and material weight

A new Pareto optimal set is shown in Fig. 8, and solution #1 is detailed in Fig. 9, where the reference array is the same as in Fig. 7. Now the optimum solution is also suitable for practical applications. The shape of the Pareto optimal solutions in Fig. 8 is not as smooth as in the previous case in Fig. 6. One reason may be the discrete design variable N, i.e., the number of fins, which may have caused the steps. Another reason may be the MOPSO optimization algorithm, which is not gradient-based and thus does not always find exact optimum solutions but rather solutions near the optimal set. Yet—for practical purposes—nearby optimal solutions are very useful.

Table 6 Dimensions of the optimized case in Fig. 9

L [mm]	W [mm]	l [mm]	t [mm]	N [−]	b [mm]
68	256	82	0.54	36	6

The optimum geometry #1 in Fig. 9 was also analyzed with CFD. The temperature fields of our model and CFD are shown in Fig. 10, where the left heat sink is the same as in Fig. 9. In the final geometry, the symmetrical component locations are 53 mm from the heat sink side edge and 38 mm from the bottom edge. Values of other dimensions are given in Table 6. The maximum temperatures are almost the same, whereas the minimum temperatures vary, because the flow may enter from the tips of the fins in the CFD solution, whereas in our model, the flow in the channels is always one-dimensional. If the fin height l is small in comparison with fin length L, the overall convective heat transfer can be under predicted because of the assumption of one-dimensional flow.

6 Conclusions

This paper introduces a new heat transfer model for heat sinks, which can be used to optimize fin arrays cooled by natural convection. The main idea is that flow and convection heat transfer are calculated using analytical results of forced convection, because buoyancy-driven and fan-generated flows are similar. The model was tested by comparing its results with those of an isothermal 2D channel and with our CFD results. Furthermore, a reference 3D array with two heat generating components was calculated with this model and compared to numerically modelled CFD results. The CPU time was many orders of magnitude less with our model than with CFD. In addition, its accuracy was sufficient for practical applications. Consequently, our model is suitable for optimization purposes where CFD is impractical due to a long CPU time.

In practice, multi-objective optimization has an advantage over traditional single objective optimization, because the former can help us to see all the compromise solutions at once. With correct objective selection, the design can be significantly improved, and the decision maker can then choose the best design from Pareto optimal set. However, even with multi-objective optimization, the results can be impractical if, as pointed out above, the objectives are not chosen correctly.

For algorithm selection, we have observed that PSO algorithms are efficient when we have a discrete design variable, such as the number of fins.

Compliance with ethical standards

Conflict of interests   The authors declare that they have no conflict of interest.

References

1. Kraus AD, Aziz A, Welty J (2001) Extended surface heat transfer. Wiley, New York
2. Karvinen R, Karvinen T (2010) Optimum geometry of fixed volume plate fin for maximizing heat transfer. Int J Heat Mass Transf 53:5380–5385
3. Karvinen R, Karvinen T (2012) Optimum geometry of plate fins. ASME J Heat Transf 134:08101-1-7
4. Lindstedt M, Karvinen R (2017) Conjugated heat transfer from a uniformly heated plate and a plate fin with uniform base heat flux. Int J Heat Mass Transf 107:89–95
5. Bejan A (1993) Heat transfer. Wiley, Chichester, New York
6. Teertstra P, Yovanovich MM, Culham JR (2000) Analytical forced convection modelling of plate fin heat sinks. J Electron Manuf 10(4):253–261
7. Lindstedt M, Lampio K, Karvinen R (2015) Optimal shapes of straight fins and finned heat sinks. ASME J Heat Transf 137(6): 061006-1-8
8. Elenbaas W (1942) Heat dissipation of parallel plates by free convection. Physica 9(1):665–671
9. Bar-Cohen A, Rohsenow W (1984) Thermally optimum spacing of vertical, natural convection cooled, parallel plates. ASME J Heat Transf 106:116–122
10. Aihara T (1991) In: Aung W (ed) Air cooling techniques by natural convection, cooling techniques for computers. Hemisphere, New York, pp 1–45
11. Raithby GD, Hollands KGT (1985) chapter 6. In: Rohsenow WM et al (eds) Natural convection, handbook of heat transfer fundamentals, 2nd edn. McGraw–Hill, New York, pp 6–37
12. Kim TH, Kim D-K (2013) Correlation for the fin Nusselt number of natural convective heat sinks with vertically oriented plate-fins. Heat Mass Transf 49:413–425
13. Joo Y, Kim SJ (2015) Comparison of thermal performance between plate-fin and pin-fin heat sinks in natural convection. Int J Heat Mass Transf 83:345–356
14. Shah RK, London AL (1978) Laminar flow forced convection in ducts. Academic Press, New York
15. Kays W, Crawford M, Weigand B (2005) Convective heat and mass transfer, 4th edn. McGraw Hill, New York
16. Karvinen R, Lampio K (2013) Multi-objective optimization of electronics heat sink geometries (Invited paper). Proc of IWHT2013. Xi'an, China
17. Miettinen K (1999) Nonlinear multiobjective optimization. Kluwer Academic Publishers, Boston
18. Kennedy J, Eberhart R C (1995) Particle swarm optimization. Proc of IEEE International Conference on Neural Networks. Perth, Australia
19. Shi Y, Eberhart R C (1998) Modified particle swarm optimizer. Evolutionary Computation Proceedings, IEEE World Congress on Computational Intelligence. Anchorage, AK, USA
20. Mohammad RB, Zbigniew M (2014) A locally convergent rotationally invariant particle swarm optimization algorithm. Swarm Intell 8:159–198
21. Coello Coello C, Pulido G, Lechuga M (2004) Handling multiple objectives with particle swarm optimization. IEEE Trans Evol Comput 8(3):256–279
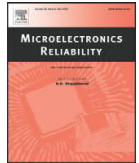
Publication V

Kaj Lampio, Reijo Karvinen

Optimization of convectively cooled heat sinks

Optimization of convectively cooled heat sinks

Kaj Lampio *, Reijo Karvinen

Tampere University of Technology, Tampere, Finland

ARTICLE INFO

ABSTRACT

Many factors of heat sink, such as its size and mass, component locations, number of fins, and fan power affect heat transfer. Owing to the opposite effects of these factors on heat sink maximum temperature, we have now a multi-objective optimization problem. A typical optimization case consists of hundreds of heat sink temperature field evaluations, which would be impractical to do with CFD. Instead, we propose to combine analytical results of convection and numerical solution of conduction to address these so-called conjugated heat transfer problems. We solve heat conduction in a solid numerically using the finite volume method and tackle convection with the analytical equation of forced convection in a parallel plate channel.

This model is suitable for forced and natural convection heat sinks, and we have verified its validity by comparing its results to measured data and CFD calculations. We use the model to improve two industrial examples, using a multi-objective version of the particle swarm optimization (PSO) algorithm. The first example is a forced convection heat sink composed of nine heat generating components at the base plate, and the other is a natural convection case with two components. In both cases, mass is minimized; the other criterion is maximum temperature for the forced convection case and heat sink outer volume for the natural convection case. Our method is many orders of magnitude faster than CFD. Additionally, we provide some LES results of pin fins with natural convection for further use in similar optimizations.

© 2017 Elsevier Ltd. All rights reserved.

1. Introduction

A typical heat sink used to cool electronics contains many discrete surface or flush mounted components. An example heat sink containing nine components with different heat dissipation is shown in Fig. 1. It is composed of rectangular plate fins and a base plate. However, the shape is not limited to rectangular, and fins can have another cross-section such as triangular and trapezoidal. The main design criterion is to keep component temperatures below safe values to prevent overheating. If the fins are far apart, a single fin heat transfer analysis is adequate, but this approach is limited in practical applications, which often require calculation of flow and heat transfer in channels between the fins. Isothermal arrays with an optimum channel width have been studied [1], but if we want to minimize mass or size, we must resort to non-isothermal analysis. Because the temperature distributions of a solid and fluid are solved simultaneously, this is a typical conjugated heat transfer problem.

Single fin optimization results do not generally correspond to optimal fin shapes for fin arrays. However, single fin results serve as a good initial guess to optimize the array geometry. Analysis of single fin heat transfer can be found in the literature, e.g., in [2]. The optimum shape of a single plate fin with a constant mass has also been studied in

[3], and easy-to-use analytical formulas for optimal fin shapes have been established for forced and natural convection cases when the fin base temperature is constant. Optimum results of fins with other cross-sections such as rectangular also appear in the literature [4]. Recently, Lindstedt and Karvinen arrived at a simple analytical solution for a fin with constant heat flux at the base, a result that helps determine in optimization the minimum fin mass when heat flux and maximum temperature are fixed [5].

Designing a fin array is intrinsically more challenging than single fin case. A fin array problem contains more variables, many of them with opposite effects such as the location of the heat generating components, the number and geometry of the fins, and the outer volume of the array. In addition, the amount of manufacturing material and the power used by pumps or fans can affect the result. In some cases, a somewhat elaborate analytical solution can be used [6], but such multi-objective optimization problems can always be solved numerically [7].

This paper presents, in addition to single fins results, a quick method to calculate the temperature field and heat transfer of a heat sink cooled by forced or natural convection. The method is suitable for multi-objective optimization, and its application is presented in the following. The main idea of the method is that convection heat transfer is solved from analytical equations, and that a numerical solution is used only for conduction. We present two practical examples of how multi-objective optimization can help determine the minimum size and mass of a heat sink for forced and natural convection cooling. First, however, we

 * Corresponding author.
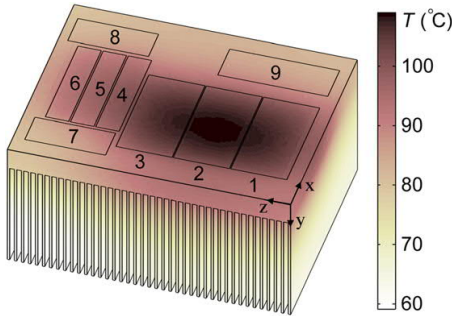   E-mail address: kaj.lampio@tut.fi (K. Lampio).

Fig. 1. Schematics and temperature field of an existing heat sink with plate fins and nine components at the base plate (array mass m = 6.65 kg).

present some analytical results of single fins, which serve as a basis for understanding the optimal fin shape and thus help design the first versions of a fin array.

2. Optimal shape of a single fin

The total heat transfer of a fin in Fig. 2 is obtained from the heat transfer of an isothermal fin ϕ_i, which is easily calculated from the correlations of an isothermal plate in text books

$$\phi = \eta \phi_i, \tag{1}$$

if the fin efficiency η is known. The efficiencies of fins with different geometries, which take into account the non-uniform temperature of a fin, are presented for *forced convection* using the non-dimensional variable
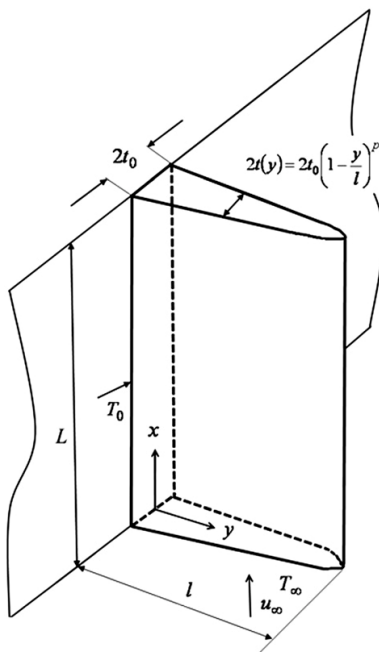
Fig. 2. Geometry of single fin.

[3,4]

$$X_* = \frac{1}{C}\frac{kt_0}{k_f l^2}\frac{L}{Re^{m_1} Pr^{n_1}}, \tag{2}$$

where the Reynolds number $Re = u_\infty L/v$, Pr is the Prandtl number = 0.7 for gases, v is the kinematic viscosity, k and k_f are heat conductivities of array material and fluid. Coefficients for a laminar boundary layer are $C = 0.332$, $m_1 = 1/2$, and $n_1 = 1/3$; and for a turbulent boundary layer $C = 0.0296$, $m_1 = 4/5$, and $n_1 = 3/5$. Fig. 2 shows the fin dimensions in Eq. (2). For instance, the efficiency of a rectangular fin in Fig. 2 (p = 0) takes the form

$$\eta = (m_1 X_*)^{1/2} \tanh(m_1 X_*)^{-1/2}. \tag{3}$$

The corresponding result of a triangular fin (p = 1) is

$$\eta = (m_1 X_*)^{1/2} \frac{I_0\left(2(m_1 X_*)^{-1/2}\right)}{I_1\left(2(m_1 X_*)^{-1/2}\right)}. \tag{4}$$

In Eq. (4), I_n is the modified Bessel function of the first kind. From Eqs. (3) and (4), it is easy to find the fin geometry to maximize heat transfer for a fixed fin mass when some of the dimensions are fixed, as we often have in actual practice. In Table 1 [4], we give an idea of how flow type and fin shape affect the total heat transfer rate by comparing the relative performance of different fins with the same mass. An optimized aluminum rectangular fin with a fin base thickness of $2t_0 = 1$ mm, and a laminar boundary layer serves as a reference with a heat rate $\phi_{ref} = 5.1$ W. We can see that the flow type, i.e., laminar or turbulent, has only a little effect on the relative values (1 and 1.18), but that the shape affects more (1 and 1.41) for laminar flow. If the mass of the fin remains the same, changing a laminar boundary layer into to a turbulent one while simultaneously modifying a rectangle shape into a triangle doubles the heat transfer relative value from 1 to 2. If the boundary layer is either laminar of turbulent, the increase in heat transfer is mainly due the increase in L, the fin length in flow direction, while the fin height l stays approximately constant, as seen in Table 1. The optimization thus suggests that there is too much mass located near the fin tip and it ought to be used as increased heat transfer surface area.

In the case of natural convection, the corresponding non-dimensional variable as Eq. (2) is

$$X_* = \frac{1}{C^4}\frac{v^2}{g\beta}\frac{1}{Pr\,\theta_0}\left(\frac{kt_0}{k_f l^2}\right)^4 L, \tag{5}$$

Table 1
Dimensions and characteristics of optimal aluminum fins with laminar and turbulent boundary layers in air flow. Fin material volume 10^{-6} m^3 (m = 2.7 g), $u_\infty = 10$ m/s, $\theta_0 = T_0 - T_\infty = 60$ °C, and fixed fin base thickness $2t_0 = 1$ mm.

p laminar	ϕ/ϕ_{ref}, $\phi_{ref} = 5.1$ W	η	L	l
0	1	0.79	0.051	0.040
1/2	1.23	0.79	0.074	0.040
1	1.41	0.78	0.100	0.040
2	1.52	0.75	0.157	0.038
p turbulent	ϕ/ϕ_{ref}	η	L	l
0	1.18	0.91	0.084	0.024
½	1.61	0.91	0.131	0.023
1	2.00	0.91	0.187	0.021
2	2.63	0.87	0.300	0.020

where

$$C = 0.503\left[1 + \left(\frac{0.492}{Pr}\right)^{9/16}\right]^{-4/9},\tag{6}$$

and the coefficient of thermal expansion $\beta = 1/T$ for air, and $\theta = T_0 - T_\infty$ is the temperature excess. The values of non-dimensional variables (2) and (5) at the optimum point are found in the literature [4].

3. Treatment of a plate fin array

In Fig. 1, heat conduction in the fins and base plate is governed by the energy equation

$$\frac{\partial^2 T}{\partial x^2} + \frac{\partial^2 T}{\partial y^2} + \frac{\partial^2 T}{\partial z^2} = 0,\tag{7}$$

which we solve numerically using the finite volume method. We treat fins as two dimensional, because their temperature gradient is negligible in the direction of their thickness. In addition, in the base plate, we consider the conduction in all three directions (details in refs. [7,8]). To solve convection between the fins and the flow, we need to know the mean velocity and flow temperature in the channel in Fig. 3.

3.1. Mean flow velocity in a channel

For *forced convection*, the open boundary at the fin tip area in Fig. 1 is assumed to be blocked completely by the ventilation channel walls. Flow is thus completely in the x-direction and we obtain the mean velocity, if not fixed, by solving the operating point from the fan and system characteristics

$$\frac{1}{2}\rho V^2\left(4f\frac{L}{d_\mathrm{h}} + \sum_\mathrm{i} \zeta_\mathrm{i}\right) = \Delta p,\tag{8}$$

where ζ is the minor loss coefficient, Δp is the pressure loss in a heat sink channel, and f is the apparent friction factor. In the case of trapezoidal fins the channel is discretized in the y-direction into part-channels. Each of these part-channels is solved individually for their mean velocity from Eq. (8) and system characteristics. For a laminar flow, we calculate the mean friction factor f, as is done in [9], from the equation

$$f\mathrm{Re} = 3.44(x^+)^{-0.5} + \frac{\frac{0.647}{4x^+} + 24 - 3.44(x^+)^{-0.5}}{1 + 0.000029(x^+)^{-2}},\tag{9}$$

where the dimensionless length $x^+ = x \,/\, (\mathrm{Re}d_h)$ and the hydraulic diameter of a channel $d_\mathrm{h} = 2d$ is used in the Reynolds number. For turbulent flow, we can use the friction factor of a fully developed flow such as [10]

$$f = 0.0791\left(\frac{2}{3}\mathrm{Re}_{d_\mathrm{h}}\right)^{-1/4}.\tag{10}$$

In the case of *natural convection*, the flow is driven by buoyancy. The open boundary at the fin tip area has only a little effect on important results, namely the maximum temperature [8]. Thus, the flow can be assumed one-dimensional in the x-direction. We calculate the mean velocity from the force balance between wall friction and buoyancy (details given in [8])

$$V = \frac{g\beta d_h{}^2}{2v(f\mathrm{Re})}(T_{avg} - T_\infty),\tag{11}$$

$$u(x,y,z)$$
$$T(x,y,z)$$
$$V = \frac{2}{d}\int_0^{d/2} u\,dz$$
$$T_m = \frac{2}{Vd}\int_0^{d/2} uT\,dz$$
$$T_w(x,y)\qquad T_w(x,y)$$
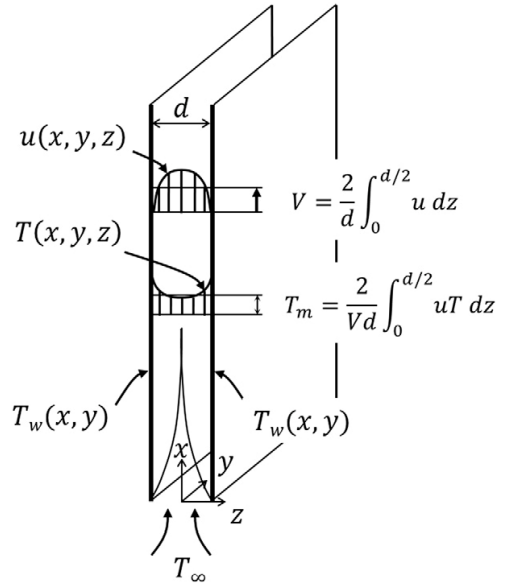$$T_\infty$$

Fig. 3. Schematics of a channel.

where T_avg is the fluid average temperature in the channel, which we obtain from the local mean temperature (see Fig. 3)

$$T_\mathrm{avg} = \frac{1}{L}\int_0^L T_m dx.\tag{12}$$

The friction factor times the Reynolds number $f\mathrm{Re}$ is obtained for a laminar natural convection from Eq. (9), but it requires the value of the mean velocity V. The mean velocity (Eq. (11)) cannot be solved until the fluid average temperature T_avg has been calculated.

3.2. Mean flow temperature T_m

Local heat transfer between the fin surface and channel flow is governed by the equation

$$\rho c_p V d\frac{\partial T_m}{\partial x} = 2h(x,y)(T_w - T_m),\tag{13}$$

where h is the local heat transfer coefficient, assuming that both walls have the same temperature distribution, ρ is fluid density, and c_p is the specific heat of fluid. The same amount of heat as in Eq. (13) must be transferred into the point (x,y) by conduction in a fin.

For a *forced laminar flow*, the local heat transfer coefficient is calculated from the result of an isothermal wall channel [9]

$$\mathrm{Nu} = \frac{h(xy)d_\mathrm{h}}{k} = 7.541 + 6.874(1000x^*)^{-0.488}e^{-245x^*},\tag{14}$$

where $x^* = x^+ \,/\, \mathrm{Pr}$; for a *turbulent flow*, it is adequate to use the mean value of a fully developed flow, which we calculate from [11]

$$\mathrm{Nu} = \frac{hd_\mathrm{h}}{k} = \frac{\frac{f}{2}(\mathrm{Re} - 1000)\mathrm{Pr}}{1 + 12.7\left(\frac{f}{2}\right)^{1/2}\left(\mathrm{Pr}^{2/3} - 1\right)}.\tag{15}$$

The temperature distribution $T_w(x,y)$ of the fin is coupled to the mean fluid temperature with the equation

$$q(x,y) = h(x,y)[T_m(x,y) - T_w(x,y)], \qquad (16)$$

where we obtain the conduction heat flux $q(x,y)$ into the point (x,y) from the numerical solution of the energy equation (Eq. (7)).

3.3. Solution algorithm

3.3.1. Forced convection heat sink
1. The mean velocity V from the fan curve operational point (Eq. (8)) or use of a given fixed value.
2. Initial guess of the $T_w(x,y)$ distribution.
3. Solving $T_m(x,y)$ from Eq. (13), to which $h(x,y)$ has been calculated from Eq. (14) or (15) for laminar and turbulent flows, respectively.
4. A new $T_w(x,y)$ distribution by solving conduction in fins and base plate using the finite volume method and combining it with the heat flux at channel walls with Eq. (16).
5. If the $T_w(x,y)$ distribution differs from the previous value, calculation is repeated starting from point 3.

3.3.2. Natural convection heat sink
1. Initial guess of the average fluid temperature and wall temperatures T_{avg} and $T_w(x,y)$.
2. The mean velocity V from Eq. (11), fRe from Eq. (9).
3. Solving $T_m(x,y)$ from Eq. (13), for which $h(x,y)$ is obtained from Eq. (14).
4. A new $T_w(x,y)$ distribution by solving conduction in fins and base plate using the finite volume method and combining it with the heat flux at channel walls with Eq. (16).
5. Updating the average fluid temperature T_{avg} from $T_m(x,y)$ values using Eq. (12).
6. If T_{avg} differs from the previous value, calculation is repeated starting from point 2.

3.4. Accuracy of the proposed model

We tested the model for *forced convection* by comparing the results with experimental data of an aluminum plate fin heat sink with one heating element generating constant heat dissipation of $\dot{Q} = 1200$ W [12]. The heat sink length was 300 mm, width 134 mm, and it contained 27 fins with fin thickness of 2 mm, and fin height of 110 mm, and the base plate thickness was 20 mm. The element location was 50 mm from the leading edge, its length was 104 mm and width the same as the base plate width, 134 mm. Temperatures were measured with thermocouples from the base plate centerline, 3 mm under the surface. The Reynolds number in the measurements was $Re = 7100$ and the inlet air
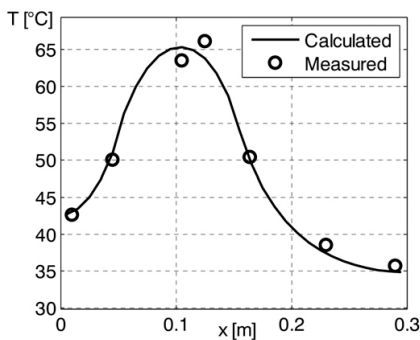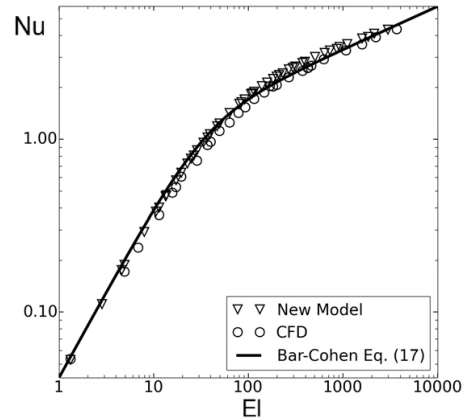

Fig. 5. Results of different methods in an isothermal 2D channel.

temperature $T_0 = 24$ °C. Fig. 4 shows the comparison and the agreement is good, when possible measuring errors are taken into account.

A *natural convection* case with a similar type heat sink was verified by comparing our results with CFD and analytical results of an isothermal channel [13]

$$Nu = \frac{hd}{k} = \left(\frac{576}{El^2} + \frac{2.873}{\sqrt{El}}\right)^{-1/2}, \quad El = \frac{g\beta(T_w - T_\infty)d^3}{v^2} \, Pr\frac{d}{L}, \qquad (17)$$

where El is the Elenbaas number. Further verification test was done with CFD results of a non-isothermal heat sink [8]. These results are shown in Figs. 5 and 6, respectively, and numerical temperatures from Fig. 6 are shown in Table 2. The agreement was not as good as in the above forced convection test case, but sufficient for design engineering purposes in optimization.

3.5. Calculation time speedup

The main advantage of our model is the speedup in the calculation CPU time. In the case of natural convection array shown in Fig. 6 the CFD calculation was done with CFD library OpenFOAM, solver chtMultiRegionFoam. The fluid region mesh had about one million cells and solid region about 50,000 cells. Solution was for a laminar flow and transient approach was chosen to guarantee the stable solution. The total CPU-time taken by OpenFOAM was about 3000 times longer than with our model. In every 3-dimensional case we have tested
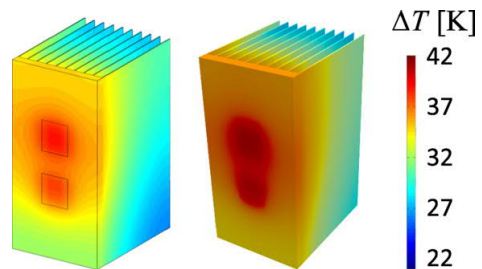

Fig. 4. Measured and calculated temperature at the centerline of the base plate in forced convection test case.

Fig. 6. Temperature fields of a fin array cooled by natural convection with our model (left) and CFD (right).

Table 2
Minimum and maximum temperature difference $\Delta T = T - T_\infty$ in Fig. 6.

	Model	CFD	Difference
$\Delta T_{\min}$	21.4	23.5	−8.9%
$\Delta T_{\max}$	38.9	41.7	−6.7%

the speedup factor has been at least one thousand. This makes the method suitable for industrial optimization purposes.

4. Natural convection of pin fin heat sinks

One possibility to increase heat transfer would be to use pin fins instead of plate fins, as shown in Fig. 7. The goal is to locate such a pin fin distribution on the base plate that temperatures of components with known heat dissipation at the other side are below given values. If we know the heat transfer of a single pin fin at a certain location on the fin base, we can use a similar approach as with plate fins. We treat each pin fin in Fig. 7 analytically using the fin efficiency formula and then combine them to numerical calculation of the base plate. However, the heat transfer of vertical pin fin stacks is generally unknown, and we study it a little here. We use CFD to model the stacks with variable pin diameters and pin spacings to determine the heat transfer coefficients of single fins. We show some preliminary results and compare them with experiments from the literature below.

4.1. Large Eddy Simulation

We calculated with CFD two vertical cylinder stacks, consisting of 10 cylinders with constant heat flux at the surface and compared the results with experimental data from [14]. In both cases, cylinder diameters were 14.4 mm, and the distances between cylinder surfaces were 10.6 mm and 50.6 mm. Each cylinder had the same surface heat flux q_w of 104 W/m². The surface temperature excess ΔT to the ambient temperature varied from 12 to 24 °C.
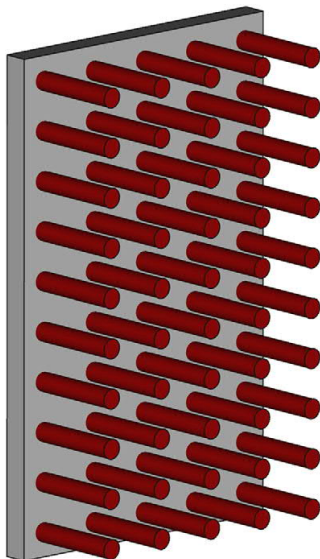

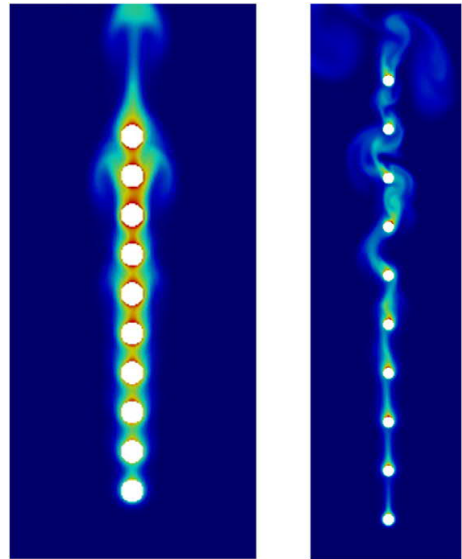**Fig. 7.** Schematics of a pin fin heat sink.

Fig. 8. Instantaneous temperature fields of vertical cylinder (d = 14.4 mm) stacks with 10.6 mm spacing (left) and 50.6 mm (right).

We assumed that the flow was mostly laminar, and that after a turbulent transition, the cross-fluctuating component of velocity did not dominate. That is, we approximated the flow as 2-dimensional. With these assumptions, we calculated CFD results using Large Eddy Simulation (LES). In general, LES is not suitable for 2D analysis, but in this case, we used it for the reasons mentioned above.

The instantaneous temperature fields of the fluid flow are shown in Fig. 8. The modified Rayleigh number is constant in both cases $Ra_d^* = g\beta q_w d^4 \Pr / k\nu^2 = 1.54 \times 10^4$. Note that on the right side of Fig. 8 temperature fluctuates as also does local heat transfer on the cylinder surface. The calculated time averaged Nusselt numbers and experimental results, shown in Fig. 9, confirm the suitability of 2-dimensional LES for an engineering approximation of the pin fin case. We made the same calculations also with k-ω SST, but the results were not as good. Consequently, we now continue to use LES as a tool to determine the Nusselt
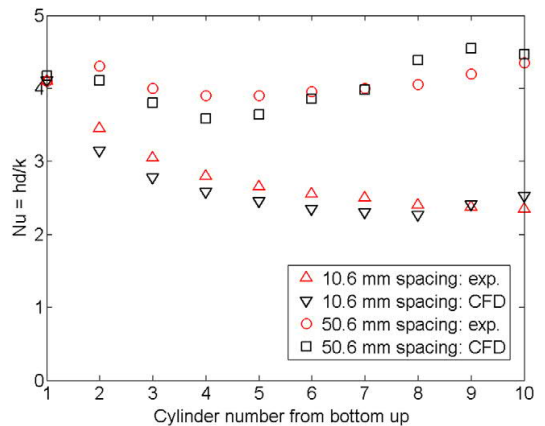

Fig. 9. Time averaged Nusselt numbers from LES computations in Fig. 8 and experiments [14].

number correlations for horizontal cylinders in the vertical stacks. We then use these Nusselt number results to optimally locate the pins. We consider also geometries other than cylindrical pins to enhance heat transfer.

5. Multi-objective optimization

In multi-objective optimization, more than one conflicting criterion is minimized simultaneously. As a result, a set of solutions (see example in Fig. 10), called Pareto-optimal solutions, are obtained. In contrast to single objective optimization, where only one optimum point is found, all Pareto-optimal solutions are mathematically equally good compromises. After multi-objective optimization, the decision maker chooses the final compromise design.

As an example, the optimization problem to minimize the mass and maximum temperature of a forced convection heat sink shown in Fig. 1 is as following:

find $x = \{N, V, d, L, b, t_b, l, d_{LE}\}$
to minimize m
such that $T_{max} \leq 109.1\,°C$
$P = 6\ W$
$pt\ Re = 3300$
$W = 242\ mm$
$d_{LE} + 156\ mm \leq L$ (18)
$156\ mm \leq L \leq 220\ mm$
$1.5\ mm \leq t_b \leq 3\ mm$
$0.3\ mm \leq t_t \leq 3\ mm$
$6\ mm \leq b \leq 26\ mm$
$4\ mm \leq d_{LE} \leq 45\ mm$
$N \in [38, 39, …, 55]$

where x is design variable vector, m mass of heat sink, T_{max} maximum temperature, P fan power, Re Reynolds number, W heat sink width, d_{LE} shortest distance of components from the leading edge ($x = 0$), L heat sink length, t_b fin thickness at the fin base, t_t fin thickness of the trapezoidal fin at tip, b base plate thickness, and N number of fins.

Multi-objective optimization may be performed with several different methods. In the weighted sum approach, the criteria are combined into a single objective function with different weights, and depending on the weights, a single Pareto-optimal point is determined. The problem here is that not all Pareto-optima are accessible with this method unless the problem is convex [15]. The constraint method is another method where only one criterion is minimized, and where the other criteria are set as constraints. With this method, one Pareto-optimal solution can be determined at a time, and all of them are accessible regardless of the convexity of the problem. This is the method used in the previous example, where maximum temperature was set as a constraint. A faster method, however, is to use multi-objective optimization

algorithms, such as genetic (GA) or particle swarm optimization (PSO), to obtain all the Pareto-optimal solutions at once. In this paper, we used a multi-objective optimization form of PSO [16] to optimize a *natural convection* array. These evolutionary algorithms can usually deal with discrete variables, such as number of fins, with no extra problems.

6. Optimized results

Heat sink design is constrained by volume or mass, locations, and power of the heat sources, and, in the case of forced convection, also by fan power. Results of two optimization cases are presented below. First for *forced convection*, an industrial case is optimized in Fig. 1 by minimizing its mass and maximum temperatures. The fin cross section is also subject to variations between rectangular, triangular, and trapezoidal shapes. Another case (details given in [8] and shown in Fig. 13) deals with *natural convection*, where the effect of the mass and outer volume of the array is shown.

In the case of *forced convection*, the mass of the array in Fig. 1 was 6.65 kg, the number of fins $N = 41$, and thickness $t_b = 2$ mm. With plate fins, the optimized mass was 3.41 kg (see circle in Fig. 10), and component locations were changed, $t_b = 1.5$ mm and $N = 48$. The best result was obtained if also trapezoidal fins were selected (see square in Fig. 10). Fig. 11 shows the optimized array geometry from Fig. 10: mass is 2.75 kg, $t_b = 1.71$ mm, $t_t = 0.33$ mm, $N = 53$, and component maximum temperatures are the same as in Fig. 1. Notice, that if

Fig. 11. Optimized heat sink with trapezoidal fins from Fig. 7, m = 2.75 kg.
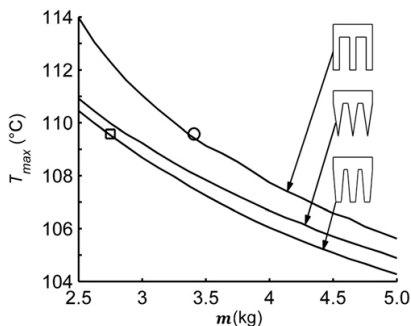

Fig. 10. Pareto-optimal solutions of a multi-objective optimization problem of forced convection array. Optimal array with the same maximum temperature as in Fig. 1 with rectangular fins (circle) and trapezoidal optima (square).
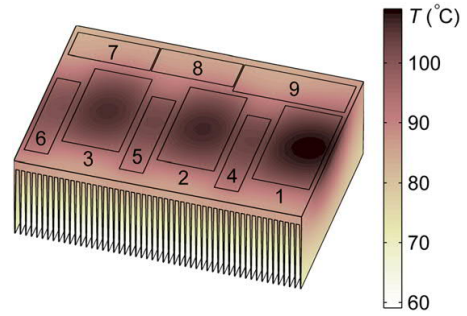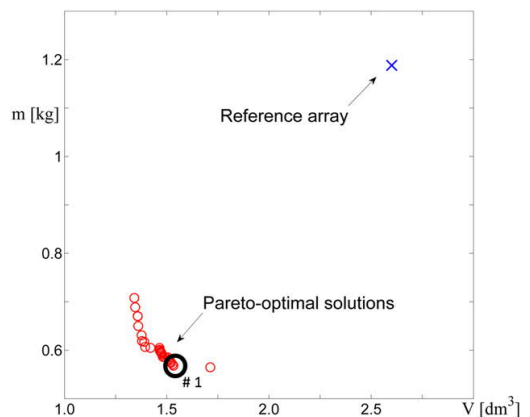

Fig. 12. Pareto-optimal solutions of a multi-objective optimization problem of natural convection array. Optimal array with the same maximum temperature as in Fig. 6.
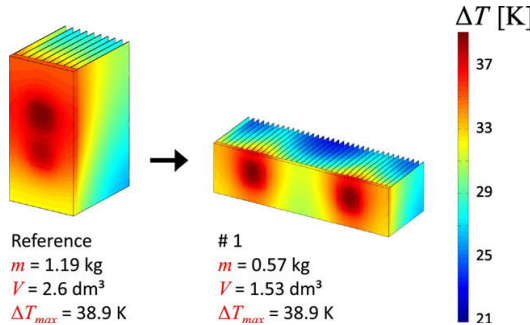
ΔT [K]

Reference
$m = 1.19$ kg
$V = 2.6$ dm³
$\Delta T_{max} = 38.9$ K

 # 1
$m = 0.57$ kg
$V = 1.53$ dm³
$\Delta T_{max} = 38.9$ K

Fig. 13. Reference array (left) and selected Pareto-optimum #1 from Fig. 12 (right).

the maximum temperature is different as above in Fig. 10, i.e. 109.1 °C, also whole geometry changes.

Another example shows how optimization reduces the mass and volume of a *natural convection* array composed of two components in Fig. 6 by maintaining the same maximum temperatures of the components. In the original reference design the number of fins is 10 and fin thickness is 1 mm. The final selected Pareto-optima #1 from Fig. 12 is shown in Fig. 13 on the right, where the mass was reduced by about 50% and the outer volume by about 40%. The number of fins and thickness were 36 are 0.54 mm, respectively.

7. Conclusions

The heat transfer analysis of the heat sink in Fig. 1 can be done with CFD, but in optimization, its use requires a lot of time. Thus we present an alternative way to calculate heat sink performance in forced and natural convection cases. It combines numerical solution of conduction in a solid and analytical treatment of fluid convection. The main advantage of this method is that it is many orders of magnitude faster than CFD.

Maximum component temperatures are usually fixed and heat generation is known. Many factors affect the performance of a sink such as component locations, the mass and size of the heat sink, and fin construction. This gives a multi-objective optimization problem, whose solution requires special methods. We have noticed that PSO is well suited optimization algorithm and can easily deal with discrete variables, such

as the number of fins. On the basis of experience of the authors, we have a conclusion that electronics heat sink designs can essentially be improved if modern optimization tools are used. For example in our latter optimization case in Fig. 13 the size and mass reduced about 50%.

We have also used LES to study and obtain analytical Nusselt number correlations of pin fins, a method that can be used to optimize natural convection pin fin array heat sinks. Also some optimum results of single fins, which give an idea of how fin geometry affects heat transfer, are given.

Funding

References

[1] A. Bejan, Heat Transfer, John Wiley & Sons, 1993.
[2] A.D. Kraus, A. Aziz, J. Welty, Extended Surface Heat Transfer, Wiley, New York, 2001.
[3] R. Karvinen, T. Karvinen, Optimum geometry of fixed volume plate fin for maximizing heat transfer, Int. J. Heat Mass Transf. 53 (2010) 5380–5385.
[4] R. Karvinen, T. Karvinen, Optimum geometry of plate fins, ASME J. Heat Transf. 134 (2012) (pp. 08101-1-7).
[5] M. Lindstedt, R. Karvinen, Conjugated heat transfer from a uniformly heated plate and a plate fin with uniform base heat flux, Int. J. Heat Mass Transf. 107 (2017) 89–95.
[6] M. Lindstedt, K. Lampio, R. Karvinen, Optimal shapes of straight fins and finned heat sinks, ASME J. Heat Transf. 137 (6) (2015) (061006-1-8).
[7] R. Karvinen, K. Lampio, Multi-objective optimization of electronics heat sink geometries, Proc. of IWHT 2013, October 18–21, 2013 (Xi'an, China).
[8] K. Lampio, R. Karvinen, A new method to optimize natural convection heat sinks, Heat Mass Transf. (2017) (in print).
[9] R.K. Shah, A.L. London, Laminar Flow Forced Convection in Ducts, Academic Press, New York, 1978.
[10] F. White, Fluid Mechanics, McGraw-Hill, 1986.
[11] V. Gnielinski, New equations for heat and mass transfer in turbulent pipe and channel flow, Int. Chem. Eng. 16 (1976) 359–368.
[12] R. Karvinen, K. Lampio, Combined numerical and analytical method for fin array heat transfer, Proc. of CHT-12, July 1–6, 2012 (Bath, England).
[13] A. Bar-Cohen, W. Rohsenow, Thermally optimum spacing of vertical, natural convection cooled, parallel plates, ASME J. Heat Transf. 106 (1984) 116–122.
[14] K. Kitamura, A. Mitsuishi, T. Suzuki, F. Kimura, Fluid flow and heat transfer of natural convection induced around a vertical row of heated horizontal cylinders, Int. J. Heat Mass Transf. 92 (2016) 414–429.
[15] K. Miettinen, Nonlinear Multiobjective Optimization, Kluwer Academic Publishers, 1998.
[16] C. Coello Coello, G. Pulido, M. Lechuga, Handling multiple objectives with particle swarm optimization, IEEE Trans. Evol. Comput. 8 (3) (2004).